Temperature Inversions in the Bergen Valley and Testing of Low-Cost Temperature and Air Quality Measuring Instruments

Master Thesis in Meteorology

Karoline Seilen

June 2018

UNIVERSITY OF BERGEN
Faculty of Mathematics and Natural Sciences

Acknowledgement

First of all, I would like to thank my supervisors Joachim Reuder and Tobias Wolf-Grosse. I could not have done this without you. I really appreciate all the help and guidance you have provided me. I am grateful for getting the opportunity to combine my two favorites; meteorology and mountain hikes. I would also like to thank Anak Bhandari, who made this project possible. I am thankful for all the help and for the hours you spent carrying heavy instruments up and down Løvstakken.

I will also thank Per Hallstein Fauske from Bergen Municipality, who made the testing of the Air Quality Eggs possible. And Dirk from Wicked Device, for helping me to solve the problems with the Air Quality Egg.

There is a large number of people I would like to thank: Ole Edvard Grov and Jan Asle Olseth for providing the data from the "Bergen Weather" project. Mona Waagsbø from NILU, for giving me access to air quality data. To Hordaland Fylkeskommune for the scholarship for writing about local climate. It made it possible to purchase the Air Quality Egg. Andrew for helping me with Latex tricks. Experimental meteorology group for weekly discussions. The people who helped carrying the instruments in February 2017.

I would like to thank my family and friend, for motivating me and cheering me up during though periods. Thanks to Hege Beate and Joachim for helping me out with programming and proofreading. And my dog Rosa, for always cheering me up. And my fellow students. I can't believe my time at GFI is over after all these years.

Abstract

This study aimed at two goals, the testing of simple low-cost measurement sensors for temperature and air pollution, and the investigation of temperature inversions in the Bergen valley. For this we conducted a 13 months measurement campaign between February 2017 and February 2018. In addition to already existing measurement stations we deployed a dense vertical transect of stations along a mountain side directly next to the city center.

The largest part of the ground-based temperature inversions were found to be shallow, most frequently with tops not exceeding 100 m asl. These were in general short lasting with more than 75 % shorter than two hours. Ground-based inversions are associated with high pollutant concentration events, but during the campaign no such events occurred. Elevated inversions were found to occur most frequently between 225 and 300 m asl and again more than 75 % lasted less than two hours. The synoptic situation during the study period, with a lot of frontal passages and a total amount of precipitation of more than 3000 mm, was likely to be the reason for the low number of long lasting inversions. The dense network of stations was instead used for a detailed study of a strong but comparatively short lasting temperature inversion over the Bergen valley caused by warm air advection.

The testing of low-cost temperature loggers (EasyLog), showed that solar radiation was a major problem. The loggers were prone to overheating when exposed to solar radiation. Removing all data when the solar radiation exceeded 20 W/m^2, resulted in a RMSD that decreased from a value between 1.7 and 3.6 % to a value between 0.4 and 0.7 %, and a increase in the correlation from a value of 0.58 and 0.82 % to 0.98 %.

Testing of low-cost air quality measuring instruments (Air Quality Egg), showed a questionable and non-reproduceable behavior. When comparing the Air Quality Egg to an official air quality measuring station in Bergen, we found a RMSD of 128.9 % and a correlation of 0.24, for the Air Quality Egg measuring NO_2. After intensive testing of these instruments we therefore decided to abandon the initial plan of field deployment of the Air Quality Eggs and advice against their usage for scientific studies without further thorough testing.

Contents

List of Figures

List of Tables

Acronyms

AADI Aanderaa Data Instruments AS

AQE Air Quality Egg

AWS Automatic weather station

AWSA Automatic weather station from AADI

AWSI Automatic weather station from ITAS

BK Bergen municipality reference station

BL Boundary Layer

CO Carbon monoxide

DSU Data Storage Unit

EL EasyLog data logger

GFI Geophysical Institute

ITAS Instrumenttjenesten AS

m asl m above sea level

MTP MTP-5HE

NaN Not a Number

NILU Norwegian Institute for Air Research

NO_2 Nitrogen dioxide

PP Particulate pollution

ppb Parts per billion

RMSD Root Mean Square Deviation

SO_2 Sulphate Dioxide

1 Introduction

High pollutant concentrations can be a problem in Bergen, Norway, especially during wintertime. From time to time the pollutant concentrations exceed the legal thresholds and can lead to health and environmental issues (Miljødirektoratet 2018). These situations are associated with temperature inversions in the urbanized Bergen valley that lead to reduced turbulent dispersion of the pollutants emitted within the city. Long lasting events with high concentrations of Nitrogen dioxide (NO_2) and Particulate pollution (PP) (Wolf et al. 2014) have repeatedly resulted in large media and public attention. This resulted in a societal request for a better understanding of the circulation and inversion conditions inside the valley.

Information about the local air quality is easily accessible nowadays. The air quality in Bergen is monitored and can be seen online at `www.luftkvalitet.info`. In addition, the Meteorological Institute in cooperation with the Norwegian Institute of Air Research (NILU) provides an air quality forecast available for everyone. These forecasts have, however, still shortcomings in the accurate prediction of, in particular, the highest pollutant concentrations (Ødegaard, Gjerstad, Abildsnes & Olsen 2011).

The temperature inversions have been investigated in years and the connection to the air quality has been known for a long time. E.g. Fitje (1972) investigated the temperature inversions in connection to Sulphate Dioxide (SO_2), by mounting instrumentation on the cable car going up and down Mt. Ulriken, which is located on the southeast side of the valley.

The Bergen Valley has a complex topography, with Mt. Ulriken southeast of the city and Løvstakken to the west. These mountains affect the circulation in the city, the mountains act as a shelter (Jonassen et al. 2012). The formation of ground-based temperature inversions often occur during relatively calm synoptic conditions with a strongly negative heat balance (Wolf et al. 2014). In addition, elevated inversions can occur through differ-

ent advective processes. The inversion height is correlated to the pollutant concentrations, where the high concentrations of NO_2 and $PM_{2.5}$ were associated with heights between 170 and 270 m above sea level (m asl).

To better understand the connection between the air quality and temperature inversions, information about the atmospheric stability, i.e. the vertical temperature structure and the circulation in the valley is needed. Previous studies of this problem have used microwave remote sensing measurements (Wolf et al. 2014), teathersondes (Berge & Hassel 1984) and ground based measurements spread over the Bergen valley (Fitje 1972, Valved 2012) , all with different focus, advantages and shortcomings. In addition, these previous studies do not fully agree on the inversion characteristics and the circulation during the temperature inversions. In this study we therefore aim to readdress the problem of the temperature inversions and the circulation in the valley during such conditions though a combination of high quality in-situ measurements with automatic meteorological stations together with newly available simple and low-cost temperature and air quality sensors. All additional instrumentation used in this study should be deployed as a vertical transect along a mountain side next to the area with the supposedly highest air pollutant concentrations in the city center, giving high resolution vertical information. For the low-cost sensors a thorough testing of their accuracy and usefulness in the field is a natural part if this study, as reports on their performance are still scarce and strongly deviating from the information provided by the manufacturers (Castell 2017). The aim of the study is therefore twofold to first deploy a dense network of measurement points along the mountain side in order to establish a measurement basis for the analysis of the local temperature inversions and circulation. Simultaneously, the low cost sensors should be tested and compared to accredited measurements. Dependent on their performance then, the low cost sensors should also be field deployed in order to establish a very dense network of measurements.

In this thesis chapter 2 is a presentation of the theory relevant for the weather and temperature inversions in the Bergen Valley. In chapter 3, we present the instrumentation used for the campaign, followed by an overview of the data applied and how we handled it. In chapter 5, the results from the campaign are presented, starting with testing of the low-cost temperature sensors EasyLog data loggers (ELs), in section 5.1, followed by the results from the testing of low-cost air quality measuring instruments (Air Quality Eggs (AQEs)), in section 5.2. In section 5.3, the general weather situation during the campaign compared to the climatology and previous studies is presented. In section 5.4 the results of

the measured temperature inversions are presented, and last, a case study of an inversion situation due to warm air advection is analyzed in detail in section 5.5. In chapter 6 a summary and conclusion of the results are presented.

2 Theory

The climate within a valley is largely varying and is influenced by both local and large-scale processes. In order to understand the climatic conditions and the processes that affect the Bergen Valley, we have to consider a large variety of effects. The large scale features can explain the overall synoptic and climatological situation, while the local scale effects explain the variations within a smaller area. When considering local climate it is defined by the range of 100 m to 50 km on horizontal scale (Oke 1987). The Boundary Layer (BL) is the lowest part of the atmosphere and is characterized by efficient turbulent transport processes. It is directly influenced by the surface with a timescale of an hour or less (Stull 2009). On a summer day the BL can have a vertical extension of 1-2 km, while during a cold and calm night it can be less than 100 m (Oke 1987). This large difference is caused by the variability of vertical mixing and depends on the atmospheric stability.

The Bergen Valley is of complex terrain and the city center is located on the valley floor with mountains surrounding it. The highest mountain is Ulriken at 643 m above sea level (m asl) located southeast of the city and the second highest is Løvstakken at 477 m asl, located west of the city. The valley is curved and mostly oriented in a southeast - northwest direction. The Bergen Fjord is located at the northwest end of the valley, and a few kilometers to the west is the open sea, the North Sea. Towards the east it is only a few tens of kilometers before the mountain ranges reach altitudes of 1500 m and above. The large variation in topography and surface characteristics, affects the climate in the city. In this chapter, I list the most relevant driving forces for the weather in Bergen, and explain the effects. First, I present some of the previous studies on temperature inversions and air quality linked to inversions. Then, the large scale features are described, e.g. frontal weather and sea and land breeze. How the stability of the boundary layer affects the atmosphere, will be presented. Followed by the local scale processes, e.g. radiation, wind flow and the heat island effect. Different types of temperature inversions will be

presented, to better understand why temperature inversions are important in the city, and how the driving forces contribute to temperature inversions build-up, amplification and break-down. Last, I explain the importance of air quality and how the air quality is linked to temperature inversions.

2.1 Previous Studies

Temperature inversions have been a well known subject within the field of geophysics for a long time. The Bergen School of Meteorology started in 1917 and was the beginning of meteorological studies in the city. Today we find several research institutions in Bergen, e.g Bjerknes Center for Climate Research, Geophysical Institute (GFI), Nansen Environmental and Remote Sensing Center (NERSC), Norwegian Meteorological Institute (MET) and UNI Research. Because of a large community in the city there are several previous studies about temperature inversions and the pollution situation in the city, some of them are mentioned in the next paragraphs.

In 1972, Fitje studied the temperature profile in the Bergen Valley by in-situ measurements and mounted instruments to the cable car going up Ulriken. The aim of the study was to look at the connection between the temperature profile and the concentration of Sulphate Dioxide (SO_2), from 1969 to 1970. The result of the study showed that most of the inversions were 100 and 150 m deep for short lasting events. For the longer lasting events, the depth increased. Further on, Hanssen-Bauer (1985) developed and tested a simple model for diffusion of SO_2 in Bergen, with input from SO_2 from four stations in the city. The purpose was to develop a model for analysis and forecast of daily mean SO_2 concentrations in the area.

Berge & Hassel (1984) used a regression model and performed measurements of temperature and wind profiles, by tethersonde, under inversion events. The purpose of the study was to investigate the dispersion of pollutants in the city. In addition to the tethersonde measurements, pollutant measurements were collected together with measurements of wind and temperature from stations in, and around the city. The result of the study was that inversions, that built up within 1-2 hours can reach 50 m height. For longer lasting inversion events the typically maximum heights were 100-120 m. Utaaker (1995) address the micro-meteorology and climate in the Bergen area and based the study on meteorological measurements with weather stations in the Bergen area.

Jonassen et al. (2012) and Valved (2012) both used a network of several Automatic weather stations (AWSs) to study the flow in the Bergen valley. They both found channeling of the winds to occur in the valley. Jonassen et al. (2012) studied how wind speed in the Bergen valley correlates to 850 hPa wind speed for different wind directions. Valved used the observations from the AWSs and simulations from the Weather Research and Forecasting Model (WRF) to investigate temperature inversion situations in the Bergen Valley. The result of the study was that inversions in the Bergen valley are normally associated with easterly or southerly winds. For inversions occurring in easterly and northeasterly winds, sheltering by topography was assumed to be the main reason. She reported strongest inversions when wind comes from east.

Wolf et al. (2014) used measurements with a microwave radiometer to analyze the temperature inversions in the Bergen Valley. In addition, they studied the circulation in and above the valley during temperature inversions and the connection between the inversions and air pollution situations. A result of the study was that ground-based temperature inversions usually occurred under the presence of down-valley winds. Above the valley it was a distinct occurrence of southeasterly winds. The inversions were also connected to NO_2 and $PM_{2.5}$ air pollution events. They found that inversion tops were most frequently located at about 70 m asl, with the maximum top at 220 m asl. For inversions lasting longer than 2 hours, the mean tops were uniformly distributed up to 270 m asl, with a maximum around 170 m asl. During the two years of investigation only four events of ground inversion tops reaching above 470 m asl were reported.

2.2 Synoptic and Mesoscale Meteorology

Bergen is known for its rainy climate. The normal precipitation in Bergen, between 1961-1990 is 2250 mm, which is more than two times the normal precipitation globally (Bergen Municipality 2017*b*, NOAA National Centers for Environmental Information 2015). In this section I highlight the synoptic and mesoscale meteorology contributing to the climate in Bergen and the west coast of Norway. First I will present the different types of precipitation and then the sea and land breeze.

2.2.1 Frontal weather

In Norway most of the precipitation is connected to the passage of synoptic scale fronts (Sorteberg 2014). Fronts are associated with the distinction of two air masses of different temperature. The three main types of fronts are cold, warm and occluded, determined by the temperature behind the front, when it has passed (Oke 1987). The fronts have different origin, they typically occur as parts of mid-latitude cyclones, but can also be independent and behave stationary. A cold front is a front where cold air takes over for the warm air at the surface. Cold air is denser and therefore heavier (Wallace & Hobbs 2006). The cold front is therefore lifting the warmer air. The isobars will bend sharply along the front and the wind shifts. As the warm air rises, it is object to adiabatic cooling. This eventually leads to a saturation of the air parcel due to the decreasing saturation mixing ratio with decreasing temperatures. Clouds are formed, leading to precipitation.

A warm front has a less steep front, than the cold front, and warm, less dense air will take over for the cold air (Wallace & Hobbs 2006). The isobars will tighten resulting in a stronger wind that will shift. In front of the the surface warm front there is cloud formation and precipitation. For temperature inversions, the warm fronts are the most interesting ones. When the warm front has passed, precipitation normally stops and a warm sector occurs. In this warm sector there are normally light winds and little clouds, giving rise to nocturnal temperature inversions by radiative cooling. An occluded front, or an occlusion, occurs when a warm front is caught and overtaken by a cold front (Ahrens 2012). There are two types of occluded fronts, a cold occlusion and a warm occlusion. The cold occlusion has colder air behind the front than ahead of it and the opposite for the warm occlusion, where it is warmer air behind the front than ahead of it.

2.2.2 Precipitation

In addition to the precipitation from the fronts, described above, orographic precipitation is a well-known type of precipitation in the Bergen area. Orographic precipitation is sometimes associated with fronts, because if the winds are directed towards a topographic barrier, the humid air is forced over the mountain, results in a cooling of the air as it rises and saturation is reached if the air is cooled enough (Sorteberg 2014). Due to condensation, clouds are formed, leading to precipitation. The mountains surrounding the city of Bergen are tall enough to cause orographic precipitation, but they are not the main contributors.

Higher mountains, such as Gullfjellet (988 m asl), located east of the city, have a larger impact on the formation of orographic precipitation (Bergen Municipality 2017*a*).

Another type of precipitation that normally occurs in the summer, is the showers. Heating of the ground by solar radiation can cause rising air and cloud formation that results in showers (Sorteberg 2014). The showers are short lasting, local processes, which occur in the summer due to strong heating of the surface and unstable ascending air.

2.2.3 Sea and Land Breeze

Due to temperature differences between the land surface and the ocean/water surface, a horizontal pressure gradient can result in a breeze across the shoreline (Utaaker 1991). The temperature over land can vary largely during the day, while the temperature over the ocean varies only slightly. During the day it is normally warmer over land and colder at night, compared to the ocean.

The result of the temperature difference is the sea breeze at daytime, as illustrated in figure 2.1(a), and the land breeze during the night, illustrated in figure 2.1(b) (Oke 1987). Because of a more rapid heating over land during the day, a sea breeze is generated from the sea towards the land (Utaaker 1991). The air over land warms and expands, leading to higher pressure aloft, over land compared to the same level over sea. This induces a motion from this local high towards the sea, leading to a pressure decrease over land and a corresponding increase over the sea that finally triggers the observed sea-breeze at the ground. The sea breeze front can form sea breeze cumulus clouds, as it transports cold and more humid air from the sea (Oke 1987). An upper-layer return flow will bring the warm air from land to the ocean where it sinks. The clouds are transported towards the sea where they dissolve, because of adiabatic heating causing the air to be unsaturated (Utaaker 1991).

During the night a land breeze is generated because the air over land cools rapidly and the air over water is now warmer (Utaaker 1991). The low pressure over land is no longer present because of the cooling over land. Eventually high pressure develops over land and low pressure aloft. The cooling of the land surface is greatest in anticyclonic summer weather, because the cloudless sky and weak winds cause the largest temperature difference during day and night. If the ocean is colder than the land surface the sea breeze will continue through the night.

The sea breeze is stronger, both horizontally and vertically, than the land breeze, because the instability is greatest during the day, the excess heat over land is higher (Oke 1987). The sea breeze can blow at 2-5 m/s, extending 30 km inland and have a vertical extent of 1-2 km in tropical areas. Because of this extent the breeze might be affected by the Coriolis force, which can result in a breeze bended to the right in the northern hemisphere, leaving the breeze almost parallel to the coast. For northern latitudes the horizontal extent is about 15-40 km and the vertical extent is 50-200 m (Utaaker 1991). The land breeze can blow at 1-2 m/s and can have a smaller extent both in the horizontal and vertical directions (Oke 1987).

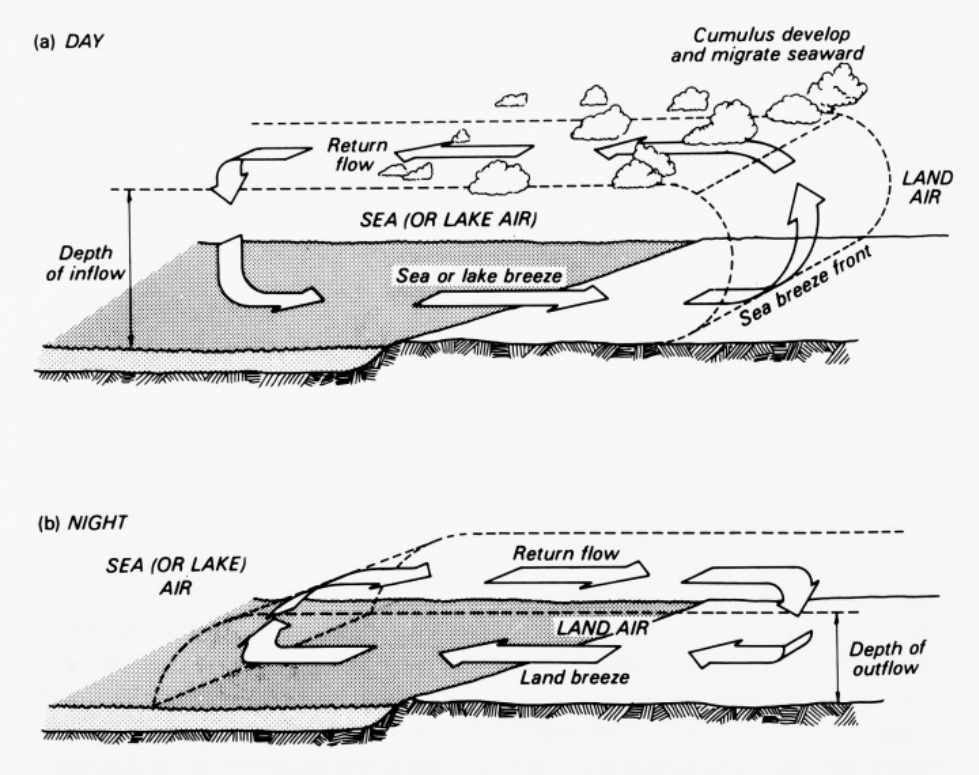

Figure 2.1: Illustration of (a) sea breeze circulation during daytime and (b) land breeze circulation during nighttime. Figure from Oke (1987)

2.3 Topoclimate

The word topoclimate was introduced in 1953 by C. W. Thorntwaite, because the topography is of great importance for the climate on local scale, and is used instead of local climate (Utaaker 1991). In this section I will go through some of the important features affecting the climate on local scale, especially for the climate in a valley, like in Bergen.

2.3.1 Radiation

The amount of solar radiation received at the ground is affected by both the orientation and the angle of the slope of the surface (Utaaker 1991). It is mainly the direct radiation that is affected. A flat surface will get a larger amount of solar radiation than a sloped surface, which leads to a large variability within a valley. The amount of solar radiation also varies throughout the year and time of the day. During the winter the days are shorter and the strength of solar radiation is weaker, leading to more cases of temperature inversions, especially during cold and calm periods. The largest variation in incoming solar radiation on sloped surfaces occurs during the spring. At night radiative cooling at the surface is a result of the negative energy balance at the surface (Oke 1987). How radiative cooling leads to temperature inversions can be seen in section 2.4.

2.3.2 Wind

Topography affects the circulation in a valley. Winds can be generated because of large temperature variations within the valley, especially when it is calm and fair weather (Oke 1987). In the summer, in anticyclonic weather the thermal differences are largest and the winds are best developed. How the winds behave depends on the orientation of the valley, as well as the geometry. Even small obstacles can modify the local wind circulation. In figure 2.2, typical patterns of the airflow affected by topography is illustrated. Figure 2.2(a) shows how topographic features with moderate slopes can influence the airflow. There will be a speed-up when the contour lines are getting closer and a slow-down when the contours are further apart. As seen in the upper panel on the left side in figure 2.2(a), a ridge causes a speed-up close to the ridge, with a maximum at the top of the ridge, because that is where the contours are closest. For the valley, a slow-down is caused because the contours are farther away from each other. A small upward step also causes a speed-up, while a

step down causes a slow-down. For a three-dimensional hill or island, the vertical contours are closer when the air goes over and around the hill, causing a speed-up. The maximum speed-up is reached after passing the hill. The last example showed that when the transects of the valley gets closer together a speed-up occurs.

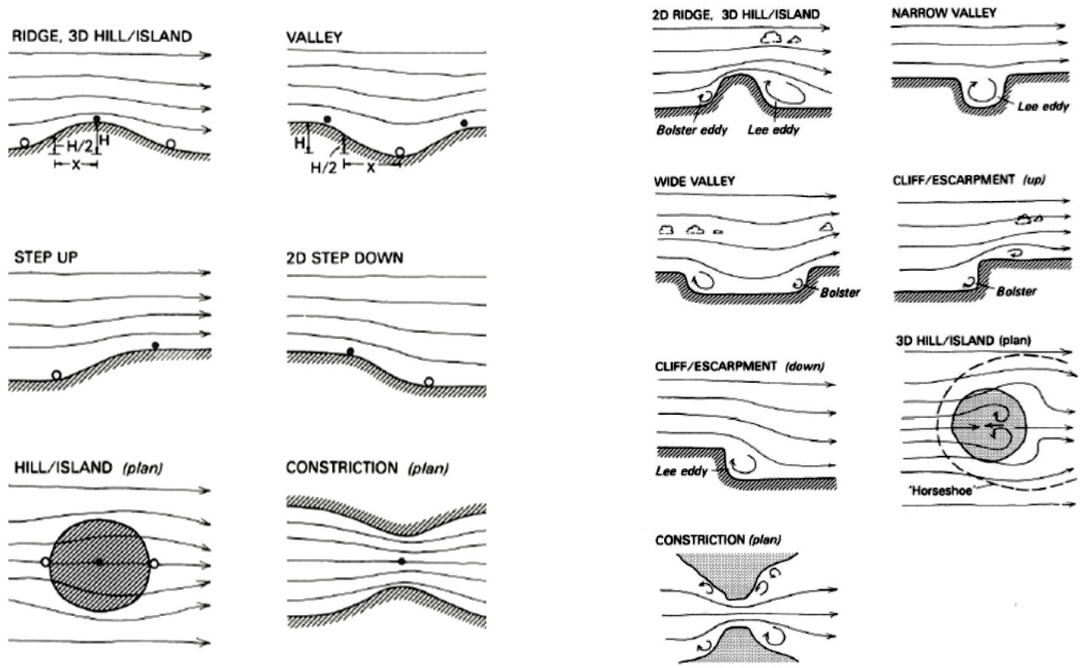

(a) (b)

Figure 2.2: Illustration of how topography influence can the airflow. (a) shows typical pattern of airflow over moderate topography, and (b) over steep topography. In (a) the white points illustrate the location of minimum wind speed, and the black points the maximum wind speeds. Figure from (Oke 1987)

The influence of topographic features with steeper slopes is illustrated in figure 2.2(b) where there is a flow over steep topography (Oke 1987). The steep topography influences the air flow and separates it from the terrain, which means the flow can not fully adjust to the terrain. In front of a steep ridge the pressure builds up and most of the flow will flow over the ridge, causing a speed-up, with maximum on the top of the ridge. The air left behind, moves downwards, creating a bolster eddy, an eddy circulating in the opposite direction to the flow. After the flow reached the top of the ridge it gets separated and form a lee eddy. At the surface, the lee eddy also circulates in the opposite direction to the mean

flow. The area is somehow sheltered but can experience short-term gusts. The air above the eddy is capable of forming convective clouds. If the flow has a stable stratification it can form decreasing lee waves and lee wave clouds downstream. When the airflow passes a narrow valley, most of the airflow will pass, but a lee eddy will form in the valley. This lee eddy can cause variable winds in the valley. When the airflow passes a wide valley with steep walls the result is a combination of the two previous examples. A lee eddy is formed as along the transect where there is a drop in the surface elevation. The airflow will start to adjust to the valley, before it speeds-up in the other end, and a bolster eddy is created. When the airflow reaches a cliff with a steep step, eddies may form at the base and on the top of the cliff, and clouds are likely to form. When there is a steep step down a strong lee eddy is formed. A steep three-dimensional hill will cause a speed-up both over the hill and on the sides of the hill. On the other side lee eddies are produced, but the flow behind the hill is complicated, since the flow comes from different directions. The result is a horseshoe shaped turbulent wake of the wind, that extends downstream for a considerable distance. A sharp constriction in the landscape causes a speed-up of the flow in addition to bolster and lee eddies both before and after the passage.

On clear or partly cloudy days the temperature within the valley will vary largely. The air just above the surface on the valley slopes will be warmer than the air at the same altitude in the middle of the valley (Oke 1987). This gives rise to a horizontal buoyancy gradient that develops an anabatic wind, upslope in the valley, as seen in figure 2.3(a) (Markowski & Richardson 2010). The strength of the anabatic winds vary and the maximum is reached a few hours after sunrise, when the temperature contrast is at its largest. Typically, the anabatic winds have a peak speed of 1-5 m/s at 10-20 m above the surface. If there is sufficient moisture present, anabatic winds can form anabatic cumulus clouds along the valley ridge. Sinking air in the center of the valley compensates for the rising warm air along the slope (Zardi & Whiteman 2012). In addition to the anabatic winds, an up-valley wind, known as valley-wind, is also present in the valley during the day (Markowski & Richardson 2010). The horizontal pressure gradient drives the valley wind and it is due to the temperature differences between the valley and the plain further down the valley. The valley is warmer than the plain, causing an up-valley flow. The valley wind lasts until it is replaced by a down-valley wind, normally shortly after sunset. A counter flow, named anti-valley wind, flows down the valley above the ridge during the day (Oke 1987).

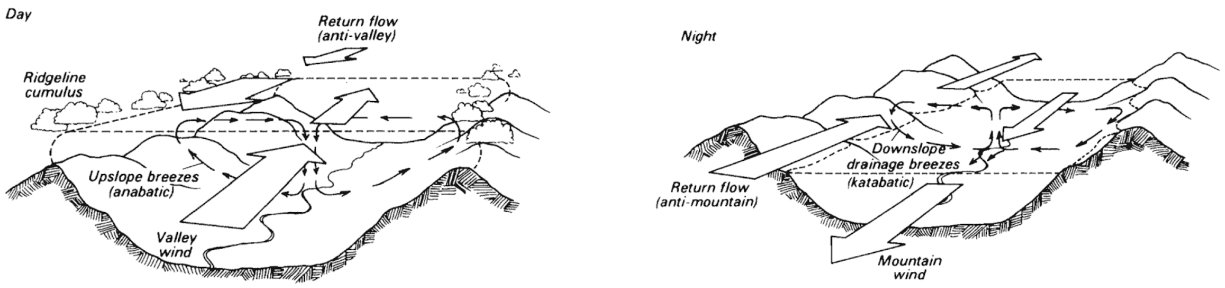

(a) Daytime

(b) Nighttime

Figure 2.3: Illustration of circulation in a valley, (a) during daytime with valley winds, and (b) nighttime with mountain winds. Figure from (Oke 1987)

Cross winds occur when only one side of the valley is in direct sunlight, resulting in anabatic winds, while the other flank is in the shadow (Oke 1987). Then the anabatic wind result in a cross wind that goes across the valley over to the top of the other slope. On the other transect air is colder and a weak down-slope wind occurs. The result is a circulation in the valley with upslope, anabatic, wind on one transect and downslope, katabatic, wind on the other transect.

During the night, the surface cools by radiative cooling, causing down-slope winds, known as katabatic winds, as seen in figure 2.3(b) (Oke 1987). Due to gravity, air sinks down the slopes. Like for the anabatic winds, the driving force is the buoyancy force (Markowski & Richardson 2010). The katabatic winds have a peak speed of 1-4 m/s at 1-3 m above the surface. Because of obstacles in the slope of the valley, the flow of air down the slope is not continuous. The flow goes rather slow, but because of obstacles a build-up of air can cause sudden intense flows. As the air is transported down the slope some of it converges in the middle of the valley and rises, while some of it is combined and flows down-valley as the down-valley wind, known as mountain wind (Oke 1987). The combined airflow of mountain wind and katabatic winds are known as a drainage wind (Markowski & Richardson 2010). The mountain wind normally starts around sunset and can last a few hours after sunrise, it lasts until the valley wind takes over. Due to friction, the mountain wind has its maximum speed in the middle of the valley, away from the surface, causing the mountain wind to have a jet-like shape in the vertical profile (Zardi & Whiteman 2012). The mountain wind is therefore referred to as a down-valley jet. Like for the valley wind, the mountain wind also has an counter flow, known as anti-mountain wind (Oke 1987).

The anti-mountain wind flows up the valley at a higher altitude. Katabatic winds can also occur over surfaces of snow and ice. The cold surface causes katabatic winds to be present during the day over e.g. glaciers.

2.3.3 Heat Island Effect

Heat island is another word for a city being warmer than the surrounding areas, normally a countryside (Stull 2009). The origin of the name is that when looking at a weather map the isothermals of the city look like the topographic contours of an island. Cities are generally warmer and emit more pollution, than the countryside. Normally large areas of the cities are covered in asphalt, concrete and other material with low albedo and large heat capacities, resulting in storage of a large amount of the incoming solar radiation.

The intensity of the heat island is the temperature difference between the city and the surrounding areas (Utaaker 1991). The heat island effect is strongest during night, when the temperature difference is largest. Due to temperature differences, horizontal temperature gradients can cause a closed circulation above the city during calm and cold nights. Tall buildings can cause strong winds in the streets, due to downward deflection og higher momentum air from above down into the city (Oke 1987). After sunrise the city can be colder than the rural areas, resulting in a negative heat island effect, because the city is warming slower than the rural areas (Utaaker 1991). After sunset the cooling of the city is slower, most likely due to a thicker layer of warm air that needs to be cooled. In the middle of the night the cooling in the city is faster than in the countryside.

The heat island effect depends on the population in the city. Small cities with a population of 1000 can have a temperature difference of 2-3 °C between the city and the landscape next to it (Stull 2009). The temperature difference increases with increasing population. Having a population of 1 million can lead to temperature differences of 8-12 °C. This temperature difference can prevent temperature inversions to occur in the city. Bergen has a population of less than 100 000 in the city center and the temperature difference is expected to be somewhere in between the two examples. The anthropogenic heat input in the city can cause a shallow convective mixed layer to be maintained during the night, preventing inversions to occur (Stull 2009, Utaaker 1991).

2.4 Temperature Inversion

The temperature in the atmosphere normally decreases with altitude. When the potential temperature increases with altitude within an atmospheric layer it is known as a temperature inversion. There are several types of temperature inversions, categorized by how they form or in what height they are located. The two types associated with height are the ground-based and the elevated inversions. As the names say, a ground-based inversion is an inversion that reaches the ground, while an elevated inversion is an inversion located higher up in the atmosphere. For this study the ground-based inversion is the one of most concern, as it traps pollutants that are emitted within the surface layer. Elevated inversions may also be problematic, because they can lead to fumigation of stack emissions.

Radiation inversion is the most well-known type of inversion. Radiation inversions are low atmospheric ground-based inversions that normally extend 50-100 m (Oke 1987). They typically occur during nights with no or little clouds and weak winds. Because the ground cools faster, than the air above due to long-wave radiative cooling , the atmospheric surface layer is cooling from below. Normally this inversion breaks up a few hours after sunset because the solar radiation heats the ground. During winter at high latitudes with weak or even no solar radiation the inversion can last for days or even weeks. Another type of radiation inversion is the elevated one, which is typically based on an active elevated surface, such as polluted layers or cloud tops. In addition, temperature inversions occur in the internal boundary layer, which is the layer of air within the boundary layer that is modified when it flow over a surface of different roughness (Stull 2009).

Frontal inversions are elevated inversions which occur in the upper-layer of fronts. The inversion is located at the boundary between cold and warm air, as the warm air overrides the cold air for warm fronts, and cold air wedging under warmer air for cold fronts. Therefore, inversions are always present in fronts. For air pollution considerations, frontal inversions are normally not of interest, since the frontal inversions are short lasting events In addition they are typically associated with wind and precipitation, both factors preventing local accumulation of pollutants. Sometimes, when the slope of the warm front is slight and the front is slowly moving, the mixed layer gets thinner, which increases the inversion. This can be problematic for the air quality because the elevated warm air is getting closer to the ground. Especially when there are pockets of cold air trapped on the ground and the warm air acts as a lid preventing vertical mixing.

Subsidence inversion is an elevated inversion occurring due to large scale downward vertical motion in a high pressure system (Oke 1987). In an anticyclonic region the air sinks and heats adiabatically The lapse rate reduces and the air can be heated to a point where it is warmer than the underlying air, and an inversion occurs. Underneath the inversion the air is well mixed, but the inversion acts as an efficient lid, trapping pollution within the layer. If the high pressure system is strong and lasts for a long period, the air quality can get poorer, as the pollution is trapped. This is a common type of inversion over the European continent because of high pressure systems (Utaaker 1991).

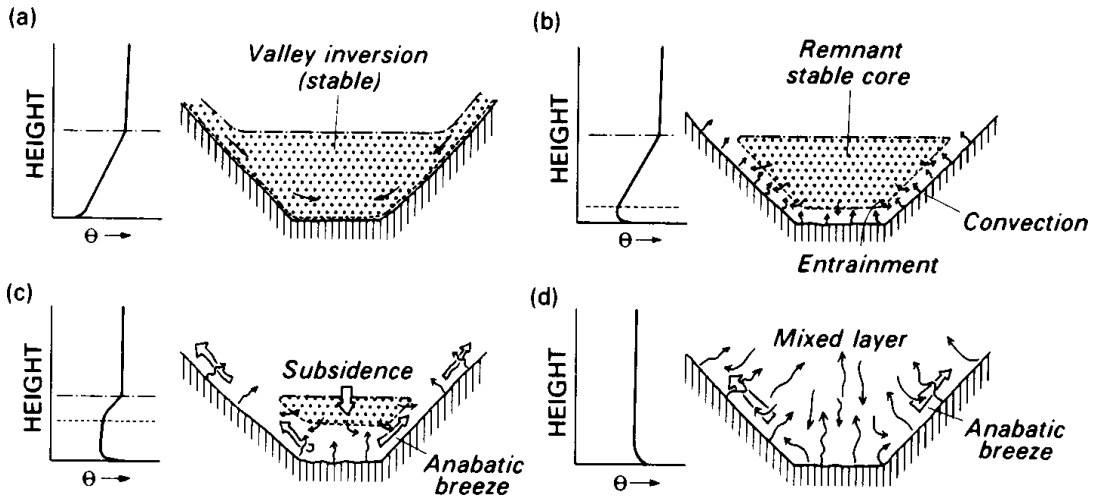

Figure 2.4: One type of mechanism showing how a temperature inversion in a valley can break up. a) Valley inversion, with katabatic winds along the transects, b) after sunrise, in the lower layer of the valley convection leads to a break-up of the inversion, an inversion in the core is still present, c) anabatic winds occur and the stable core sinks, d) The valley is fully mixed and no inversion left. Figure from Oke (1987)

Valley inversion is a common type of inversion in the Bergen Valley. Calm and clear nights are favorable, because the radiative cooling of the surface is then largest (Oke 1987). Similar to the katabatic winds a flow of about 1 m/s down-slope and small obstacles allow the coldest air to settle in the lowest levels, causing an inversion, as the temperature increase up the valley, illustrated in figure 2.4(a). This built-up of cold air in a valley is known as a cold pool. Above the cold pool, the temperature decreases with heigh. When the cold air sets in the valley and a stable stratification occurs, the warmer air that flows

down-slope will not reach the cold pool in the valley as the cold air acts as a lid. This may cause the warmer air to oscillate, giving rise to gravity waves. If the temperature in the cold pool reaches the dew point, radiation fog will occur in the lowest lying points.

After sunrise the solar radiation starts to heat the ground, a shallow mixed layer is generated by a sensible heat flux from the ground, as illustrated in figure 2.4(b). The cold, stable air in the core is still present. Anabatic winds are generated and the stable core sinks, illustrated in figure 2.4(c). As the core sinks the air is warmed adiabatically. 3-5 hours after sunrise the inversion is dissolved and the layer inside the valley is a mixed layer, as illustrated in figure 2.4(d). Sometimes during cold and calm days in the winter, the solar radiation is too weak to break up the inversion, leading to long lasting events. Inversion periods of 8 to 10 days may occur in the Bergen Valley (Utaaker 1995).

2.5 Pollution

Normally the emitted pollution is dispersed both horizontally by winds and vertically by turbulence (Oke 1987). Both wind speed and direction is important for the transport. The weather is also an important feature for air quality. Processes related to precipitation, known as wet scavenging, can improve the air quality by removing pollutants. The most favorable state of the BL, seen from a convective standpoint, is during a strong instability and a deep mixing layer, because this leads to a better dispersion of pollutants. Temperature stratification is crucial for the dispersion of pollutants. The air quality is affected by temperature inversions, since the pollutants are trapped within limited volume, leading to higher concentrations of hazardous substances. The elevated inversions act as efficient lids and the pollutant can not escape. The temperature stratification also determines the turbulence and the efficiency of mixing within a layer.

About 90 % of the particles in the atmosphere come from natural sources (Oke 1987). The rest is from anthropogenic sources, like combustion, building activity and industrial processing. Air pollution is a health problem and to be able to solve the problem it is necessary to know the source of the pollutants. Figure 2.1 shows an overview of some of the pollutants and their sources. In this thesis, mainly three pollutants are of interest, PM_{10}, $PM_{2.5}$ and NO_2. These three are measured by the Bergen municipality at several locations in the Bergen city. PM_{10} and $PM_{2.5}$ are particulate matter of a particular size less than 10 µm in aerodynamic diameter for PM_{10}, and less than 2.5 µm in aerodynamic

diameter for $PM_{2.5}$. These are small particles that can stay in the atmosphere for a long time and the state of the atmosphere is hence important for the dispersion.

Table 2.1: Overview of pollutants and their sources. Information from NILU (2015)

Source / Contribution	**NO2**	**PM_{10}**	**$PM_{2.5}$**	**SO2**	**CO**
Exhaust emission	Alot	Some	Much	-	Little
Wear of road, tires and brakes	-	Alot	Some	-	-
Sprinkle sand	-	Alot	Some	-	-
Wood combustion	-	Much	Much	-	-
Industry	Some	Some	Some	Some	-
Ship traffic	Some	Little	Little	Some	-
Long-transported pollution	Little	Some	Much	Little	-

There are several removal processes in the atmosphere. Gravitational settling is one, where particles settle at e.g. the ground, due to gravity (Oke 1987). It is an efficient process as most of the particulate matter larger than 1 µm is removed. Particles smaller than 1 µm are more affected by turbulence and may remain in the atmosphere days to weeks. Another one is dry deposition, which is a surface absorption, where the surface acts as a sink for the pollutants. How easy the pollutants are absorbed is dependent on, e.g. the water tension for the water surfaces, and the bacteria activity for the soil surfaces. Processes related to precipitation, as mentioned above, can remove pollutants by e.g. wet scavenging, which is a removal of pollutants in the atmosphere by the falling precipitation.

In Norway the regulations for air pollution, the air quality criteria, is set together by the Norwegian Institute of Public Health and the Norwegian Environment Agency (Norwegian Institute of Public Health 2017). It is only the unwanted health effects that are considered in the air quality criteria. The numbers are the legal thresholds and the pollutant concentrations should be kept below these thresholds. The numbers can be seen in table 2.2. The goal is to protect most of the population against harmful effects. Another value for describing the levels of air pollution in Norway is the national goals, that are health-based and include the ambitions for local air quality. The third type of regulation is the limit value, which is based on pollution regulations. These regulations can come from different sources, like World Health Organization (WHO), who have established the

Table 2.2: Air quality standard. The numbers are the legal thresholds and the pollutant concentrations should be kept below these thresholds. Numbers from Folkehelseinstituttet (2018)

Averaging period / Component	**15-minutes**	**1 hour**	**24 hours**	**1 year**
NO_2	300 µg/m^3	100 µg/m^3	-	40 µg/m^3
PM_{10}	-	-	30 µg/m^3	20 µg/m^3
$PM_{2.5}$	-	-	15 µg/m^3	8 µg/m^3
CO	80 mg/m^3	25 mg/m^3	-	-
SO_2	300 µg/m^3	-	20 µg/m^3	-
Ozone	-	100 µg/m^3	-	-

air quality guidelines for Europe. Economics and practical considerations are also included in the limit values.

3 Instrumentation and Data

In this chapter I describe the instruments and data used for the campaign and how the data are handled.

3.1 Instrumentation

Various data sources have been used in the presented study. A considerable portion of the data have been collected with instrumentation that was specifically deployed for the purpose of this campaign. Meteorological measurements along the slope of the Bergen Valley have been performed by Automatic weather stations (AWSs) (five from Instrumenttjenesten AS (ITAS) three from Aanderaa Data Instruments AS (AADI)) and five low-cost temperature loggers from EasyLog. In addition two Air Quality Eggs (AQEs) have been purchased for the project, one measuring particulate matter, the other CO and NO_2. This section shortly describes the instrumentation used.

3.1.1 Automatic Weather Station from ITAS (AWSI)

The Automatic weather station from ITAS (AWSI) measures temperature, humidity, pressure, shortwave radiation, wind (speed, gust and direction) and precipitation (ITAS 2015). The sensors are connected to a logger box with a data logger (Campbell Scientific CR1000) and mounted on a tripod mast. The data logger is connected to the mobile network via modem (Maestro 100 GSM/GPRS) and allows for two way communication for remote access and data download. Table 3.1 shows an overview of the sensors and their specifications.

Table 3.1: Sensor specification for the AWSI. Numbers from (ITAS 2015)

Parameter	**Sensor**	**Measurement range**	**Accuracy**	**Unit**
Temperature	Vaisala HMP155	-80 to +60	± 0.2 @ -80 to +20 °C ± 0.06 @ +20 to +60 °C	[°C]
Relative humidity	Vaisala HMP155	0 to 100	± 0.6 @ 0 to 40% RH ± 1.0 @ 40 to 97% RH	[%]
Atmospheric pressure	RM Young 61302V	500 to 1100	± 0.2 hPa RMS @ 25 °C ± 0.3 hPa RMS @ -50 to +60 °C	[hPa]
Wind speed	RM Young 5106-45 Alpine	0 to 100	± 0.3 m/s or 1 % of measurement	[m/s]
Wind direction	RM Young 5106-45 Alpine	0 to 360	± 3 %	[°]
Shortwave incoming radiation	Apogee SP110	0 to 1000	<1%	[W/m^2]
Precipitation (Tipping bucket)	Pessl IM523	0 to 12	± 5 % of measurement	[mm/min]

3.1.2 Automatic Weather Station from AADI (AWSA)

The AWS from AADI measures in the configuration used for this project only temperature and wind (10 min mean wind speed, wind gust, and direction). The Automatic weather station from AADIs (AWSAs) consist of a 2 m mast, a sensor arm, a logger box with a data logger, a battery and a Data Storage Unit (DSU) (Aanderaa Data Instruments AS 2016*b*). The sensor specifications can be found in table 3.2. The wind sensors are measuring the average wind speed and direction in the selected sampling interval (Aanderaa Data Instruments AS 2016*a*,*b*). The maximum wind speed over a two second period during the 10 minute interval is recorded as wind gust. The DSU can store up to 65,000 readings

(Aanderaa Data Instruments AS 2012).

Table 3.2: Sensor specification for the AWSA. Numbers from (Aanderaa Data Instruments AS 2016*a*,*b*,*c*)

Parameter	**Sensor**	**Measurement range**	**Accuracy**	**Unit**
Temperature	3455	-43 to +48	± 0.1 % of range	[°C]
Wind speed	2740	0 to 79	± 2 % or ± 0.2 m/s, whichever is greater	[m/s]
Wind Direction	3590	0 to 360	± 5 °	[°]

3.1.3 EasyLog

The EasyLog data loggers (ELs) used for this project are low-cost temperature loggers of the type EL-USB-1. Information about the loggers can be found in table 3.3. They have a memory capacity of 16,382 samples (DATAQ Instruments 2018). The temperature sensor and logger is located inside a black plastic housing and thus complying with IP67 standard, which means that they are protected against dust and can handle water immersion up to 1 m depth (Resource Supply 2008).

Table 3.3: Sensor specification for the EL-USB-1. Numbers from (DATAQ Instruments 2018)

Parameter	**Measurement range**	**Accuracy**	**Unit**
Temperature	-35 to +80	± 1 °C	[°C]

3.1.4 Air Quality Egg

The AQEs used for this project are low-cost air quality instruments. They are version 2 instruments and one measures Particulate pollution (PP) and the other measures Nitrogen dioxide (NO_2) and Carbon monoxide (CO). They are wireless and can store data while being offline. The data can be transferred via WiFi. The AQE measuring PP detects

particles of size between 0.5 and 10 µm (Wicked Device 2016*b*). Both AQEs also monitor temperature and relative humidity. Information about the AQEs can be seen in table 3.4 for the one measuring PP and in table 3.5 for the one measuring NO_2 and CO.

Table 3.4: Sensor specification for the AQE measuring particulate pollution. n/a*: no accuracy information given by the manufacturer. Numbers from (Wicked Device 2016*b*)

Parameter	**Measurement range**	**Accuracy**	**Unit**
Temperature	0 to +40	0.2	°C
Humidity	0 to 95	1.8	%
Particulate Pollution	0 to 20 000 particles	n/a*	µg/m^3

Table 3.5: Sensor specification for the AQE measuring NO_2 and CO. n/a*: no accuracy information given by the manufacturer. Numbers from (Wicked Device 2016*a*)

Parameter	**Measurement range**	**Accuracy**	**Unit**
Temperature	-20 to +40	0.2	°C
Humidity	0 to 100	1.8	%
NO_2	0 to 20 ppm	n/a*	ppb
CO	0 to 1000	n/a*	ppm

3.1.5 Remote Sensing Temperature Profiler (MTP-5HE)

A ground-based remote sensing temperature profiler, MTP-5HE (MTP), from Attex, was used in this project. It is an angular scanning type microwave radiometer. The instrument scans the irradiation at the sensor head in the 56.7 GHz oxygen absorption channel for different angles between 0 and 90 deg (Wolf-Grosse 2016). The vertical temperature profile up to a height of 1000 m above the instrument is calculate by an internal inversion algorithm.

3.2 Data

In addition to the data from the instruments specifically installed for the the purpose of the campaign, several other data sets have been used, listed in table 3.6. The different datasets were used for variable cases. The data from the measurement stations at Ulriken and Geophysical Institute (GFI) were used throughout the whole year, as additional information for detecting temperature inversions. Due to problems with an already existing AWSA on top of Ulriken, a new AWSI was installed in November 2017. Data from the "Bergen Weather" campaign, measurements from Davis weather stations located at a number of schools in the Bergen area, were used for additional information for the case study in section 5.5, to get information about the spatial variability in the Bergen area. The "Bergen weather" project is a collaboration between the municipality of Bergen and the University of Bergen (Bergensværet 2018). Data from the Norwegian Institute for Air Research (NILU) were used for testing the AQEs. The MTP data were used for a comparison with our in-situ measurements.

Table 3.6: Overview of the dataset used for the campaign

Dataset	Provided by	Description
The Bergen weather project	Bergensværet, by Ole Edvard Grov	Data from Davis weather stations, measured at schools in the Bergen area
Air quality measurements at Danmarksplass	NILU, by Mona Waagsbø	Access to admin.luftkvalitet.info. Hourly mean data from the measuring station at Danmarksplass, owned by Bergen Municipality
AWSI at GFI & AWSA at Ulriken	Accessed via Metdata	Data from the ITAS station located in the garden at GFI
MTP	Tobias Wolf-Grosse	Access to the computer, to download the MTP data

3.3 Data handling

This section describes how the data are handled.

3.3.1 Automatic Weather Station from ITAS (AWSI)

Data from the AWSIs are transmitted via a modem to a computer at GFI once a day. The data are saved and can be accessed online. The modem is turned on automatically at 10.00 UTC every day and runs for 30 minutes. We used this regularly to monitor the battery power.

3.3.2 Automatic Weather Station from AADI

The AWSAs at Skillingsbollen (150 m above sea level (m asl)) and Svingen (250 m asl) only measure temperature. To convert the data from the AWSA to a readable format, we used different constants for the sensors and applied the conversion equation (eq. 3.1 and 3.2). The constants are listed in table 3.7 and 3.8. The transfer was done by connecting the DSU to a data reader, called DSU reader 2995, and we used the program Data Reading Program 5059. Since the DSUs were old, it was important to make sure they were connected to a power source all the time. We may lose the data if the DSU internal battery is empty. Therefore, the DSU was connected to a power source while transported from the measurement location to the computer as well as during the transfer. This causes a large uncertainty in the project, if there were problems with sensors or loggers, we get false data or no data at all. Some of the DSUs were not giving the correct date of the measurements and therefore it was important to write down start/end date and time when we changed the DSUs or restarted the instruments.

For the wind speed sensor 2740 and the wind direction sensor 3590, the calibration equation is:

$$Wind(m/s) = A + BN + CN^2 + DN^3 \tag{3.1}$$

Where N is the raw data reading. The required calibration constants are listed in table 3.7. For the temperature sensor 3455, the calibration equation is:

$$T(^\circ C) = A + BN + CN^2 + DN^3 \tag{3.2}$$

Where N is the raw data reading. The constants are listed in table 3.8

Table 3.7: Conversion constants for wind measurements, applied in equation 3.1.

Constant	Sensor	
	2740	**3590**
	wind speed	**wind direction**
A, C, D	0	0
B	$7.770*10^{-2}$	$3.516*10^{-1}$

Table 3.8: Conversion constants for temperature measurements, applied in equation 3.2.

Constant	Serie		
	462	**469**	**482**
A	$-4.347*10^{-1}$	$-4.347*10^{-1}$	$-4.331*10^{-1}$
B	$8.064*10^{-2}$	$8.140*10^{-2}$	$8.063*10^{-2}$
C	$9.628*10^{-6}$	$9.191*10^{-6}$	$9.996*10^{-6}$
D	0	0	0

3.3.3 EasyLog

For set-up and downloading data we used the EL-WIN-USB Software. Before starting measurements, the name, sample rate, high/low alarm, start date and time have to be set. Since the start date and time were optional it was easier to control the measurements. It also made it easier to install the loggers out in the field the first time, as we did not need to bring a computer to set it up, nor start the measurements before a certain time, to prevent using storage for unnecessary data. When restarting the measurement in the field, we brought a computer, downloaded data at the measuring sites and restarted the measurements.

3.3.4 Air Quality Egg

The data from the AQE were in Parts per billion (ppb), while the data from the reference station were in micrograms per cubic meter ($\mu g/m^3$). Therefore we had to convert the

AQE values into µg/m^3. The calculation was done by the following equation:

$$NO_2[\mu g/m^3] = NO_2[ppb] \cdot \frac{M \cdot T_0}{V_m \cdot T} \tag{3.3}$$

M = 46.0055 [kg/mole], which is the molecular weight of NO_2, T_0 = 273 [K], V_m = 22.41 [dm^3/mole], which is the molar volume and T [K] is the temperature measured by the AQE, converted to absolute temperature [K] (APIS 2017). This equation assumes an atmospheric pressure is 1013.25 hPa. The reason for this assumption is that there are no pressure information at the measuring site.

For the AQE tests in section 5.2 we had to covert the data from AQEs into hourly mean, to be able to compare them to the data from the air quality station at Danmarksplass. The data provided by NILU were divided into hourly mean from e.g. 10.00 to 11.00. To be able to compare them to the data from AQE we sat the value from 10.00 to 11.00 to be the value at 10.00. The same was done for the data from the AQEs, the measurements from 10.00 to 11.00 was converted into a hourly mean at 10.00. The reason for doing this was to make sure the values are comparable.

4 Campaign overview

In this chapter I describe the campaign.

4.1 Bergen

Figure 4.1: Map of the Bergen Valley.

The campaign took place in the Bergen Valley from February 2017 to February 2018. Bergen (60.4°N, 5.3°E) is the second largest city in Norway, located at the western coast. The city is located in a narrow valley with complex terrain. An overview of the Bergen Valley and its topography is given in figure 4.1. There are approximately 280,000 inhabitants in the Bergen municipality (SSB 2018). The area around Danmarksplass is the densest populated area, where more than 40,000 people live (SSB 2017). The valley is curved and mostly oriented in a southeast - northwest direction, from the Bergen Fjord at the northwest end and Nordåsvannet at the south end. The valley is approximately 10 km long and is at its minimum 1 km wide.

There are six mountains surrounding the Bergen Valley. These are divided into two mountain massifs, Fløyen (400 m above sea level (m asl)), Ulriken (643 m asl) and Sandviksfjellet (417 m asl) to the east, and Løvstakken (477 m asl), Damsgårdsfjellet (317 m asl) and Lyderhorn (396 m asl) to the west

(Bergen Municipality 2017*a*). The mountains act like a shelter, that protects the city from storms, but also favors temperature inversions to occur (Jonassen et al. 2013, Wolf et al. 2014). Due to its topography and latitude, there are just a few hours of daylight in the Bergen Valley during the winter. On the shortest day, there are less than two hours of sun at Geophysical Institute (GFI), because of the surrounding mountains.

The climate is maritime and winters are normally mild and wet, causing a well-mixed layer over the city. The mild and wet climate is caused by the warm Norwegian Current and south westerly winds transporting warm and moist air towards western Scandinavia. These warm and moist winters are interrupted repeatedly by cold and dry periods leading to an increased occurrence of temperature inversions and connected air pollution episodes. The types of temperature inversions are described in section 2.4. Temperature inversions can cause long lasting problems with polluted air in the valley, and strong nocturnal temperature inversions can form. Sometimes these do not break up during the day and a re-stratification by long wave radiative cooling of the ground takes over, leading to temperature inversions that can persist over days at a time.

4.2 Location

The reason for choosing Løvstakken as the measuring site is because Løvstakken is located close to the city center and Danmarksplass, where we find high pollutant concentrations. It is favorable to have meteorological stations close to Danmarksplass, because here we find one of the busiest traffic junctions in the city, in addition to an air quality measurement station, owned by the Bergen municipality. Since the stations are located close to GFI, where the MTP-5HE (MTP) is located, we get a better basis for comparison when comparing the MTP measurements and the in-situ measurements along the Løvstakken transect. A map of the Løvstakken transect with the stations marked, is shown in figure 4.2

An overview of the weather stations and instruments used for the campaign can be seen in table 4.1. Pictures of the individual stations and measurement sites are presented in figure 4.3. The stations are placed in a dense network to get detailed information, especially of the vertical temperature profile. From December 2017, there were temperature measurements every 25 m, from 75-250 m asl. Based on the study by Wolf et al. (2014) the stations are located in a denser network around 75-250 m asl, because most of the

Figure 4.2: Map of the Bergen Valley with station marked. The blue marks are the Automatic Weather Stations and the red marks are the EasyLogs. Map from Google Maps.

inversions are expected here. Since the Automatic weather station from ITAS (AWSI) and Automatic weather station from AADI (AWSA) are placed every 50 m, except for the one AWSI at 225 m asl, we find it not to be a problem that the EasyLog data loggers (ELs) are only measuring for a shorter time period. The ELs are included as additional information.

For the AWSI, the original plan was to install them at 100 m asl, 200 m asl and 300 m asl. Because of challenges in topography the 200 m asl station was located at 225 m asl. Since there were less trees around the station at 225 m asl, it was more suitable for measurements, to get more undisturbed information about the circulation in the valley.

In addition to the 50 m interval covered by the Automatic weather stations (AWSs), an AWSA located at Løvstakken (450 m asl) was used. It was included to give information about temperature inversions above 300 m asl and the wind conditions for the circulation in the valley. Also, when comparing the temperature from in-situ measurements and the MTP, it is favorable to have measurements between the AWS at 300 m asl and the one at Ulriken (605 m asl).

(a) Ulriken

(b) Løvstakken

(c) Strandafjellet

(d) Svingen

(e) Gapahuken

(f) Skillingsbollen

(g) EL2

(h) Solheimslien

(i) GFI

(j) Air Quality Eggs

(k) GFI rooftop

Figure 4.3: Overview of the instruments used in the campaign (a) AWSI at Ulriken (605 m asl) (b) AWSA at Løvstakken (450 m asl) (c) AWSI at Strandafjellet (300 m asl) (d) AWSA at Svingen (250 m asl) (e) AWSI at Gapahuken (225 m asl) (f) AWSA at Skillingsbollen (150 m asl) (g) EasyLog (125 m asl) (h) AWSI at Solheimslien (100 m asl) (i) GFI (12 m asl) (j) Air Quality Egg (k) MTP-5HE located at the rooftop of GFI (45 m asl)

Table 4.1: Overview of stations used in the campaign

Station number	**Station name**	**Altitude [m asl]**	**Altitude [m agl]**	**Latitude °N**	**Longitude °E**	**Description**	**Logging interval**
S1	Løvstakken	450	2.1	60.362	5.320	AWSA	10 min
S2	Strandafjellet	300	2.0 and 3.2	60.372	5.323	AWSI	1 min
S3	Svingen	275	1.8	60.370	5.326	AWSA	10 min
S4	Gapahuken	225	2.0 and 3.2	60.371	5.327	AWSI	1 min
S5	Skillingsbollen	150	2.1	60.374	5.325	AWSA	10 min
S6	Solheimslien	100	2.0 and 3.2	60.376	5.325	AWSI	1 min
S7	GFI	12	2.0 and 3.2	60.383	5.333	AWSI	1 min
S8	Ulriken1	605	4.0	60.377	5.382	AWSA	10 min
S9	Ulriken2	605	2.0	60.377	5.382	AWSI	1 min
S10	Løvstien	75	1.8	60.376	5.328	EasyLog	10 min
S11	EL2	125	2.1	60.375	5.327	EasyLog	10 min
S12	EL3	175	1.9	60.373	5.327	EasyLog	10 min
S13	EL9	200	1.8	60.373	5.326	EasyLog	10 min
S14	Gapahuken2	225	1.6	60.371	5.327	EasyLog	10 min
S15	GFI2	45	0	60.384	5.332	MTP-5HE	5 min
S16	Danmarksplass	20		60.374	5.340	Air Quality Eggs	1 min

4.3 Campaign

The aim of the campaign was to assess how the temperature inversions are distributed throughout the year, in height and duration. As well as comparing the MTP with the in-situ measurements along the Løvstakken transect. A previous study by Wolf-Grosse (2016) shows how the temperature inversions are distributed in height, using the MTP, and in this campaign we wanted to see how in-situ measurements compare to these results. In addition, we wanted to test two low-cost air quality instruments produced by Wicked Device.

For the measurements from February to September 2017, seven ELs were installed at different locations. Four of them were located at the same location as another station, either AWSI or AWSA. This was done to check the quality of the measurements by EL.

During the first months one went missing and one was destroyed, leaving five loggers left. The loggers were covered with a yoghurt box, to protect them from precipitation and solar radiation. Because the loggers needed ventilation it was important that the loggers were not covered too much, as the air can be trapped and give false data. In September 2017 the loggers were taken down and the measurements analyzed. Based on the result the loggers went trough two tests to check whether the loggers measured the same temperature at the same location. The tests are described in section 5.1.

Based on the test results, data from the ELs were only used from December 2017 and onward. The locations for the ELs are listed in table 4.1. To make sure the loggers measured the correct temperature, we installed one of the sensors at the same location as the AWSI, at 225 m asl. By doing this we could correct the other loggers by the difference between the EL at 225 m asl and the reference AWSI. This may lead to errors, as the loggers were placed at different locations and under different conditions. The advantage of a dense network of temperature measurements is that we can check whether the ELs are giving realistic values.

Since Aanderaa no longer produces weather stations, the sensors, Data Storage Units (DSUs) and the software are outdated. We had problems with the wind sensors, as one slowed down and the other speeded up. Due to this problem, which was discovered early fall 2017, we had to change both the wind speed and direction sensors at the top of Løvstakken. Another problem we had during the winter 2017/18 was that the sensors froze during the cold and humid weather. The problem was discovered 1st of February 2018 and due to this problem the wind measurements cannot be fully trusted, especially during periods of temperatures below 0 °C.

5 Results

In this chapter I present the result of the study. I start with the results of the tests of low-cost EasyLogs in section 5.1 and the results of the tests of low-cost air quality measuring instruments (Air Quality Eggs) in section 5.2. In section 5.3 I will summarize the meteorological measurements from the 13 months of deployment, before focussing on a statistical analysis of temperature inversions, in section 5.4. Finally, I will present a case study on an inversion caused by warm air advection in section 5.5.

5.1 Test of EasyLogs

As mentioned in chapter 4 the EasyLog data loggers (ELs) went through two tests in order to check their performance in the field. Because of the limited resolution, of 0.5 °C, and an accuracy of 1 °C, the data loggers should not be trusted equally to the other temperature sensors used in the campaign, e.g the temperature sensor on Automatic weather station from ITAS (AWSI) (DATAQ Instrument 2018). In addition they have no appropriate radiation shield and are therefore prone to overheating when exposed to solar radiation, e.g. shown in a study by Nordhagen (2014). Based on this, and the results from the first months of measurements for this thesis, the loggers were tested against each other and the AWSI in the observational garden at Geophysical Institute (GFI).

The first test lasted for 12 days (25.10-06.11.17), where the loggers were put in a box and placed close to the radiation shield of an already installed AWSI (figure 5.1(a)). The temperature measured by the AWSI were used as reference. The box had semi-transparent walls with small holes for ventilation and an opaque lid. The reason to test this setup was that we wanted to install the ELs out in the field at least with a basic radiation protection. Since the radiation shields available at GFI were too small for the loggers we needed to find another cover and wanted to test the box as a low-cost solution.

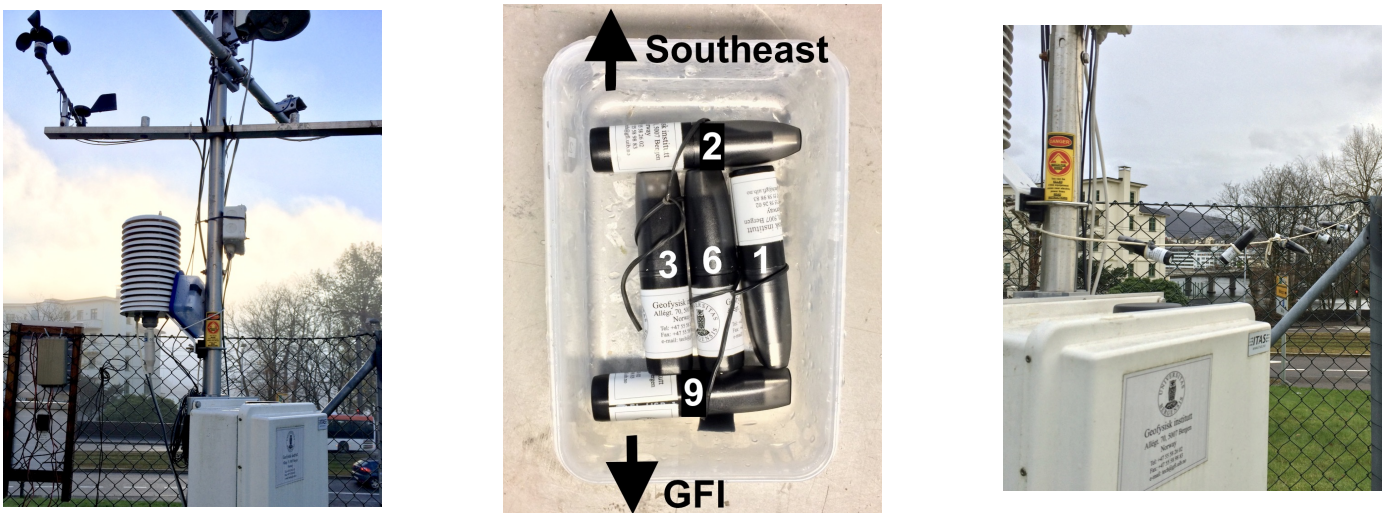

(a) (b) (c)

Figure 5.1: Setup for the EL tests in the observational garden at GFI. a) Mounting of the plastic box with the 5 EL sensors inside close to the radiation shield of the AWSI during test 1. b) Detailed view of the location of the EL sensors inside the box. c) Unprotected mounting of the EL sensors on a rope during test 2.

The result of test 1 is shown in figure 5.2(a). It shows large temperature variations both between the ELs themselves and especially in comparison to the reference station. As expected, the variations were largest during the day with exposure to solar radiation and smaller during the night. Since the instruments were installed in a box, with semi-transparent walls, as seen in figure 5.1(b), the loggers were clearly affected by solar radiation. The box was located close to the reference temperature sensor, as seen in figure 5.1(a), with one side pointing towards south. This was most likely the reason for the large variation between the loggers, as one logger was in direct sunlight, while the others experienced partial or full shadow. The box might also not be ventilated enough, as there were only small holes in it. EL2 showed the highest temperature and this was the logger that was located at the side of the box facing the sun (figure 5.1(b)).

Another advantage of comparing the ELs to an AWSI was that the reference station also measured incoming solar radiation. We could therefore remove measurements that were taken during times, when the solar radiation exceeded a certain threshold. This allowed us to test our hypothesis that the ELs are highly sensitive to solar radiation. The results after the removal of all cases with more than 20 W/m^2 are shown in figure 5.2(b). The

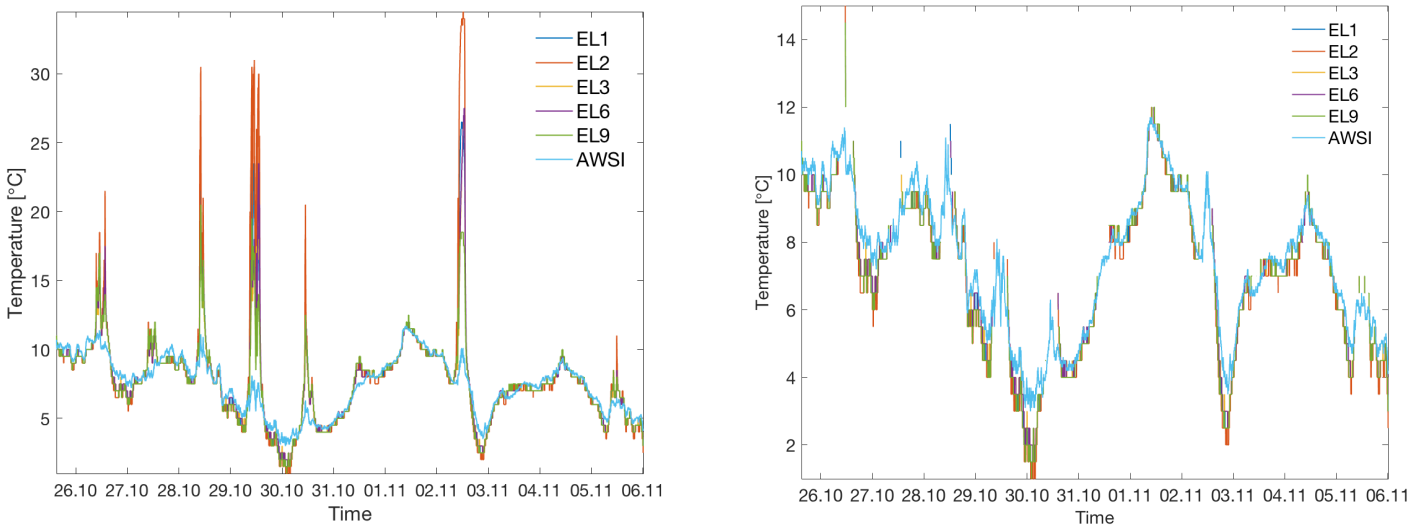

(a) (b)

Figure 5.2: Temperature series of the first test in the observational garden at GFI. a) shows the raw data and b) the filtered data, where measurements when the solar radiation measured at the AWSI exceed 20 W/m^2 are removed.

result showed great improvements. Even after applying the filter there were situations with large differences between the loggers and the reference station, especially on 26.10.17. In figure 5.4, information about global radiation can be seen. When looking at the situation on 26.10.17 we can see that the sky was partly cloud covered that day in the time period when the temperature measured by ELs were higher than the reference temperature. A possible explanation for this was that a cloud covered the sun, resulting in a measured radiation below the threshold. Therefore the temperature measured by the ELs were not removed. However, as a result of build-up and storage of heat due to limited ventilation of the box, the temperature loggers in the box measured higher temperatures than the reference station. The loggers are black and this can also have affected the temperature measurements.

The result also showed that during the night the ELs measured temperatures of up to 2 °C lower than the reference station. Apparently, the box and/or the loggers were subject to longwave radiative cooling, leading to reduced temperatures compared to the ventilated AWSI sensor. During the day the loggers will be heated by solar radiation and during the

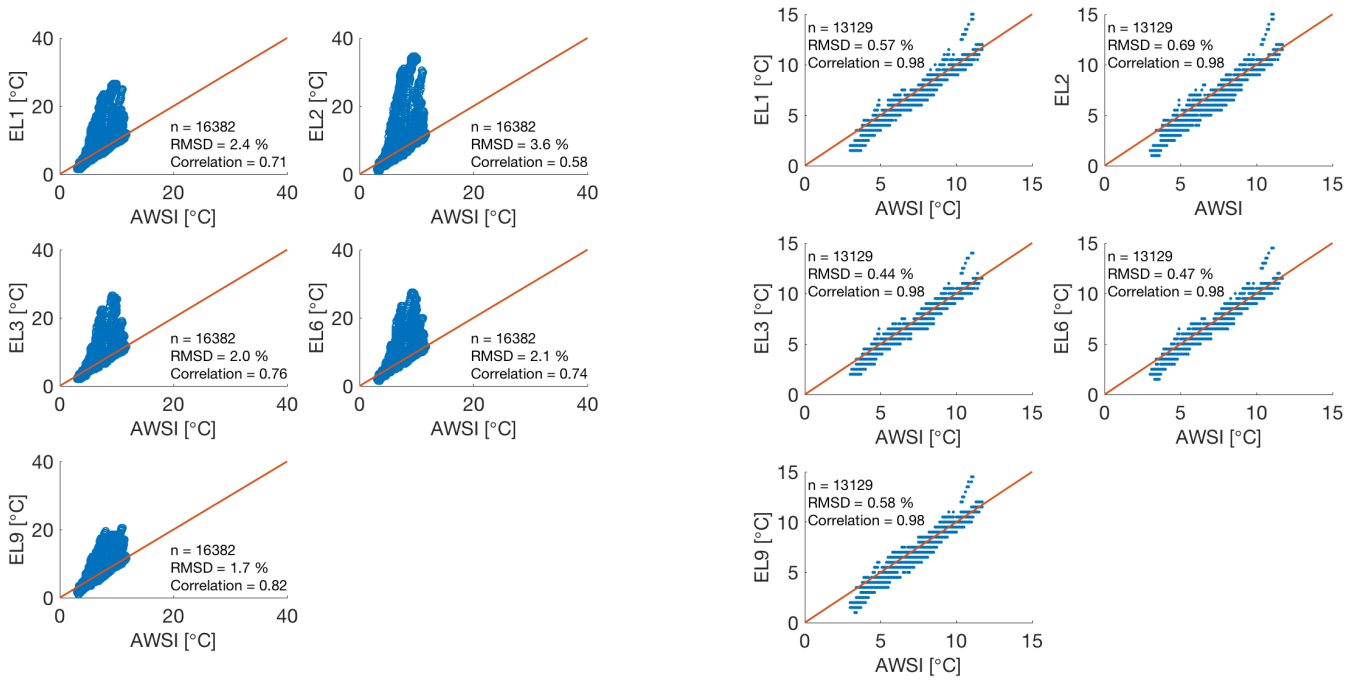

Figure 5.3: Scatter plot of the first test in observational the garden at GFI. a) shows the raw data and b) the filtered data, where measurements when the solar radiation measured at the AWSI exceed 20 W/m^2 are removed.

night they can be cooled. A slowness in the box system resulted in false measurements at the given time. This was likely to be a calibration error.

Figure 5.3 shows scatter plots of the ELs compared to the AWSI, both for the raw data and the filtered data. It was clear that the filtering improved the results considerably. The Root Mean Square Deviation (RMSD) decreased from values between 1.7 and 3.6 % to values between 0.44 to 0.69 %. After being filtered, the ELs had a correlation of 0.98, compared to the correlations in the range of 0.58 to 0.82 before applying the filter. Some issues remain, in particular with too low night temperatures measured by the ELs. Test 1 revealed clear disadvantages of placing the ELs inside a box, both with respect to overheating by solar radiation during daytime and by excess longwave cooling during nighttime. Therefore, a second test was conducted with uncovered ELs at the same location

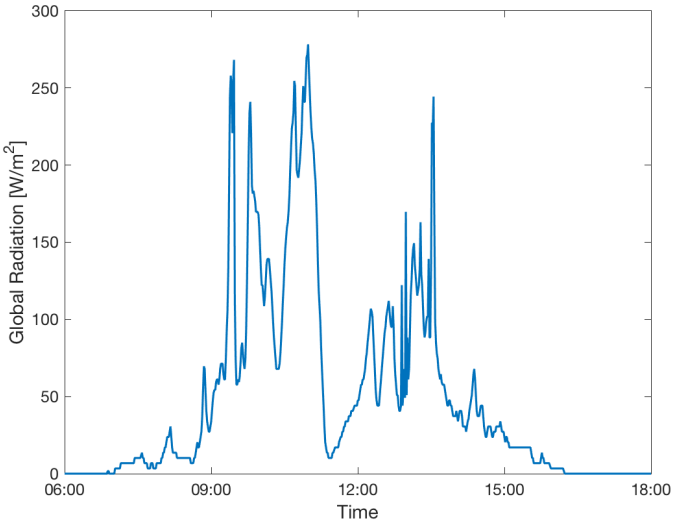

Figure 5.4: Measured global radiation by AWSI on 26.10.17

in the period from November 17 to 23, 2017.

In the second test, the loggers were attached to a rope, hanging between the reference AWSI and the fence, as shown in figure 5.1(c). The main goal of this second test was to check whether the loggers could be used without additional shielding, at least during the hours of no or weak solar radiation. The result of the test is shown in figure 5.5. It confirmed the outcome of the first test, with an overestimation of temperatures when exposed to direct sunlight. The corresponding scatter plots are presented in figure 5.6, where 5.6(a) is the raw data and 5.6(b) is the filtered data. The result was similar to the result of the first test. For the raw data, the problem was mainly too high temperatures, while for the filtered data the ELs were generally measuring too low temperatures. Overall, there was a negative bias most of the time and short bursts of a positive bias seem to be more indicative of a calibration error. Due to the spikes, the mean of the sensors was set too low in order to have a low mean error. Because of the low resolution and accuracy of the loggers, the filtered result was acceptable, as there were only a few degrees difference. The most important result was that they have a high correlation or follow a regression line with slope 1. This was the case, the ELs had high correlations, of 0.98, after applying the filter.

The filtering was an efficient way to get rid of the positive spikes, but it did not affect the negative spikes, as seen in figure 5.5. A slight systematic underestimation was

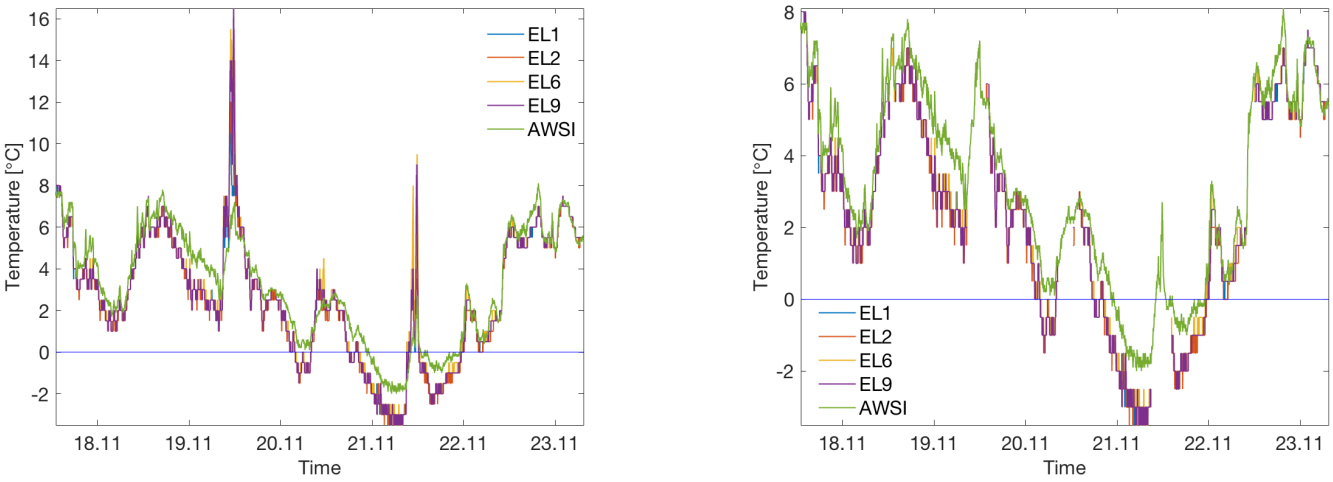

(a) (b)

Figure 5.5: Temperature series of the second test in the observational garden at GFI. a) shows the raw data and b) the filtered data, where measurements when the solar radiation measured at the AWSI exceed 20 W/m^2 are removed.

remaining after being filtered, which can indicate a potential calibration error. Since the underestimation was largest during nighttime in both tests it was likely that the instruments themselves were the problem and not the box. This can be an indication of an error due to longwave radiative cooling of the ELs housing and sensor. Since the ELs were overall measuring the same absolute temperature, the gradient measured by the ELs can be used in the field for further analysis.

There was a risk for the sensors to be covered with a thin layer of ice, leading to false temperature measurements. Therefore it was an advantage that during the second test period the temperatures were below 0 °C for some of the measurements. This we could see whether larger differences between the loggers and the reference existed when the temperature was below 0 °C. The test showed that the loggers were measuring a lower temperature when the temperature was below 0 °C, but we can not conclude that the difference was due to ice on the loggers.

As a result of the two tests, we decided that the loggers should be uncovered for further analysis, as we did not have a proper cover. In addition, we filtered the data by removing the measurements when global radiation was above 20 W/m^2. The Bergen Valley only

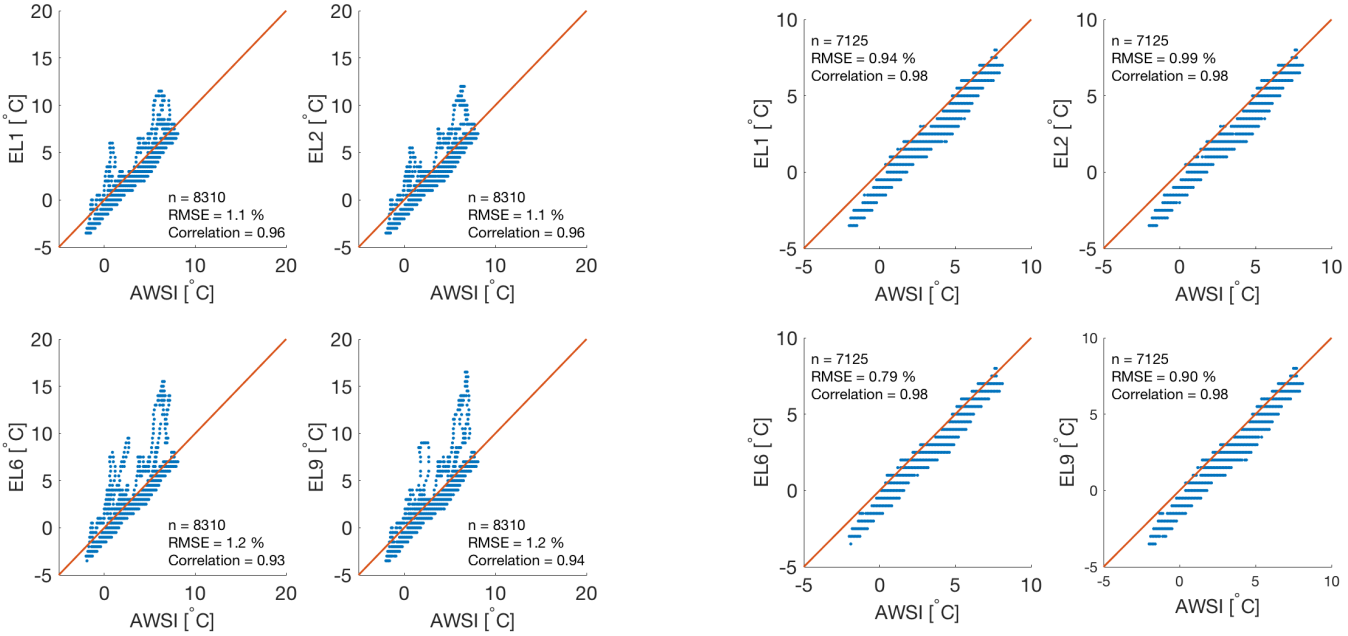

Figure 5.6: Scatter plot of the second test in the observational garden at GFI. a) shows the raw data and b) the filtered data, where measurements when the solar radiation measured at the AWSI exceed 20 W/m^2 are removed.

has a few hours of sunlight during the winter, leaving us with several hours of useable measurements after applying the filter. It was a disadvantage that the loggers are black, because they get heated by the sunlight. For further use, it should be considered testing the loggers when they are painted white.

After the second test, the ELs were installed in the field, at five different locations, listed in table 4.1. To make sure the loggers measured the correct temperature, we installed one of the loggers close to the temperature sensor on the AWSI, at 225 m above sea level (m asl). This made it possible to correct the other loggers by the difference between the EL at 225 m asl and the reference, AWSI. The ELs were also filtered by removing the measurements where the AWSI at Gapahuken measured radiation above 20 W/m^2.

5.2 Test of Air Quality Eggs

In autumn 2017 two Air Quality Eggs (AQEs) were purchased for this campaign, one measuring Nitrogen dioxide (NO_2) and Carbon monoxide (CO), and one measuring Particulate pollution (PP). In addition, both measure temperature and relative humidity. Initially the AQEs were meant to measure the air quality at different altitudes in the Bergen Valley during inversion periods, to get more information about the distribution of pollutants in the valley. Since we did not have any experience with the eggs, we wanted to test their performance before using them for field measurements. The eggs went through three tests. For the first two, the instruments were tested against the air quality measuring station, located at Danmarksplass, owned by the Bergen municipality (figure 5.7(a)). We used data provided by Norwegian Institute for Air Research (NILU), from the station at Danmarksplass. No temperature or relative humidity measurements exist at that site, therefore the temperature and relative humidity measured by AQEs during these tests were compared to the ones measured by AWSI in the observational garden at GFI. For the temperature comparison it has to be kept in mind that both stations are located ca. 1 km apart from each other. The third test has been performed in the observational garden of MET at GFI, to test the AQEs temperature measurements in more detail against an AWSI.

(a)

(b)

(c)

(d)

Figure 5.7: Setup for the tests at Danmarksplass. a) Overview of the measurement site. b) Setup for the first test. c) Cover for the second test. d) Setup of the third test.

We experienced some problems with the eggs, the offline logging did not work, because

of issues with the program software. The problem were fixed by the supplier of the instruments, Wicked Device. It also turned out that the GPS and altitude indications were not working properly. After resolving the technical issues described before, the two tests of the AQEs were done in mid January and the beginning of February. In addition, a third test took place in April 2018, to test the temperature measurements against an AWSI in the observational garden at GFI.

The AQEs are temperature dependent and are in general rather limited with respect to the environmental conditions they can be operated in. They should not be exposed to unusual cold (0 °C for the PP sensor and -20 °C for the CO/NO_2 sensor) or heat (+40 °C for both AQEs, as well as they should not be placed in direct sunlight, because it can destroy the instruments (Wicked Device 2016*a*). The instruments should in addition not be exposed to precipitation, which is a challenge in Bergen. They can therefore not be used without proper protection. For our tests, two types of covers were used, as seen in figure 5.7(b)-(c). Since it is a lot of precipitation in Bergen it was problematic to find an appropriate period without rain. Initially, the second test was intended to last longer, but because of heavy rainfall forecasted, the eggs had to be taken down.

The first test lasted for approximately 34 hours, from 11.01.18 at 10.00 to 12.01.18 at 19.55. During the first test the minimum temperatures were outside the operational range of the AQE for PP, we therefore could only test the AQE measuring NO_2 and CO. Because the instrument needed some time to adjust, we only used data from 11.01.18 at 12.00 to 12.01.17 at 18.00. The setup for the first test can be seen in figure 5.7(b). For the test, an external USB power bank was used as power supply, limiting the duration of the test.

The result of the first test can be seen in figure 5.8. It is only the NO_2 that is included here because the Bergen municipality reference station (BK) does not measures CO. The curve from the AQE was following the curve from the reference station, but there was a substantial offset between the two curves. The BK was at the most 76 µg/m^3 higher than the NO_2 value measured by the AQE. At its minimum, the reference was more than 5 µg/m^3 higher than the AQE. The mean of the reference station (76.6 µg/m^3) was more than twice the amount of NO_2 measured by the AQE (34.4 µg/m^3). The two temperature curves are following the same path, but the temperature measured by AQE was between 1 and 4.8 °C higher than the temperature measured by the AWSI. The same we see for the relative humidity, which was expected, because when temperature increases the relative humidity decreases. The relative humidity measured by the AQE is between 6 and 21.7 %

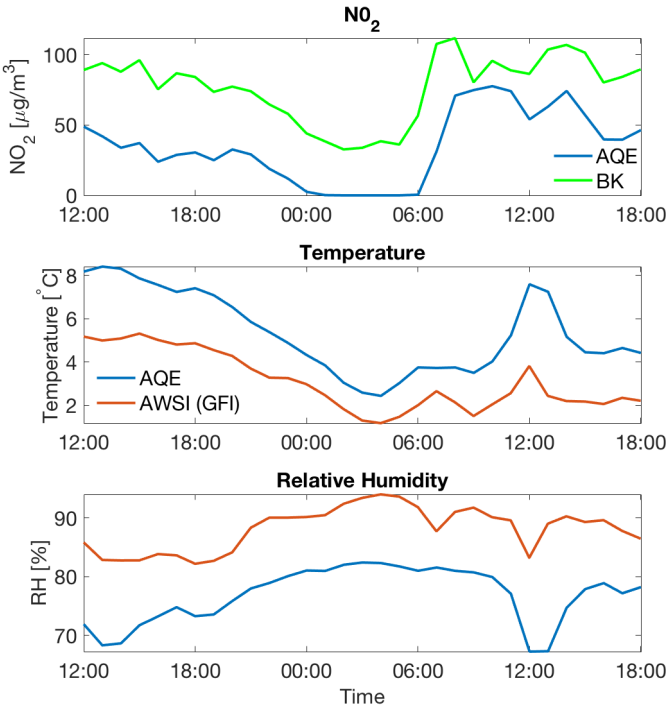

Figure 5.8: Time series for the first Air Quality Egg test. The (upper panel) shows the No_2 concentrations measured by the AQE and the reference station (BK), (second panel) the temperature measured by AQE and the AWSI in the observational garden at GFI, (third panel) the relative humidity measured by AQE and AWSI.

lower than the relative humidity measured by the AWSI.

Figure 5.9 shows the corresponding scatter plots for both NO_2 and temperature. In figure 5.9(a) temperature is included as color coded background information and in figure 5.9(b) relative humidity is included as color coded background information. Figure 5.9(c) shows the scatter plot for temperature measurements, where the AWSI in the observational garden at GFI was used. The scatter plots visualize the results of the time series and confirmed that the AQE was underestimating the NO_2 concentration. As seen in the two first figures, there was no systematic dependency on temperature and humidity visible in the scatter of the data. For the NO_2 measurements the RMSD was 44.2 % and the correlation is 0.85. The temperature measured by the AQE was too high and had a RMSD of 2.4 % and a correlation of 0.92. The temperature increased around midday which was due to solar radiation. We corrected the temperature measured by the AQE with a constant

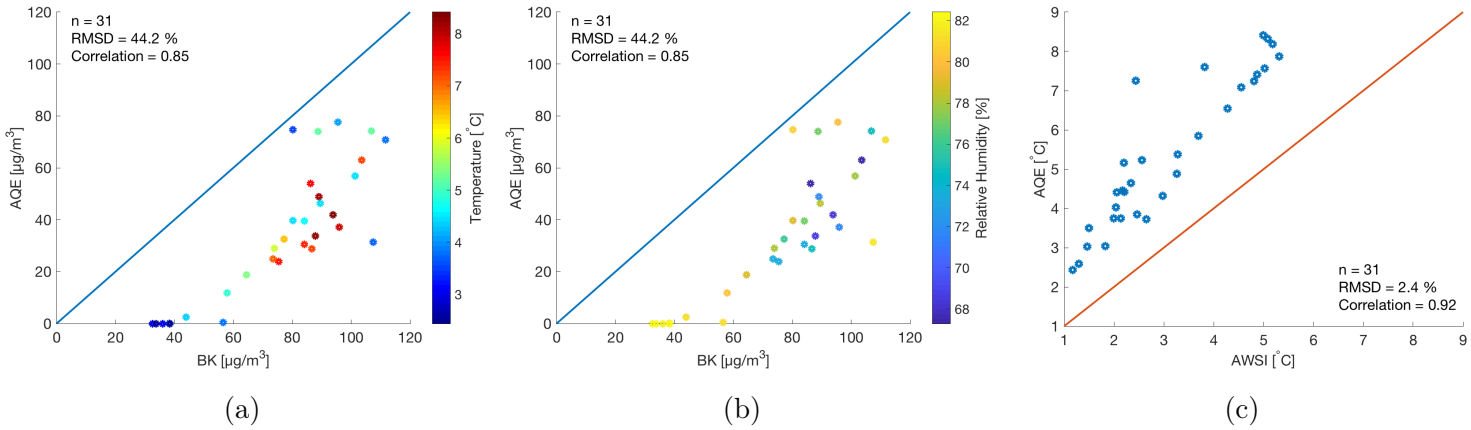

(a) (b) (c)

Figure 5.9: Scatter plots of the first test. a) shows NO_2 with color coded temperature information, b) NO_2 with color coded relative humidity information and c) temperature

offset of 2.3 °C. This was calculated by taking the mean of temperature measured with the AQE and subtracted it from the mean of the AWSI. The RMSD then decreased to a value of 0.81 %.

A possible explanation then for the large differences in temperature between the AQE and the reference stations might be the use of protection for the AQE. Although, the cover was ventilated from below the instrument this ventilation might not have been efficient enough. A corresponding build-up and storage of heat could have caused an increase in temperature for the AQE. The NO_2 measurements are dependent on the temperature and the instrument should not be exposed to direct sunlight, which it was. The cover should have been painted, to reduce the exposure of solar radiation. Another possible explanation for the observed differences was the location of the instrument approximately 30 to 40 cm above the ground. It should have been located further up, but due to limited available options at the measurement site and since it was installed at one of the instruments measuring PP owned by the Bergen municipality, we could not have installed the AQE higher on the mast in order to prevent potential effects on the official PP measurements.

To make sure that the results of the first test were representative, we did a new test, lasting for almost a week, from February 1st to 7th, 2018, at the same location. For this test we used a 220 V power supply that made it possible to test the AQEs for a longer period. Both AQEs were used in this test. In addition to check whether the performance of the AQE measuring NO_2 was similar to the result of the first test, we wanted to test

how the AQE measuring PP reacted to low temperatures, especially temperatures below 0 °C, as the operational range is from 0 to 40 °C. Pictures from the setup of this test are not available, due to limited time available at the measurement site. Figure 5.7(c) shows the protective covers used for this test.

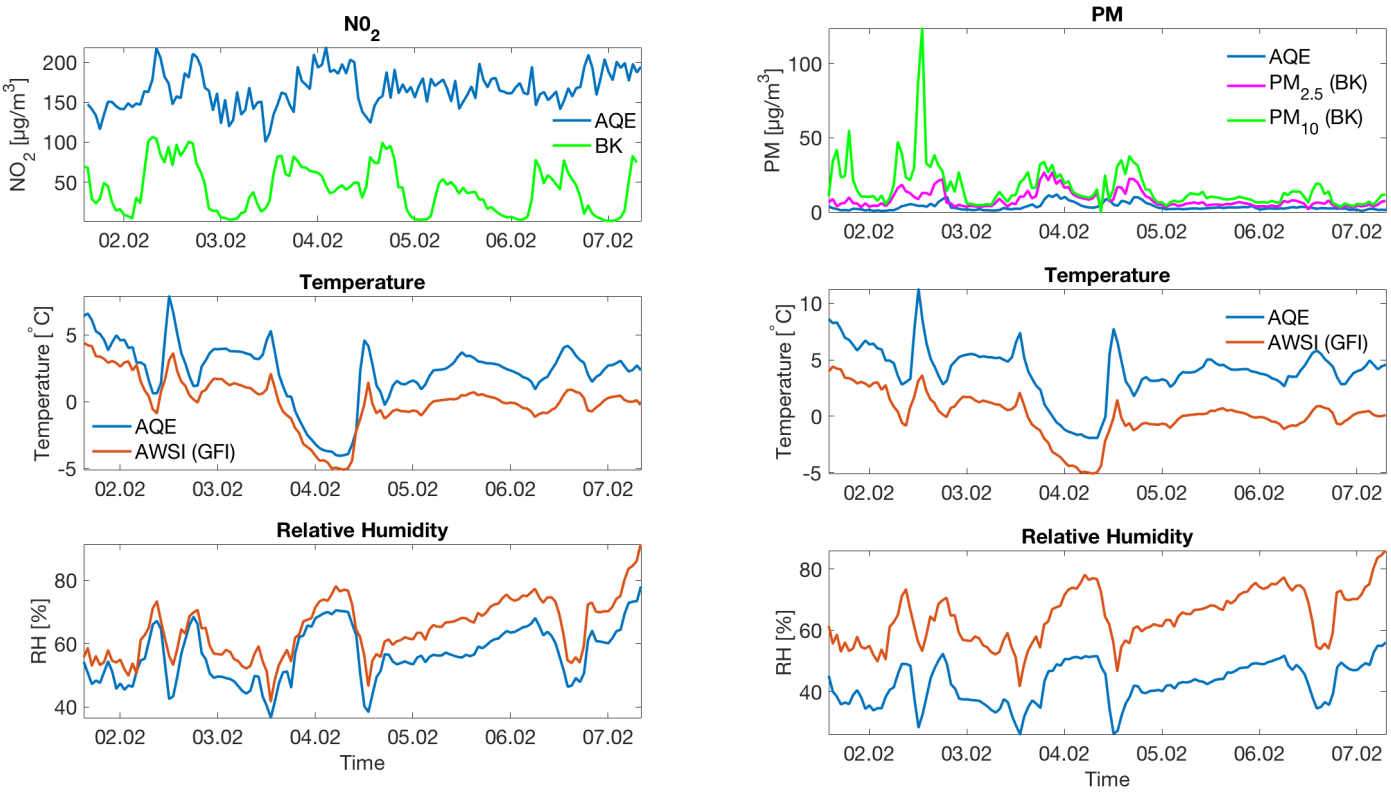

(a) (b)

Figure 5.10: Time series for the second Air Quality Egg test. (a) shows the measurements by the AQE measuring NO_2, where the (upper panel) shows the NO_2 concentrations measured by the AQE and the reference station (BK). (b) shows the measurements by the AQE measuring particulate pollution. For both, (second panel) the temperature measured by AQE and the AWSI in the observational garden at GFI, (third panel) the relative humidity measured by AQE and AWSI.

The result from the second test can be seen in figure 5.10. Figure 5.10(a) shows the result for the AQE measuring NO_2. In the beginning, the NO_2 was somehow following the curve of the reference station, but from 03.02.18 and onward there were large differ-

ences. The AQE is temperature dependent and it seems to be a huge problem when the temperature decreased around 04.02.18. With this temperature decrease, the NO_2 was increasing, while the NO_2 measured by the reference station was decreasing. Compared to the first test, this result shows the opposite, as the BK measures lower concentrations of NO_2 than the AQE. The measured NO_2 by AQE was at the most 199 µg/m^3 higher than the NO_2 concentration measured by BK. At its minimum, the AQE was more than 50 µg/m^3 higher than the reference. The mean of the AQE measurements are four times the mean of the reference. The temperature and relative humidity follow the path of the AWSI. The temperature difference was up to 4.8 °C and the relative humidity difference was up to 16 %.

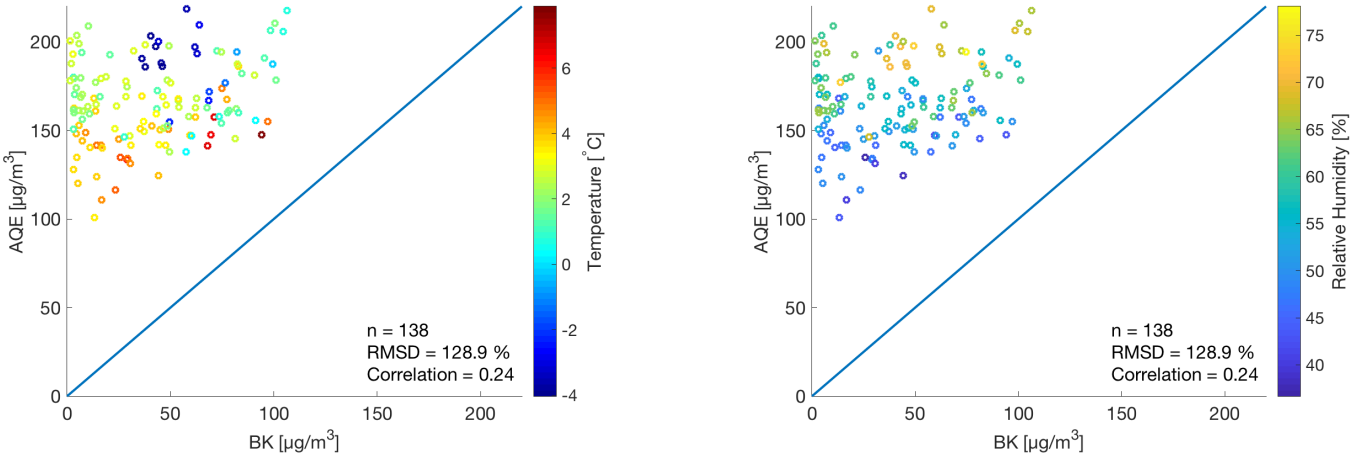

(a) (b)

Figure 5.11: Scatter plot of the second test, where a) shows the scatter plot of NO_2 with temperature background information and b) the NO_2 with relative humidity background information.

Figure 5.10(b) shows the result for the AQE measuring PP. The reference station measures PM_{10} and $PM_{2.5}$ separately, while the AQE is also supposed to measure PM_{10}. As seen in the figure, the measurements by BK were in general much higher than the ones measured by the AQE. The measured PM_{10} by BK was at the most 119 µg/m^3 higher than the PP concentration measured by the AQE. The mean of the BK measurements were almost five times the mean of the AQE. The temperature and relative humidity followed the path of the curve of the reference (AWSI) but the differences were larger than for the AQE measuring NO_2. The temperature difference was between 2.2 and 8.2 °C and the

relative humidity difference was between 12.3 and 30.1 %. The peak of measured PM_{10} by BK was because of high particle concentrations in the mid range from 2.5 to 10 µm and do not include particles below 2.5 µm. A possible explanation of the peak is that the ground is dry and particulate matter from the road is transported into the air by strong winds and turbulence close to the ground.

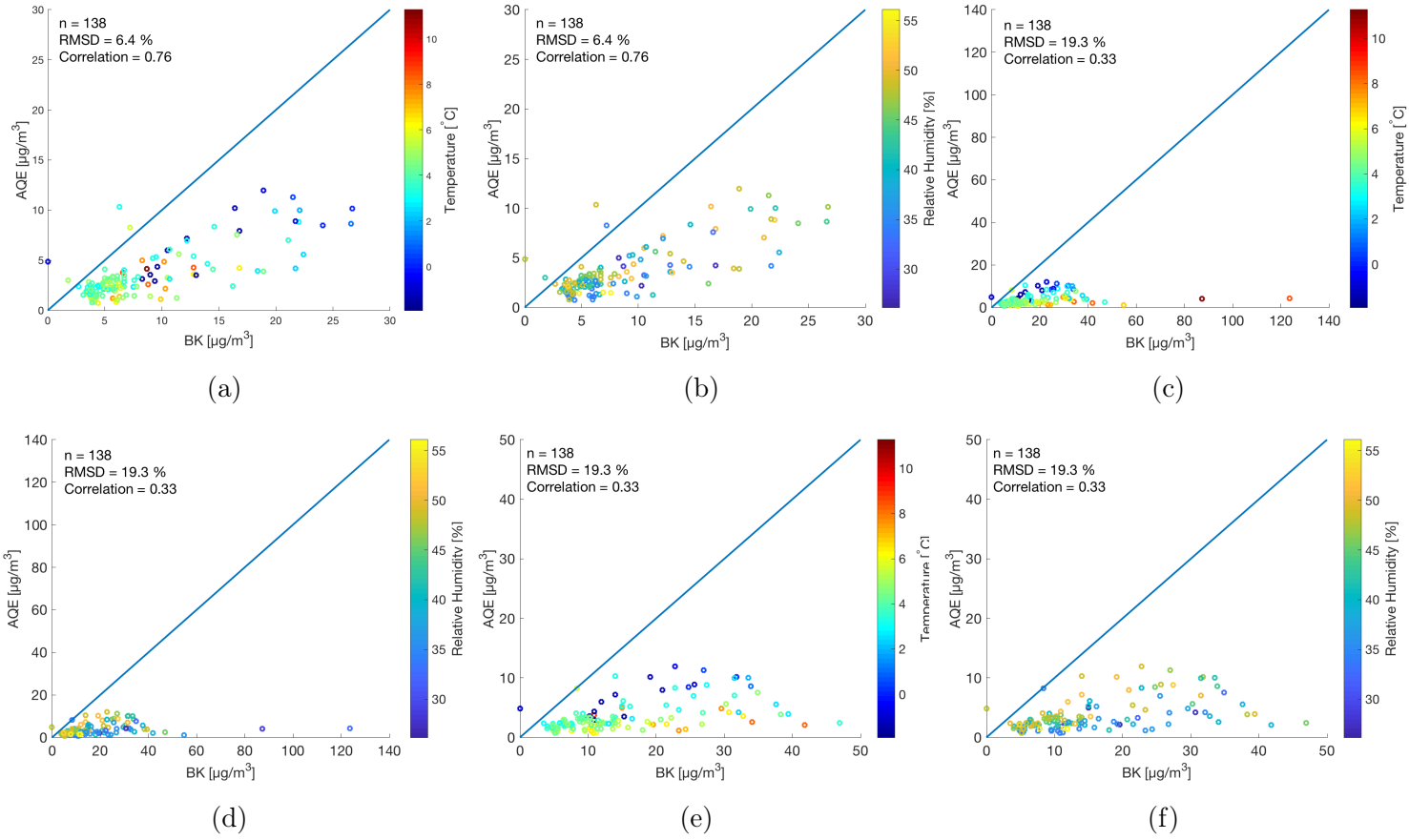

Figure 5.12: Scatter plot of the second test, where particulate pollution measured by the AQE is compared to $PM_{2.5}$ and PM_{10} by BK. a) shows the scatter plot of $PM_{2.5}$ with temperature background information, b) the $PM_{2.5}$ with relative humidity background information, c) the PM_{10} with temperature background information, d) the PM_{10} with relative humidity background information, and e)-f) shows the same as c)-d) with a smaller interval.

Figure 5.11 shows the corresponding scatter plots for NO_2 with temperature (figure 5.11(a)) and relative humidity (figure 5.11(b)) as color coded background information. The AQE was largely overestimating NO_2 with a RMSD of 128.9 % and a weak correlation

of 0.24. The highest temperatures are closest to the regression line with slope 1. The coldest temperatures are gathered in a cluster. The coldest temperatures appeared on the 4th of February, as seen in figure 5.10(a). It was easier to see a cluster of temperatures when looking at the relative humidity in figure 5.11(b). The lowest relative humidities are closest to the regression line and as the distance from the line increases, the value of relative humidity increases.

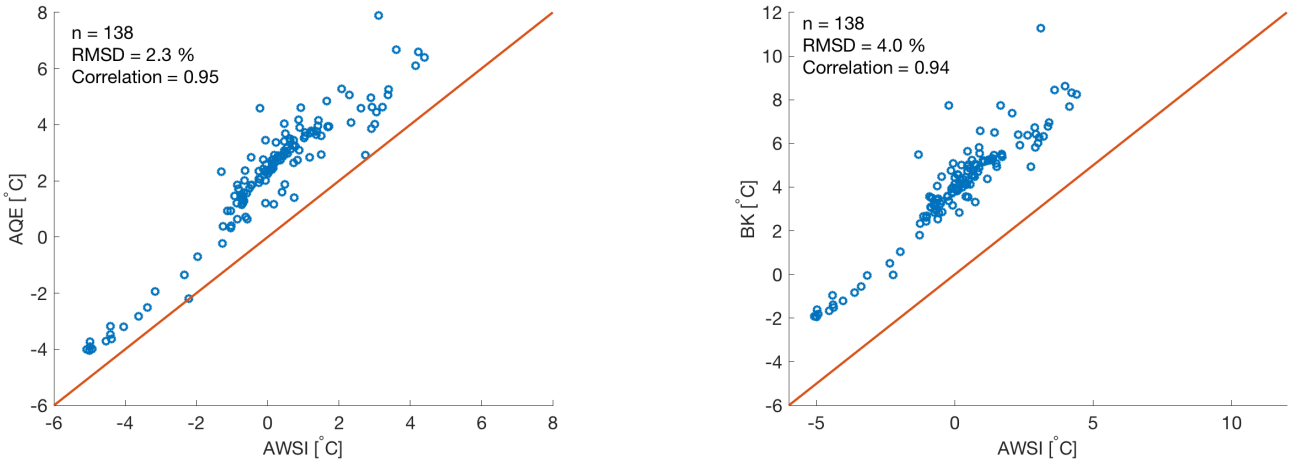

(a) (b)

Figure 5.13: Scatter plots of the second test, where temperature measurements by AWSI are compared to the AQEs measuring NO_2 and particulate pollution. a) shows the temperature comparison to the AQE measuring NO_2 and b) the temperature comparison to the AQE measuring particulate pollution.

Scatter plots of the PP is presented in figure 5.12. Since the reference station at Danmarksplass measures PP of two different sizes, $PM_{2.5}$ and PM_{10}, the PP measured by AQE is compared to both. Even if the PP measured by the AQE detect particles of a dynamical size less than 10 µm, the result of this test shows something else. Figure 5.12(a) and 5.12(b) show the scatter plots of PP measured by AQE compared to $PM_{2.5}$, with temperature and relative humidity background information, respectively. The AQE was underestimating the amount of $PM_{2.5}$. The AQE detects the smallest amounts of PP best, and as the concentration increases the ability of the egg to detect the particles decreases. The RMSD when we compared the PP from AQE and the $PM_{2.5}$ from BK was 6.4 % and the correlation was 0.76. Figure 5.12(c)-(f) show the scatter plots of PM_{10} compared to PP measured by the AQE. The two first shows the whole range, with temperature

and relative humidity background information. An interesting result was that the highest concentrations of PM_{10} occured at high temperatures. Since there were only a few values in the upper range, we decreased the interval of the scatter plot to be able to see how the temperature and relative humidity were distributed (figure 5.12(e)-(f)). In figure 5.12(e) we can see a clustering with respect to temperature, where the PP measured by the AQE increased with decreasing temperature. When we compared it to PM_{10} the RMSD was 19.3 % and the correlation was 0.33. None of the results were satisfying and indicate a general problem in PP measurements by, at least the tested version of, the AQE.

The corresponding scatter plots for temperature measurements for the two AQE can be seen in figure 5.13, where (a) shows the temperature for the AQE measuring NO_2 and (b) shows the temperature for the on measuring PP. It was obvious that the AQE measuring NO_2 performs a more accurate temperature measurement. This was confirmed by the RMSD and the correlation, which was 2.3 % and 0.95 for the AQE measuring NO_2 and 4.0 % and 0.94 for the one measuring PP. Since the two eggs were located close to each other, with a distance of a few cm, we expected the eggs to measure the same temperature.

One explanation of the large differences in the measurements is the exposure of solar radiation. The protection used for the second test, seen in figure 5.7(c), was made of a more opaque material than the protection used in the first test. The hope was that they would protect the instruments better against the exposure of solar radiation. The protections used for the second test were also better ventilated underneath the instrument. Again, a problem of build-up and storage of heat due to no ventilation above the instrument could also be a problem, especially for temperature measurements. Since the air intake and fan was underneath the instrument the absence of ventilation on the top should not be a problem. As for the first test, the location of the instruments were likely too close to the ground. This might have influenced the result. It seems that the instruments have a calibration error, because the they are overall measuring too low or too high values. For the AQE measuring PP the poor performance can be because the egg was exposed to temperature below its operational range.

Comparison of the two test shows that it is likely that the instrument protection used for the first test affected the result more than what the protection of the second test did. The first test showed lower concentrations of NO_2 than the reference while for the second test the AQE measured higher concentrations than the reference. This might be because of the limited ventilation of the first test. Both tests show that the instruments

were affected by solar radiation. The results show that the AQEs have major problems of measuring the correct concentrations of NO_2 and PP, which they are designed for. Based on the performance during these two tests it was clear that the eggs do not fulfill the requirements for a scientific application.

The result of the temperature and relative humidity measurements are better, but not perfect. Since the reference station was 1 km away, a third test was conducted to see how well the eggs measure temperature and humidity when co-located with the reference sensors. This test was preformed from April 11th to 12th, 2018 in the observational garden at GFI, close to the temperature sensor at the AWSI. The setup of the test can be seen in figure 5.7(d).

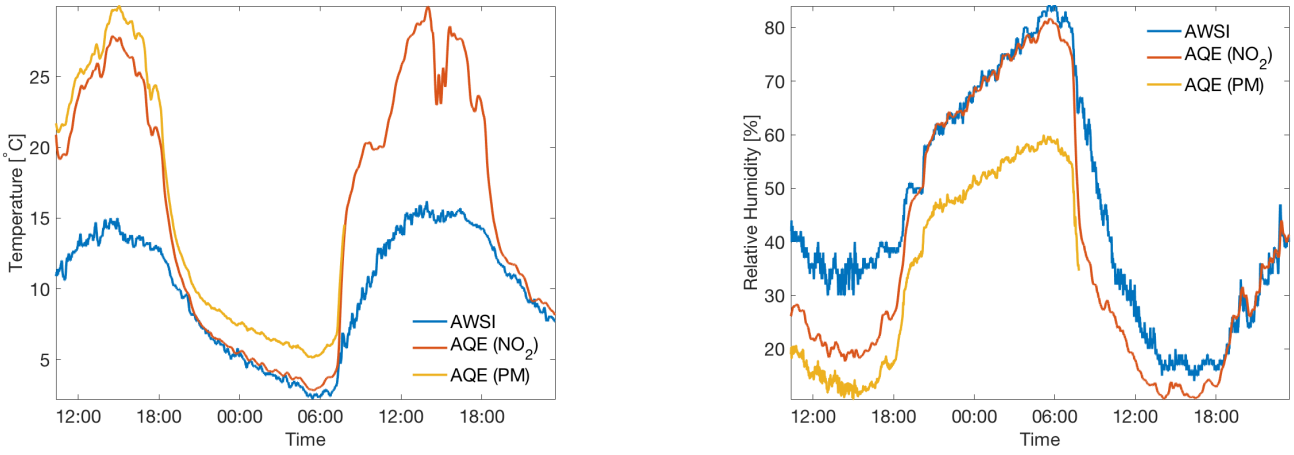

(a) (b)

Figure 5.14: Time series of the third test where a) shows the temperature and b) the relative humidity.

The result of the test can be seen in figure 5.14, where (a) shows the temperature measurements from the AWSI, the AQE measuring NO_2 and the AQE measuring PP. The AQE measuring PP ran out of battery in the morning of 12.04.18 and therefore the temperature and relative humidity series are shorter than the ones for NO_2. It was clear that the eggs were affected by solar radiation. A positive result of this test was that we can see that during the nighttime or periods of no or weak solar radiation, the AWSI and the AQE measuring NO_2 measured the same temperature. At the same time, the AQE measuring PP measured a systematically higher temperature. It seems that the AQE measuring NO_2 can measure the correct temperature under conditions with no or

weak solar radiation. However, we can not draw a sound conclusion because of the short measurement period.

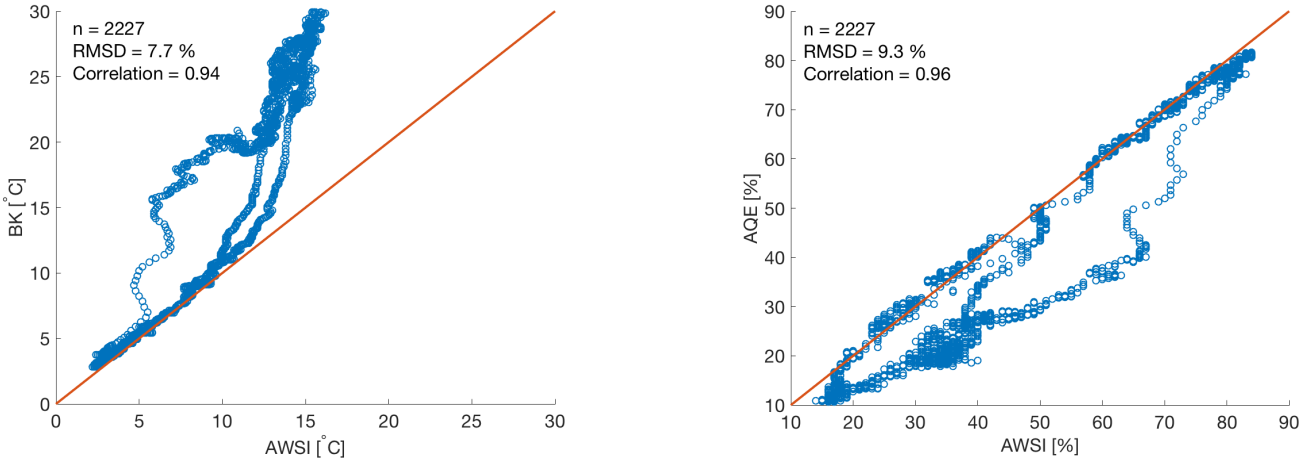

(a) (b)

Figure 5.15: Scatter plots of the third test, where AWSI is compared to the AQE measuring NO_2. a) shows the temperature and b) the relative humidity.

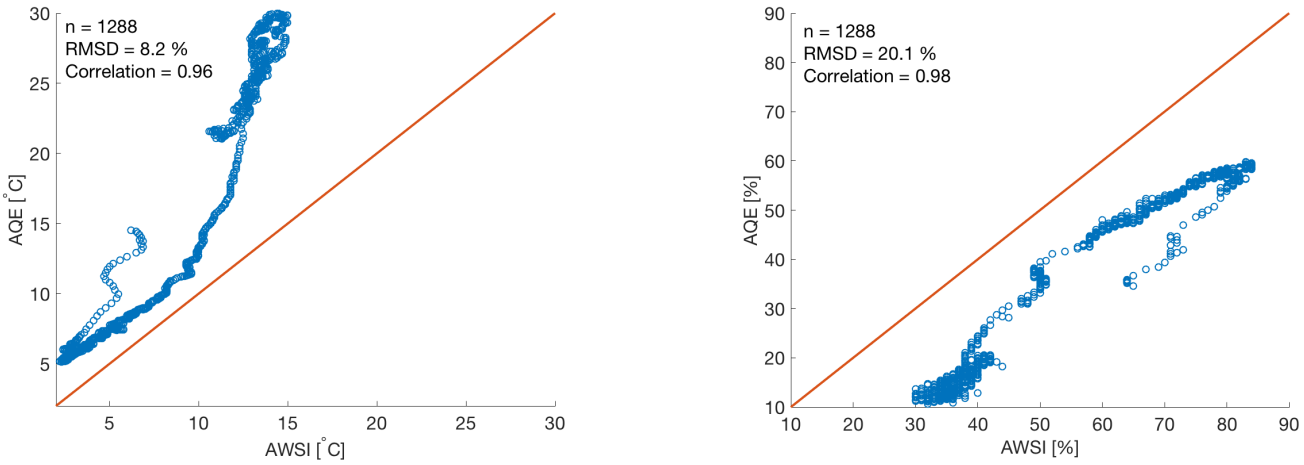

(a) (b)

Figure 5.16: Scatter plots of the third test, where AWSI is compared to the AQE measuring particulate pollution. a) shows the temperature and b) the relative humidity.

The corresponding scatter plots for the AQE measuring NO_2 can be seen i figure 5.15.

The AQE measured the correct temperature partly in the beginning, where it followed the regression line, but eventually it measured too high temperatures (figure 5.15(a)). The RMSD was 7.7 % and the correlation was 0.94. The relative humidity was underestimated by the egg. Also in this case the egg was partly measuring the correct relative humidity. The RMSD was 9.3 % and the correlation was 0.96. For the AQE measuring PP the scatter plots can be seen in figure 5.16, where (a) shows the temperature and (b) shows the relative humidity. The RMSD for the temperature measurement was 8.2 % and the correlation was 0.96, while for the relative humidity the RMSD was 20.1 % and the correlation was 0.98. Compared to the AQE measuring NO_2, the performance of the AQE measuring PP was poorer.

From the three tests it appears that the temperature and relative humidity measurements by the AQE measuring NO_2 are the only measurements that can be trusted, but only under certain conditions, with no or weak solar radiation. Since the instruments were prone to exposure of solar radiation they should only be used at locations that were protected from the sun. The AQEs need also proper protection since they can not be exposed to precipitation. Our tests have shown that the AQE measurements, in particular of PP, NO_2 and CO are unreliable and would therefore be of no, or at the best very low scientific value. In combination with the limited environmental robustness of the devices, we decided not to deploy those sensors in the field as part of this master thesis.

5.3 The Weather in Bergen During the Measurement Campaign

Throughout the year of the campaign the Automatic weather stations (AWSs) have collected a large amount of data. The stations have measured, among others; temperature, wind speed and direction, radiation and precipitation. In this section I present the general situation throughout the year to allow for an estimation of the representativeness of the measurement period in a longer climatological context.

Table 5.1: Overview of the deployment of the AWS and number of records and missing data, and data availability

Station	**Station deployed**	**Number of 10 min records**	**Number of missing data**	**Data availability [%]**
Løvstakken	09.02.17 13:50 UTC	55357	2258	95.9
Strandafjellet	02.02.17 11:10 UTC	56381	1097	98.0
Svingen	02.02.17 11:30 UTC	56379	3	100
Gapahuken	02.02.17 13:10 UTC	56369	2188	96.1
Skillingsbollen	02.02.17 13.20 UTC	56368	2	100
Solheimslien	02.02.17 14:20 UTC	56362	981	98.3
GFI	02.02.17 00:00 UTC	56448	3840	93.2
Ulriken (AWSA)	02.02.17 00:00 UTC	31272	612	98.0
Ulriken (AWSI)	27.11.17 10:20 UTC	13186	0	100

Information about the time of deployment, number of records, missing data and data availability are listed in table 5.1. We deployed most of the stations on the 2nd of February 2017, except the stations at Løvstakken and Ulriken. The Automatic weather station from AADI (AWSA) at Løvstakken we deployed a week later, and the AWSI at Ulriken we deployed in the end of November 2017. All stations, except the AWSA at Ulriken, measured to the 28.02.18 at 00:00 UTC. The AWSA at Ulriken stopped measuring on the 27th of September. To get the best comparison between the stations, we used the same start time; 09.02.17 at 13:50 UTC. When we combined the measurements from both Ulriken stations the resulting data availability was 83.3 %, for the whole campaign.

Since we wanted to look at the monthly mean of the data it was necessary to look at the monthly data availability. Most of the stations were missing records for longer continuous periods and this affected the monthly mean. An exception was Ulriken (AWSA), where the missing records were near evenly distributed throughout the measuring period. September, with data availability of 88.0 %, was the only month where the data availability was less than 95.0 %. For Løvstakken most of the missing records were in October, resulting in a data availability of 54.0 %. The rest of the missing records for Løvstakken was from November, with a data availability of 95.3 %. For Strandafjellet, Gapahuken and Solheimslien, all of the missing records were from May, resulting in a data availability of 75.4 % (Strandafjellet), 51.8 % (Gapahuken) and 78.0 % (Solheimslien). For GFI most of the missing records were in March, but there were also missing records in May and September. The resulting data availability for GFI was respectively, 51.5 % (March), 94.6 % (May) and 67.5 % (September). For Ulriken, October and November was not included because there were no measurement in the period from 28.09-27.11.17. The missing records resulted in uncertainties, especially when comparing monthly mean.

Monthly mean temperatures can be found in figure 5.17(a). For most of the period the stations are distributed as we expect according to the stations altitude. The smallest spread between the station was in October and the largest was in July. In May, the station at Gapahuken has approximately the same monthly mean as the station at Løvstakken. This is most likely because Gapahuken had a data availability of 51.8 % for May. We also found a peak in the temperature measured by the station at GFI that was not found for the other stations. We assume the reason was the low data availability, of 51.5 %.

Since the campaign only lasted for 13 months, it is a too short time period to draw sound conclusions for Bergen. We therefore compared the measurements from GFI to the climatology, the normal from 1961-1990, as seen in figure 5.17(b). The normal temperature is based on measurements from Florida (GFI), close to the station used for this campaign. When comparing the measurements from GFI and the normal, one should keep in mind the months with low data availability (March and September), because they only represent a part of the month. This also applies to the other stations when comparing them in between.

The comparison of GFI and the normal monthly temperature, figure 5.17(b), showed that the temperature measured during the campaign were most of the time above the normal. The difference, shown as the yellow line in the figure, is the temperature measured in the campaign subtracted by the normal temperature. The monthly average measured

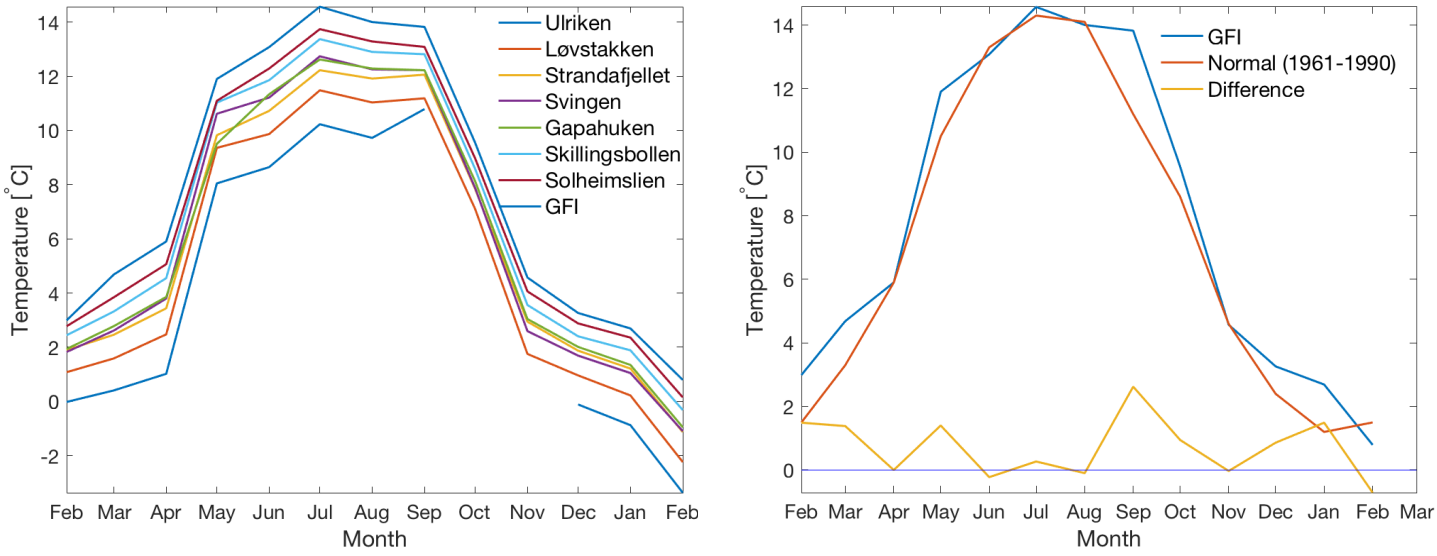

(a) (b)

Figure 5.17: The monthly mean temperature measured by the AWSs for (a) all stations, and b) GFI and the normal temperature between 1961 and 1990, in addition to the difference between the two temperatures, as the yellow line.

at GFI was 0.7 °C higher than the normal. The largest difference was in September, where the temperature measured was 2.6 °C higher than the normal. It is interesting that the temperature of September was warmer than the normal, because the GFI station were missing records from 01.-11.09.17. Normally the temperature decreases throughout the month, but September 2017 seemed to be a warm month. This is confirmed in figure 5.17. When comparing the normal temperature to the other stations, the normal temperature was the same as the temperature measured at Løvstakken in September 2017. As we will see later, September was also a dry month with only 2/3 of the normal amount of precipitation. For March, the GFI station had missing records from 10.-25.03, but also here the temperatures were higher than the normal.

In figure 5.18 the high resolution temperature series for the AWS is shown. The presented temperatures are 10 minute mean values and the figure visualizes the spread throughout the months of measurements. The black line is the Ulriken temperature, which is expected to be the lowest temperature. The bright blue is the temperature measured at GFI. This figure shows a more realistic temperature distribution, then the one in figure

5.17(b). Here we see the large spread within the months. The largest spread was during the summer and the least during the fall. In the end of February 2018 we experienced an unusual cold period in Bergen. This was due to cold air advection from Siberia (Russia).

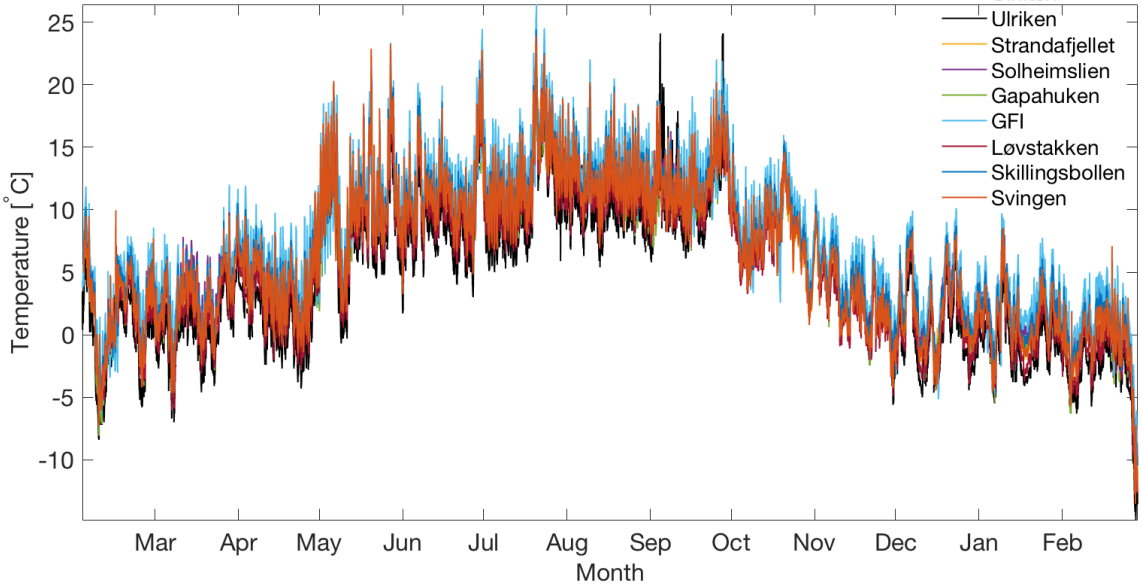

Figure 5.18: High resolution temperature series for all AWSs during the campaign.

For the measurements from the ELs, we saw in the tests of the ELs, in section 5.1, that the they needed to be corrected. We corrected the ELs by removing all records when the solar radiation measured at Gapahuken exceeded 20 W/m^2. In addition, we corrected all ELs with the difference between the temperature measured by AWSIs and EL6, at Gapahuken. The result is shown in figure 5.19. The two AWSI at Solheimslien and Gapahuken were used as boundaries, which all ELs, except EL1 which was located at 75 m asl, should not cross. For most of the time the ELs stayed within the boundaries, but in the end of January they deviate. EL9 have 1864 records of values outside these boundaries, with the maximum deviation of 6.3 °C. This means that 18 % of the measurements are showing unrealistic values. In addition 40 % are filtered and set as Not a Number (NaN), leaving 42 % left. The main problem is that we do not know whether we can trust a value or not, even after the filtering. It is problematic to use these data for detecting temperature inversions. We therefore decided not to use the ELs for further analysis. Since the other AWSs are located in a dense network, the additional information from the ELs are not of

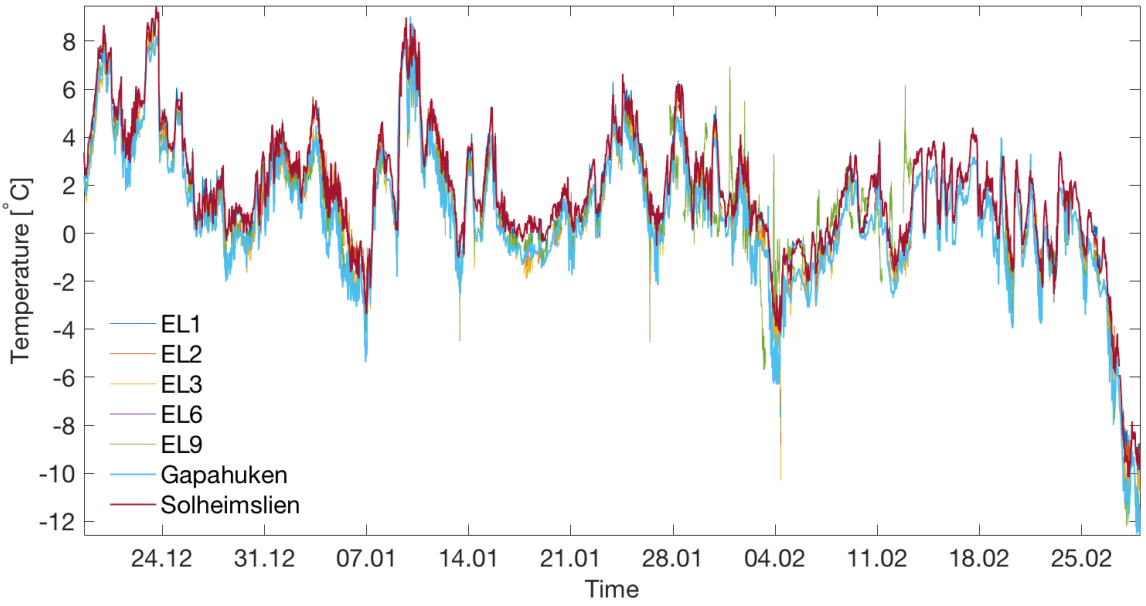

Figure 5.19: Corrected temperature measured by the EasyLogs and temperature measured at Gapahuken and Solheimslien are used as temperature boundaries.

crucial importance.

Monthly amount of precipitation from the four AWSs measuring precipitation, is be found in figure 5.20. For comparison, we include the normal (monthly mean precipitation between 1961 and 1990 in Bergen), the green bar in the figure. From the figure, it is clear that the total precipitation during the campaign was higher than the normal. This was the case for all months, except May and September. The measured precipitation was approximately the same for all of the AWS for the months without missing dates. For March and September the measurements by the station at GFI were clearly lower than the other stations. For May, all stations had missing records, but the station at GFI had a data availability of 94.6 % and the other stations had similar amount of precipitation, which was slightly less than the normal.

February 2018 is characterized by a large spread between the stations unaffected by missing records. During the winter in 2017 there was little snowfall and especially not snow laying on the ground for longer periods. In the winter of 2018 we had a larger amount of snow and continuous snow cover for days and at some places for weeks. This was most likely the reason for the spread in registered precipitation. Either the non-heated instrument was

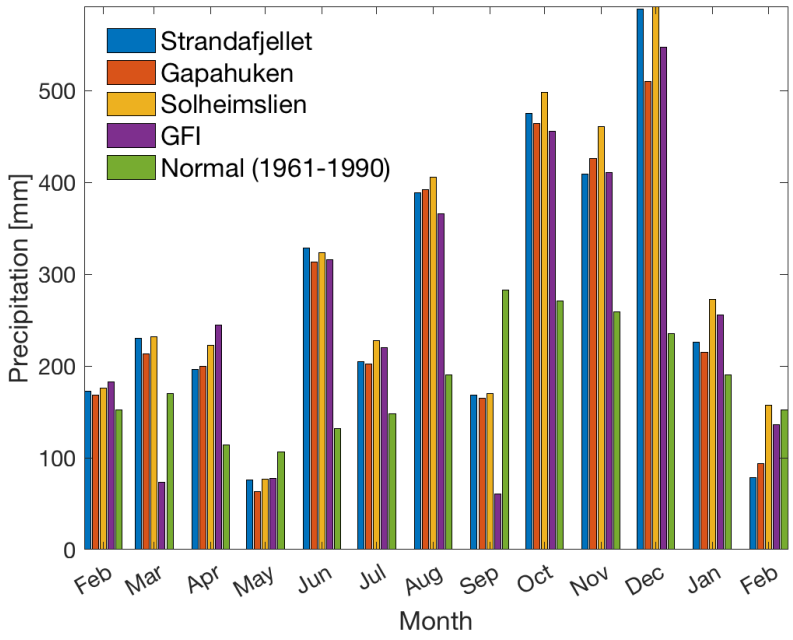

Figure 5.20: Monthly amount of precipitation measured by the AWSI compared to the normal precipitation between 1961 and 1990.

covered by snow or the rain gauge was suffering from precipitation undercatch of snow in windy conditions (Rasmussen et al. 2012, Weiss 1961). This is consistent with the fact that the two stations at higher altitudes, Strandafjellet and Gapahuken measured the smallest amount of precipitation. Solheimslien and Gapahuken are the two stations with data availability of more than 98 % and the total amounts of precipitation over the whole period of the campaign were 3815 mm (Solheimslien) and 3426 mm (Gapahuken). The normal amount of precipitation at Bergen, Florida is 2554 mm. This means that the 13 months of measurements resulted in a 34-49 % higher amount of precipitation than the normal. It has to be taken into consideration that the precipitation instrument at the AWSI were affected by winds and turbulence, because they did not have any wind shield.

Monthly mean solar radiation can be found in figure 5.21. We replaced slightly negative values during nighttime with zero. Two of the stations, GFI and Gapahuken did not have negative values and stayed the same. We can see from the measurements, in figure 5.21, that May was the month of largest irradiance. One would expect largest irradiance during June and July, but May had least precipitation and hence less clouds. We found the

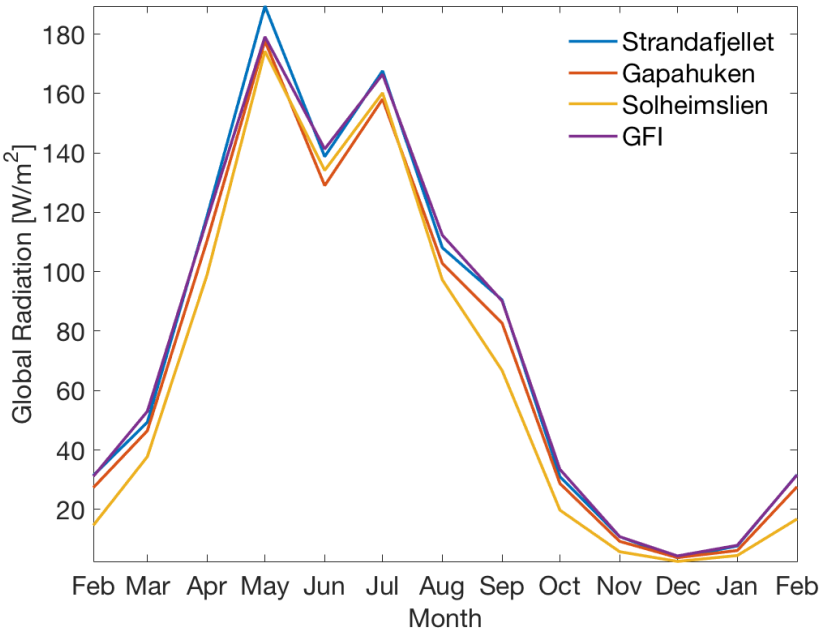

Figure 5.21: Monthly mean incoming solar radiation by replacing the negative values by zero.

opposite for June, where heavy precipitation and cloud cover decreased the incoming solar radiation. December was the month of overall least incoming radiation, both because it is the month of weakest solar radiation and because of heavy precipitation.

The most favorable location to maximize the irradiance was when the stations were located in a southwest direction. The least favorable location was when directed towards northeast. The stations at Strandafjellet was located on the top of a hill and was an ideal location for receiving solar radiation. Solheimslien was located at the least favorable location of the stations, because the Løvstakken mountain covers the sun. During the summer the stations at Solheimslien received slightly more solar radiation than Gapahuken, because of the position of the sun.

The general wind pattern and the circulation in the city from our stations can be seen in figure 5.22. The circles represent the frequency of occurrence and mark every 5 %. All stations have circles from 5 to 15 %, except Gapahuken which have circles up to 25 % because of strong channeling. They all have the same wind speed intervals, from 0 to 36 m/s, to make it easier to compare to each other. We combined the data sets for the AWSA and the AWSI measuring at Ulriken. However, we missed two months of measurements

between the end of September and the end of November.

A previous study by Valved (2012) showed the circulation in the Bergen Valley based on a network of seven AWSAs. Her measurements were based on measurements over a period of approximately 19 months, from end of November 2010 to beginning of July 2012. Since four of her stations were located at the same location or a location close to our stations, we could compare them. Our measurements were collected over a period of 13 months, where February was represented twice. Valved had two years of measurements for all months except from the beginning of July to the end of November. The two results are therefore not directly comparable, but gave us an indication of the circulation in the valley for the two campaigns.

As expected the wind speed increased with increasing altitude, and the strongest winds were found on Ulriken (figure 5.22(a)). When we compared the winds to the result from Valved (2012), the wind roses at Ulriken were in general showing the same. Both the wind directions and winds speeds were similar. There were most occurrence of south to southwesterly winds and the strong winds of more than 30 m/s occur from this direction. In northwest direction a tall mast is located, which can lead to an underestimation of winds from this direction. Winds from east might have been affected by the hill behind the station. Our measurements showed a stronger channeling for southwesterly winds than the result from Valved. This is most likely because the strongest channeling occurred during fall, and her measurements lasted for 19 months and the measurements from the fall was only included once.

The wind measurements from Løvstakken (figure 5.22(b)) showed a frequent occurrence of winds from south-southeast, but also from northwest. The station was located tens of meters from the edge of the mountain, which gave rise to these winds from northwest. Valved also had a AWSA at the top of Løvstakken, but her station was located directly on the top of the mountain, about 20 m higher than ours. The large differences in location resulted in two slightly different results. Her measurements showed most occurrences of winds from south and southwest and our measurements showed most winds from southeast. Since her station was located at a higher altitude as well as toward south, her measurements were less affected by the obstacles nearby, and the stations were located in an area of more free flow. Our stations were affected by the mountain which acted like a shelter for winds from southwest. Because our main interest was the temperature and winds within the valley, the location of our station was favorable.

The wind measurements from Strandafjellet is shown in figure 5.22(c). The winds were dominated by winds from south-southeast. The station was located at the top of a hill and was connected to Løvstakken by a ridge. Løvstakken will most likely have affected the winds from southwest, by reducing the occurrence of winds from this direction. A few meters from the station, in northwest direction, there was steep terrain which was likely to influence the measurements. The wind speeds were shigher for the winds from west and northwest. The maximum wind speed was 18.6 m/s. The result from Valved measurements showed the same wind pattern, with slightly weaker winds, with maximum wind speeds of 10-15 m/s. Both campaigns showed little or no winds from north-northeast. The absence of winds from north-northwest was probably a result of the wind circulation in the valley.

Wind measurements from the AWSI at Gapahuken, found in figure 5.22(d), showed strong channeling of south-southwesterly winds. This station had the strongest winds speed in this direction, with a maximum wind speed of 10.6 m/s. Wind measurements from Solheimslien can be found in figure 5.22(e), where the highest frequency of occurrence were winds from east. In addition, winds from northwest were also present. The winds from northwest were strongest, reaching up to 9.8 m/s. Neither of the stations at Gapahuken and Solheimslien, had any measurements to compare to.

The result from the wind measurements from GFI is found in figure 5.22(f). The southwesterly winds were the most common, but winds from west and east were also present. The stations were located in the observational garden at GFI, where the Institute building affected winds from northwest, north and northeast. As seen in the figure, there were only a few occurrences of winds from these directions. Valved used measurements from the AWSA at the roof of GFI at 48 m asl. Therefore her result differ from our measurements. Her measurements showed a channeling of winds from southeast and some from northeast. Overall, the results from the two measurement periods showed different wind directions and wind speeds. The maximum wind speed measured by the station at the roof was 15 m/s, compared to 6.5 m/s from our measurements.

5.3.1 Discussion

There are error sources associated with performing in-situ measurements. To make sure the measurements are as precise as possible it is important to follow the instructions for setups. The stations should be placed at suitable locations where the measurements are not

affected by noises. Our instrumentation were installed according to the instructions and at suitable locations. All temperature sensor at the AWS, except the one at Ulriken, were installed at heights of 1.9-2.1 m above the ground. The temperature sensor at Ulriken was mounted on a tall mast, approximately 4 m above the ground. This was probably to prevent the temperature measurement to be affected by ground processes. When we mounted the new AWSI at Ulriken we installed it at 2.5 m. The ELs were installed on threes, hanging, with a bit varying height, due to limited access. These small difference in height, at least for the AWS, should not affect the measured temperature significantly. The temperature and wind sensors at AWSA, installed at Ulriken until September 2017, was installed at 4 m.

We had problems with the AWSI regarding missing data. The reason for these missing data is a bit unclear. We know some of them are due to problems of transferring the data to the computer via the modem. The station at GFI were down for weeks because the computer receiving the data broke down. We found overlapping data that we filtered, and removed the duplicates. These duplicates had the same values and we could therefore remove them. Some of the AWSIs had negative radiation values that we replaced by zeros. The reason for choosing this method, was because these values occurred during the night. The negative values are likely due to a calibration offset. We could also have calculated the daily average and the average of solar radiation during the night. Then we could correct the daily average by adding the average during that night. Because we did not focus on the solar radiation in this thesis, we only replaced the negative values by zero.

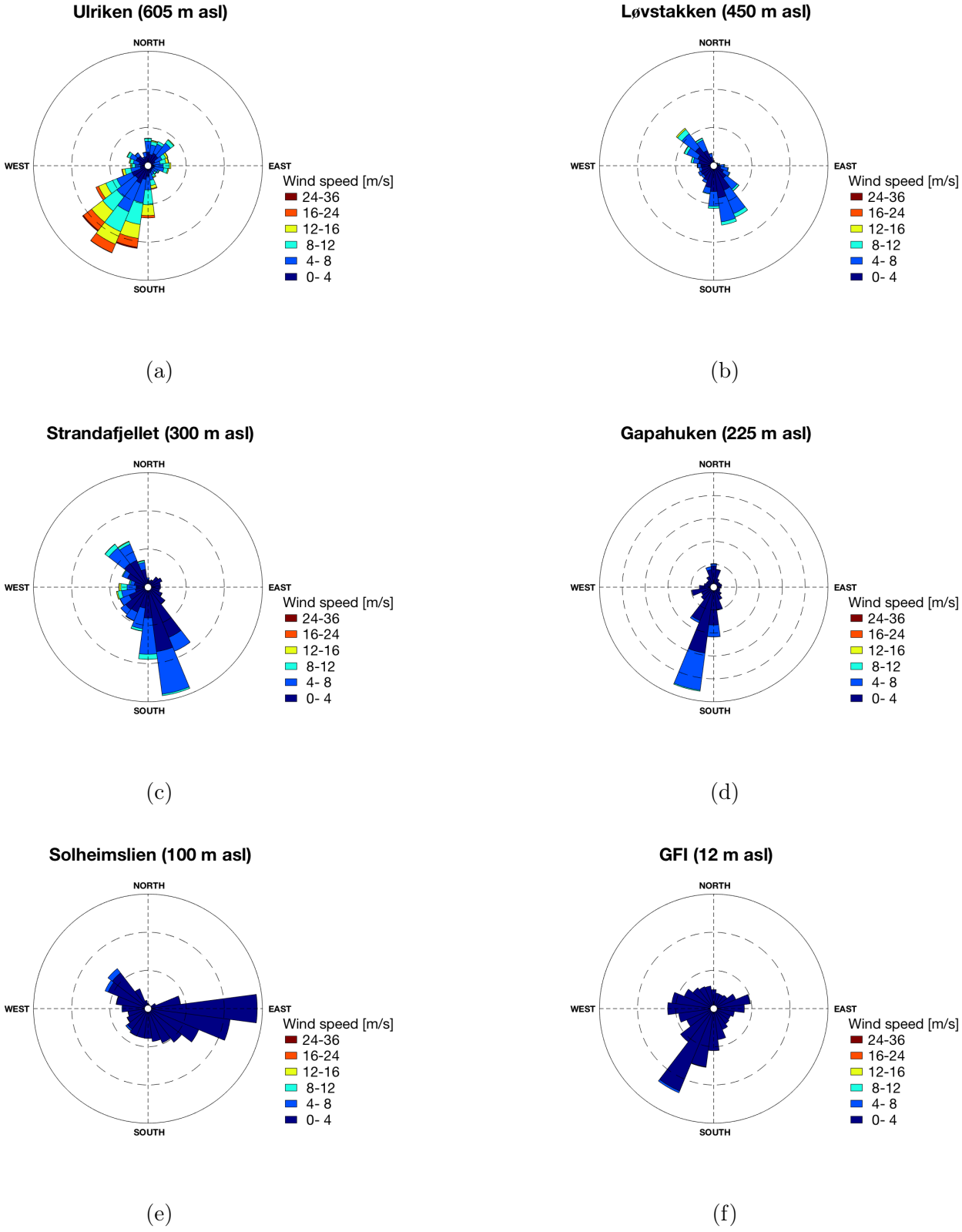

Figure 5.22: Wind roses for all of the AWSs measuring wind speed and wind direction. The circles represent the frequency of occurrence and mark every 5 %. Measurements from a) Ulriken, b) Løvstakken, c) Strandafjellet, d) Gapahuken, e) Solheimslien and f) GFI.

5.4 Temperature inversions

The transect along Mt Løvstakken together with the stations at GFI and Ulriken allow us to analyze in-situ measured vertical temperature profiles with a high vertical resolution. We use these temperature measurements to detect both ground-based and elevated inversions in the Bergen Valley. Ground-based inversions are defined as inversions between GFI, which is the station at the lowest altitude, and another station. Elevated inversions are defined as inversions between any two stations except for GFI. In this section I present the temperature inversions measured during the campaign.

In terms of the assessment of temperature inversions, in particular with respect to air pollution, it is beneficial to distinguish between short lasting inversion events and longer lasting episodes. The most relevant feature of temperature inversions in Bergen and in the context of this study is the decreased efficiency in the dilution of pollutants. Longer lasting inversion episodes have the largest impact on local air pollutant concentrations (Wolf et al. 2014). The inversion episodes defined here were identified as continuous measurements of an inversion situation at a given height interval. This means that e.g. an inversion between Solheimslien (100 m asl) and Strandafjellet (300 m asl) is recorded, whenever the temperature at Strandafjellet was higher than both the temperature at the intermediate station at Svingen (at 250 m asl) and Solheimslien. The inversion duration was defined as the length of continuous measurements of inversions, within a specific height. The inversions of 1 min durations are here referred to the single records of inversions. For all other cases, except for single inversion measurements, the basis for the analysis in this section is episodes with a multiple of 10 min duration. A 10 min episode is said to occur if at least 2 consecutive measurements within a 10 min interval have shown a temperature inversion. All 10 min intervals after the initial inversion episode are said to be part of the same inversion episode, as long as an inversion was present with the same inversion height for at least the first measurement of the 10 min intervals. This means that an episode of 20 min consists of at least three continuous records of inversions.

After grouping the inversions based on the 8 available stations between the valley floor at GFI and the highest station at Ulriken, we ended up with 28 possible vertical inversion profiles (inversions between station 1 and 2, 1 and 3, 2 and 3, etc.). The thickness of the inversions were based on the height difference between the stations. The instruments were located in a dense network, with varying height difference, in the range of 25 to 150 m. The

25 m thickness bin consisted of the inversions occurring at stations 25 m apart. Inversions only excisting between Gapahuken (225 m asl) and Svingen (250 m asl) are an example of inversions with a thickness of 25 m.

Since the inversions were defined as inversion of continuous height and duration, we had to make sure that the inversions between the stations were unique. E.g., the inversions between Skillingsbollen (150 m asl) and GFI (12 m asl) included the inversions between Solheimslien (100 m asl) and GFI. We filtered the data correspondingly and removed the overlapping inversions. All figures we present in this section are based on unique inversions for the specific height, unless otherwise stated.

A previous study by Wolf et al. (2014) defined the temperature inversions differently. They identified temperature inversions not based on in-situ measurements along a mountain transect but from microwave remote sensing measurements with the MTP-5HE (MTP). In addition, they defined inversion episodes as continuous measurements with inversions of the same type (ground based or elevated) but with the possibility of varying inversion heights. The height of single inversion episodes was therefore defined as the mean height over an episode. Since our inversions were defined differently, the results could not be directly compared to the results from Wolf et al. (2014). Treating the temperature inversion as we did, allowed us to characterize the episodes exactly during measurements with elevated air pollution more precisely. It resolves the problem that some inversions can last for a long time but with widely varying inversion height and answers directly, what inversions are typically connected to the strongest stagnation of the air flow along the bottom of the valley. This provided extended information compared to the methodology used by Wolf et al. (2014). Because of the two different definitions, our inversions last in general shorter than the ones found by Wolf et al. (2014).

The number of ground-based temperature inversion episodes against height can be found in figure 5.23. The majority of the inversion episodes were shallow, with inversion tops below 150 m asl. The maximum number of episodes reached only 100 m high. In order to give an impression of the duration of the inversion episodes, they are separated into single records (blue), episodes lasting between 10 and 110 min (red) and the episodes lasting longer than two hours (yellow). For the shallow episodes, with inversion top at 100 m asl, there were four times as many single records (1 min) than episodes lasting longer than two hours. An exponential decrease in the number of episodes with height is visible. As previously explained, long lasting episodes are of special concern, because they might

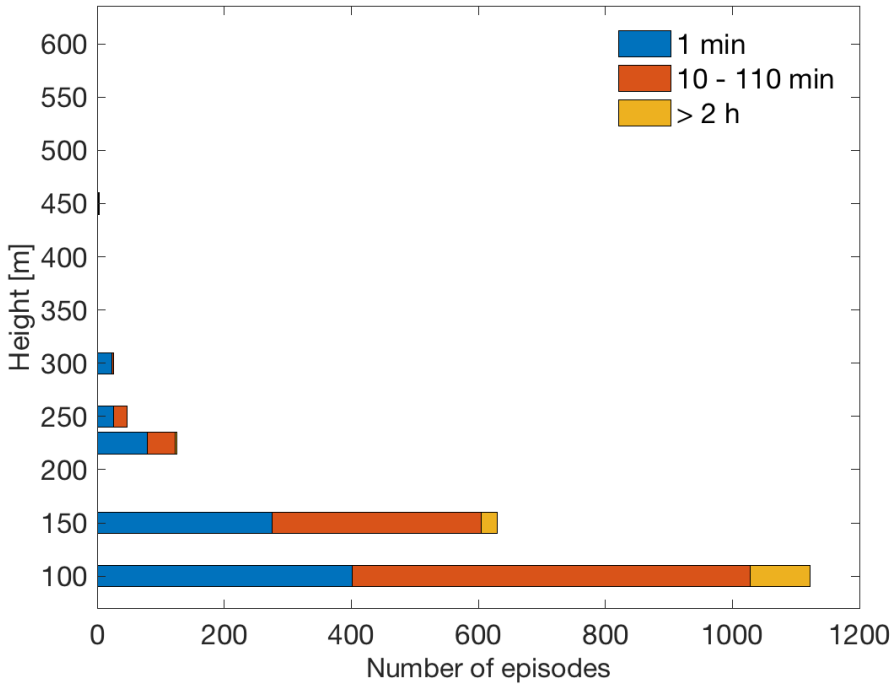

Figure 5.23: Number of episodes of ground-based temperature inversions. The (blue columns) are the single records, (red columns) the inversions lasting longer than 10 and 110 min, and (yellow columns) the inversions lasting longer than 2 h.

lead to build-up of elevated pollutant concentrations in the Bergen Valley. During the campaign there were 94 ground-based inversion episodes lasting longer than two hours, with the top at 100 m asl. The number decreased with height, to 25 episodes with the top at 150 m asl and only two episodes lasting longer than two hours at 225 m asl. No ground-based inversion episodes were measured with duration of more than two hours and tops higher than 225 m asl. We found most of the inversions to form during nighttime, as expected.

The monthly distribution of ground-based inversion episodes can be seen in figure 5.24. The single records were removed, meaning that we are only analyzing inversion episodes lasting at least 10 min or longer here. Overall, we observed most inversions during the winter season. The lowest inversions showed further the highest occurrence also in other seasons, whereas the higher inversions are more confined to winter time. As the number of inversion episodes decreased with height, the monthly variability also reduced. The ground-

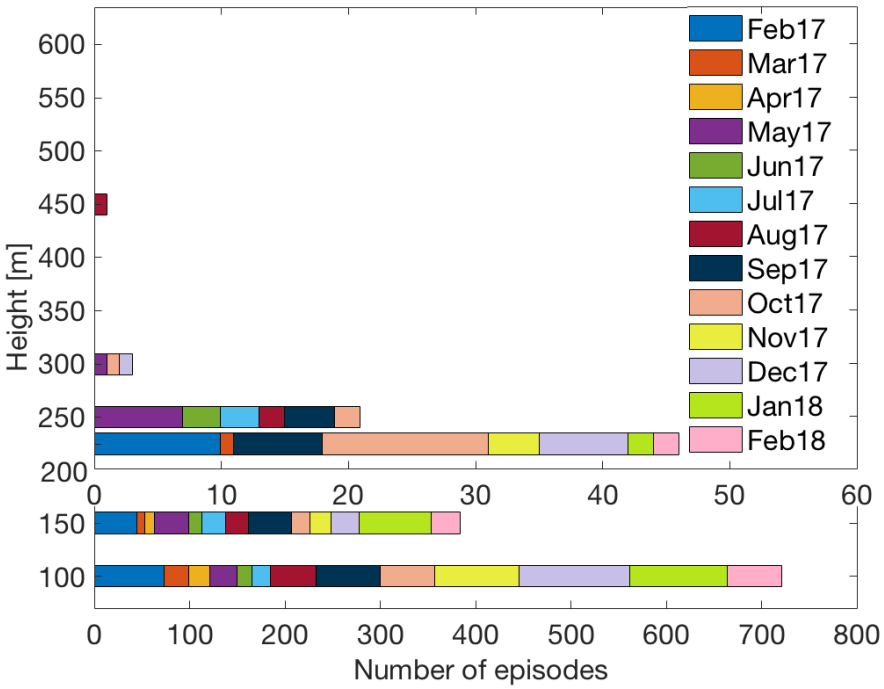

Figure 5.24: Monthly distribution of ground-based inversion episodes lasting at least 10 min.

based inversion up to Gapahuken (225 m asl) did not measure any inversions between April and August. We found the opposite for inversions up to Svingen (250 m asl), where all the inversions lasting longer than 10 min were measured between May and November.

From September 2017 and onward, we found most of the inversions episodes, lasting longer than 10 min, at all inversion heights, except for the one at 250 m asl. For the top at 100 m asl, 68 % of the episodes occurred from September 2017 until February 2018. For 150 m asl, we found 58 % and for 225 m asl, 76 %. At 250 m asl only 29 % of the episodes occurred in this range. We only found three episodes with top at 300 m asl (in May, October and December) and one at 450 m asl (August). As mentioned in section 5.3, the temperature spread between the stations were smallest during the fall (minimum in October). The smaller spread might have affected the number of inversion episodes, because even small temperature differences between the stations can result in an inversion. We found large precipitation amounts during the fall, except for September. This is likely to be the reason for the high number of episodes in September. For all stations, except the

one at 225 m asl, we found a higher number of episodes in September than October. The number of episodes can also be seen in context of incoming solar radiation. We found the largest spread of measured solar radiation between the stations, during the months of fall . Especially the station at 100 m asl has a general lower amount of monthly mean solar radiation. The station at 225 m asl showed 28 % of the occurring episodes in October. Even if this percentage of occurrence in October is larger than for the other stations, the inversions with tops at 100 and 150 m asl showed higher number of episodes in October.

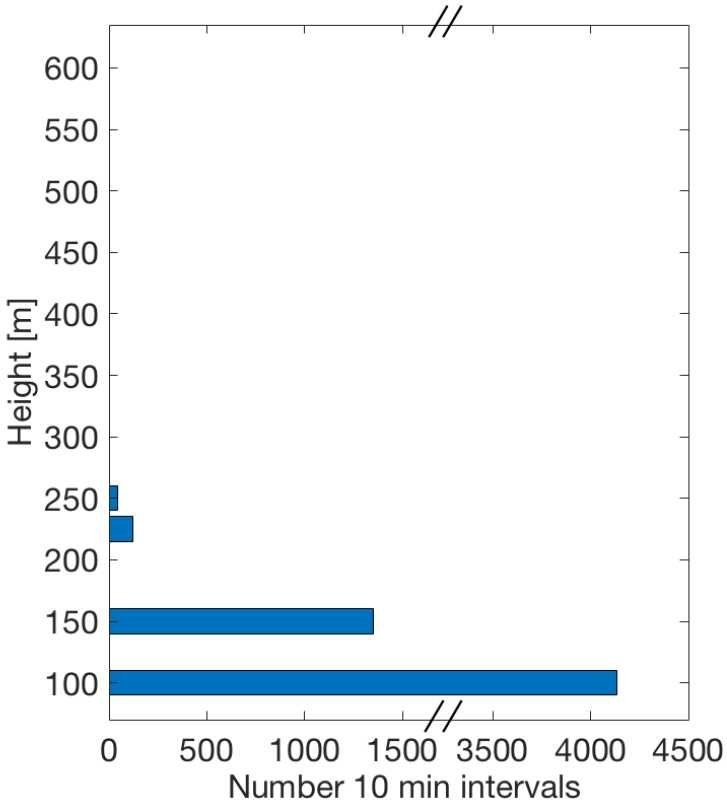

Figure 5.25: Number of 10 min intervals against height, for the ground based inversions.

The number of 10 min intervals against the height for ground-based inversions can be seen in figure 5.25. This figure is comparable to the result from Wolf et al. (2014) because they show the same, even with two different definitions. It also gives more information about the distribution of the duration of inversions, with height. The inversion tops were most frequently located at 100 m asl. There were three times as many 10 min intervals at 100 m asl than 150 m asl. This is in agreement with the result of the study by Wolf et al.

(2014). They also found the lowest inversions (in their case with a height of 70 m) to be the most frequent. However, they reported in addition a second maximum in occurrence for inversions with a height of 220 m asl. These were the inversion they found to be connected to cases of high pollution. Most of their shallow inversions were short lasting for only a few tens of minutes and they suggested airflow perturbation to be the main reason for this observation. Our results from the measurements during the campaign did not show this second maximum. Instead, the frequency decreased monotonously with height and we found 34 times less 10 min intervals at 225 m asl, than at 100 m asl.

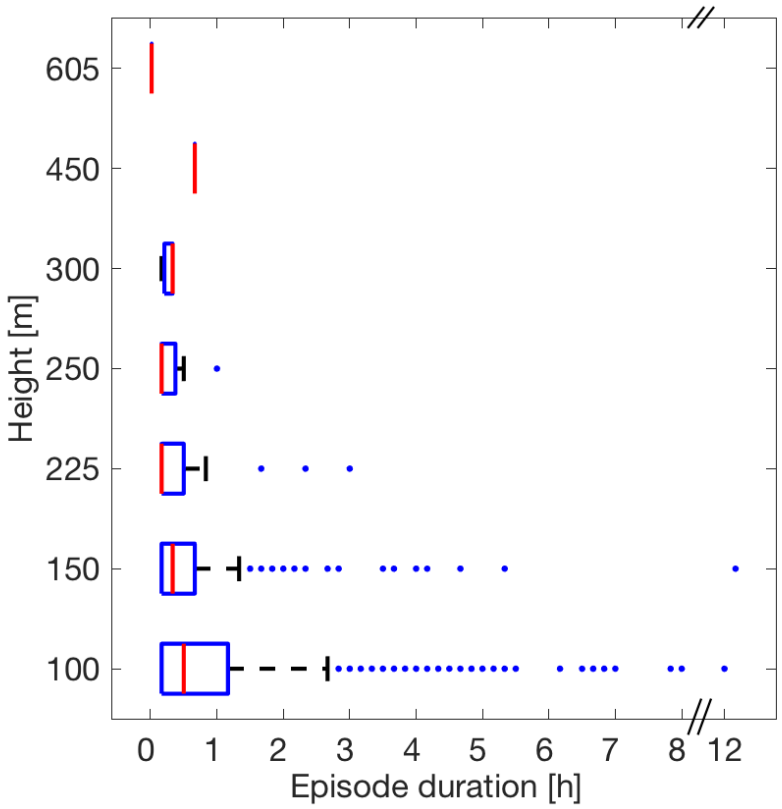

Figure 5.26: Duration of ground-based temperature inversions against height idenpendent of episode length, for inversions lasting longer than 10 minutes. The boxes show the median (red line) and 25th and 75th percentiles. The maximum whisker lengths are specified as 1.5 times the interquartile range. Outliers are marked as dots.

The episode durations against height for the ground-based inversions are found in figure 5.26. The single records were removed. The shallow ground-based inversions have the largest spread. The longest lasting episodes for both inversion tops at 100 and 150 m asl

were around 12 hours. Most of the ground-based inversions lasted less than an hour. This means that most of the inversions, because they are short lasting, do not have an impact on the local air pollutant concentrations. In context with the number of 10 min intervals in figure 5.25, we found both a low number of inversion episodes at 225 m asl and that these were short lasting. This concurs with the result of the study by Wolf et al. (2014), because we only found a few episodes and these were short lasting, we did not experience any long lasting high pollutant concentrations in the Bergen Valley during the campaign.

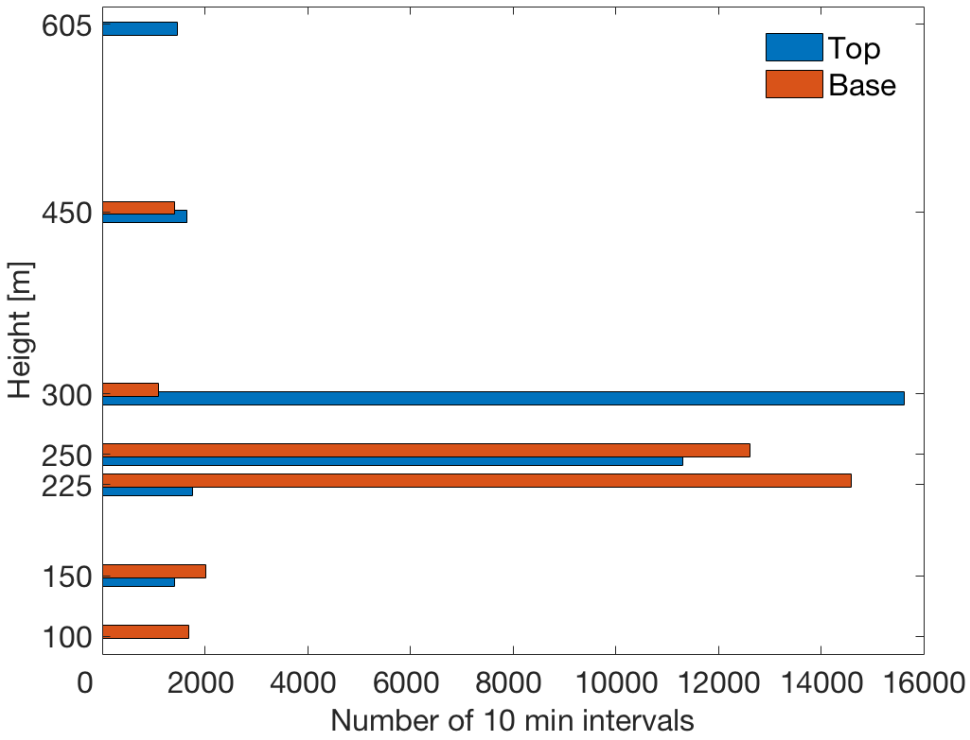

Figure 5.27: Number of 10 min intervals for bases and tops of elevated temperature inversions against height. The red column shows the inversion base and the blue the inversion top.

Our in-situ measurements are beneficial for the analysis of elevated inversions. Wolf et al. (2014) had problems with the analysis due to the poor performance of the MTP in clouds and rain, but found simultaneously a large amount of the elevated inversions to occur under these conditions. Therefore we here present an analysis of the elevated inversions. Elevated inversions are normally not connected to elevated air pollutant concentrations in

the Bergen Valley. There are only a few pollutant emitting sources high up in the valley. For the air pollution in the city, the fumigation of stack emissions is the most relevant phenomenon in connection to elevated inversions. The only large enough emission source that could possible contribute to this in the Bergen valley are the emissions from ships in the Bergen Harbour. A previous study by Wolf-Grosse et al. (2016) showed that during the period of high pollutant concentrations in the Bergen City, emission from the ships were no dominant source of pollutants over inhabited areas. This was likely due to the location of the Bergen Harbour. It is located in the northwest end of the Bergen Valley. High pollutant concentrations occurred mostly during ground-based temperature inversions. These conditions are mostly characterized by southeasterly, down-valley winds. Mixing by turbulence and stronger winds in the area, also affected the transport of pollutants.

The number of 10 min intervals for elevated inversion bases and tops against height, can be found in figure 5.27. The red columns are the inversion bases and the blue columns are the tops. The elevated inversions were most frequently distributed between 225 and 300 m asl. We found the largest amount of elevated inversions to occur between Gapahuken (225 m asl) and Svingen (250 m asl) and between Svingen and Strandafjellet (300 m asl). Therefore, the base at 225 m is mainly associated with inversions with tops at 250 m. We found the same for inversions between Svingen and Strandafjellet (300 m asl), where we found 12179 10 min inversion intervals. This is a very high number of 10 min inversions. One reason contributing to this high number of especially shallow elevated temperature inversions could be differential heating/cooling conditions at the neighboring stations. Shadowing of the lower station and not the station only 25 m higher up could cause a measurement to be identified as an inversion. The relevance of such very shallow inversions is highly debatable, since they are caused by very localized effects.

The number of 10 min intervals against thickness, for the elevated inversions can be found in figure 5.28. The thickness was defined as the distance between the stations where positive temperature gradients were measured. The inversions were grouped based on their thickness. The purpose of looking at this, was that we wanted to see whether there is a connection between the height distance between the stations and the number of 10 min inversions. In table 5.28(b) an overview of the number of vertical inversion types can be found. The 150 m thickness bin includes inversions from five inversions heights. E.g., the inversions between Løvstakken (450 m asl) and Strandafjellet (300 m asl) were categorized as inversion of thickness 150 m. Most of the inversions were shallow. Inversions

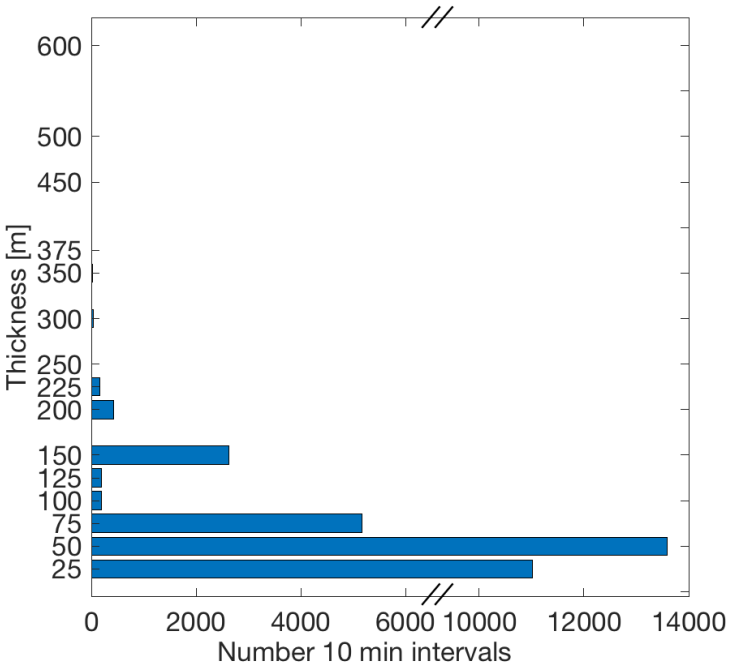

(a)

Thickness	Number of heights	Thickness	Number of heights
25	1	**250**	1
50	2	**300**	3
75	2	**350**	2
100	2	**375**	1
125	1	**450**	2
150	5	**500**	1
200	2	**600**	1
225	2		

(b)

Figure 5.28: (a) shows the number of 10 min intervals against thickness, for elevated inversions. It is only the possible thicknesses that are included in the figure. (b) shows the number of possible combinations of vertical inversion profiles with a given inversion height based on the existing measurement station network.

of 50 m thickness occur most frequently and we found barely any inversions of thickness greater than 225 m. The varying number of vertical height types, should be considered. The distance between the stations is variable and because there are not the same number of vertical height types, the thickness intervals are not directly comparable. The higher number of 10 min intervals for thickness of 150 m, is most likely because it included inversions from five vertical inversion types.

Episode duration of elevated inversions against thickness can be found in figure 5.29. Panel (a) shows the episodes lasting longer than 10 min and panel (b) shows the episodes lasting longer than two hours. We found most of the elevated inversions to be short lived. When considering the episode that lasted at least 10 min, more than 75 % of the measurements lasted less than two hours. None of the inversions with a thickness of more than 200 m, lasted longer than two hours. The longest duration of an elevated inversion

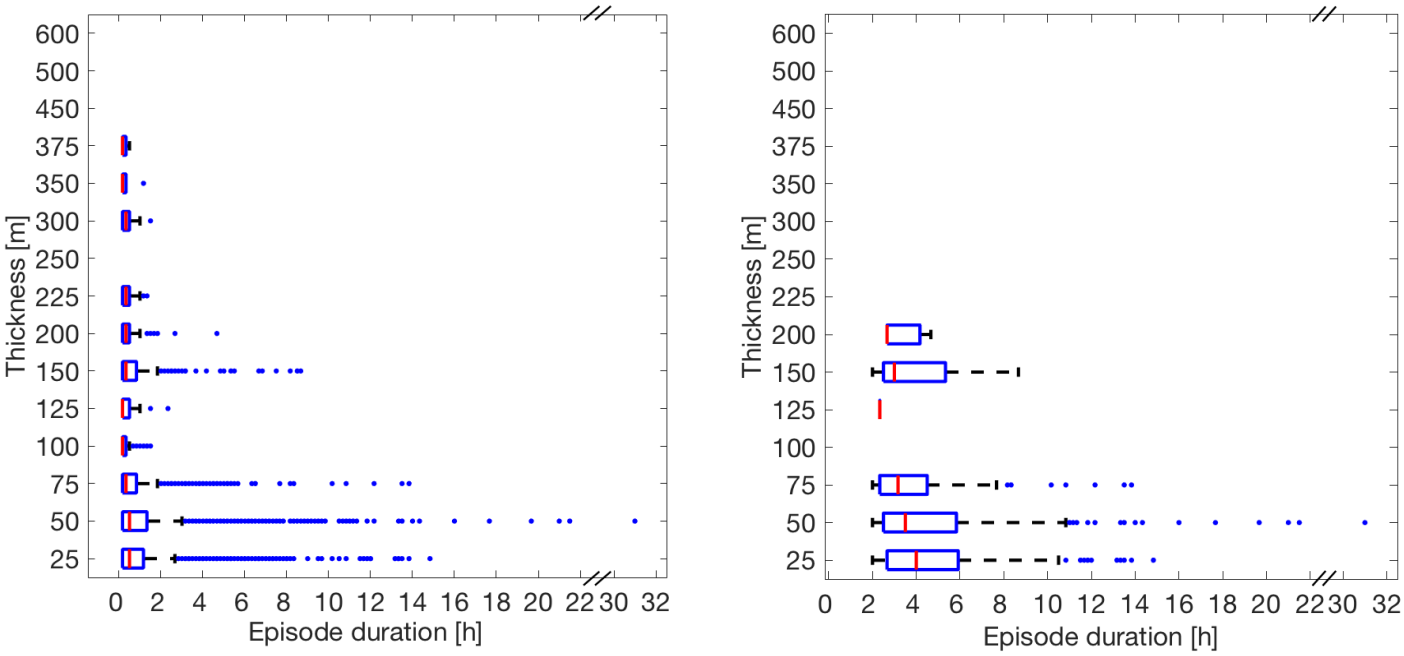

(a) (b)

Figure 5.29: Episode duration of elevated temperature inversions against thickness, for inversions lasting longer than (a) 10 min and (b) 2 h. The boxes show the median (red line) and 25th and 75th percentiles. The maximum whisker lengths are specified as 1.5 times the interquartile range. Outliers are marked as dots.

was 31 hours, with a thickness of 50 m. As mentioned before, the elevated inversions are normally not problematic in the Bergen Valley, regarding the air quality.

5.4.1 Discussion

We chose not to use the MTP for detecting temperature inversions as this was already done by Wolf et al. (2014). In addition repported Ezau et al. (2013) low reliability for the MTP during periods of high concentration of liquid water or ice, due to formation of a thin water film on the instrument housing. Therefore, Wolf et al. (2014) had to filter the data and remove all measurement during e.g. rainfall and fog. They ended up with only approximately 30 % of the measurements. It is therefore favorable to use in-situ measurements, as they are not limited by e.g. rainfall or fog and allowed us to use all

measurements. The ground-based inversions are the relevant ones regarding the air quality in Bergen, as the majority of emissions (e.g. from traffic and heating) is taking place close to the surface. The deployed dense network of in-situ measurements along the transect of the valley would give us detailed information of local variations.

Overall was in particular the winter seasons 2017 not favorable for the built-up of long-lasting inversions. The main reason for that was the synoptic weather situation in the with a lot of frontal passages and total annual precipitation of more than 3000 mm in Bergen in 2017. Because of turbulent mixing in the valley induced by the rain and increased wind speeds during frontal passages, in addition to the suppression of longwave radiative cooling, long lasting inversions that affect the air quality negatively are suppressed. In terms of air quality the precipitation also reduces the pollutants in the atmosphere by wet scavenging. As seen in section 5.3, a particularly unusual cold situation occurred in addition in the end of February 2018. Because this was a situation due to cold air advection and strong wind, it was not favorable conditions for inversions to occur. We found only a few inversion episodes during these days, the longest lasting ground-based inversion had a height of 100 m asl and lasted for only 50 min. The clear and cold conditions in February 2018 did also not result in major air pollution issues.

5.5 Case study - Advection Inversion

In the night from the 8th to the 9th of January 2018 a warm front passed over the Bergen area. It resulted in a strong ground-based temperature inversion and several elevated inversions. At the station at GFI the event was connected to two episodes of fast temperature increase at around 7 and 9 in the morning of January 9. The installed network of stations for this thesis allows for a detailed analysis of this event. In addition we also used data from the Davis stations located in the Bergen area as part of the school network, to extend our area of analysis.

5.5.1 Vertical Structure Based on AWS Profiles

The temperature series, from the AWS is found in figure 5.30. In the beginning (at 21:00) the stations were mostly evenly distributed by a temperature difference of 4 °C between the station at GFI and the one at Ulriken. The exception was the two stations at Skillingsbollen and Gapahuken that measured approximately the same temperature. This was also the case for the two stations at Strandafjellet and Svingen. On the 8th of January, at around 22:30, the temperature at Ulriken started to increase rapidly, indicating the passage of the warm front over the Bergen valley. The temperature increased by 3.6 °C in 1h 20min. Right before midnight the temperature at Ulriken was higher than the temperatures at the other stations, leading to elevated inversions due to warm air advection, where warm air flowed over a colder surface (Oke 1987). These inversions can be seen as the blue line (23:50) in the temperature profile, figure 5.31.

At the same time as the temperature at Ulriken increased, the temperature at Løvstakken also started to increase, but the increase was less steep. We assume the reason was the altitude difference. At the same time the temperatures at GFI, Skillingsbollen, Gapahuken and Svingen started to decrease. For Strandafjellet, the temperature slightly decreased, before it started to increase more rapidly from around 02:00. After a few hours, the temperature increased at the other stations, except GFI. The temperature increased at the southern and highest located stations first. The temperature at Svingen increased before the temperature at Strandafjellet, because Svingen is located a bit souther and only 50 m below Strandafjellet. We therefore assumed the warm air came from south or close to south.

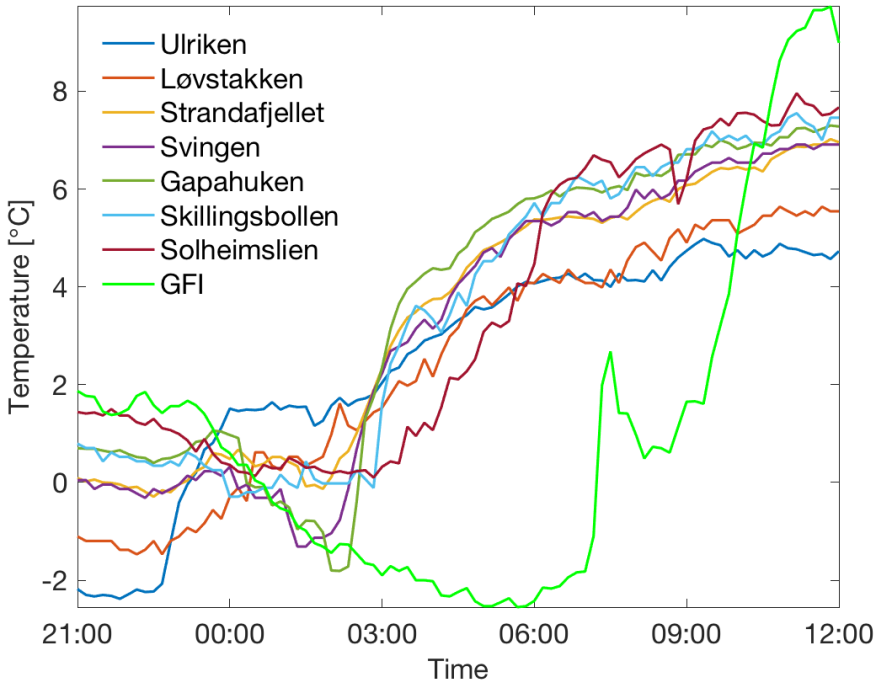

Figure 5.30: Temperature series from 08.01.18 at 21:00 to 09.01.18 at 12:00.

The temperature at GFI behaved differently than for the other stations. It decreased until 05:30 when it reached its minimum of -2.6 °C. The temperature at GFI kept decreasing several hours after the warm air reached the stations above. This could indicate both, local longwave-radiative cooling and cold pooling by drainage flows from the surrounding slopes. Due to cooling of the ground, a ground-based inversion was formed. Eventually, the warm air reached the lowest layer and the temperature at GFI increased rapidly in two steps. First by 3.8 °C/20 min, reaching a local maximum of 2.8 °C. The temperature once again decreased, before it increased rapidly again to its maximum of 9.7 °C, around 11:00. In total, the temperature increased by 12.3 °C over six hours.

The corresponding temperature profiles at five different times are presented in figure 5.31. The temperature profiles were chosen based on the ongoing situation at the given time. The first one (blue line, 23:50) shows the situation when the temperature at Ulriken increased and passed the other stations. The second line (red, 01:00), illustrates the situation when the temperatures from the other stations are very close together, to give an overview of how the temperatures were distributed with height. The third line (yellow,

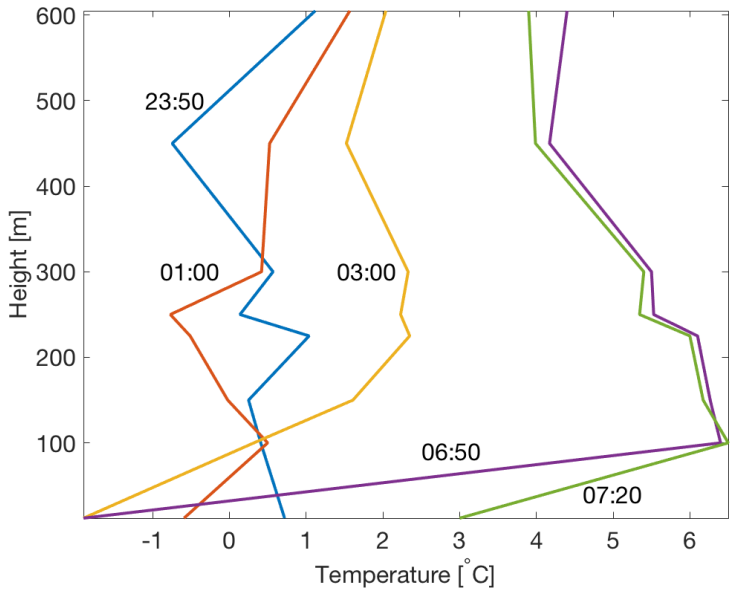

Figure 5.31: Temperature profiles at five given times; 23:50 (08.01.18), 01:00, 03:00, 06:50 and 07:20.

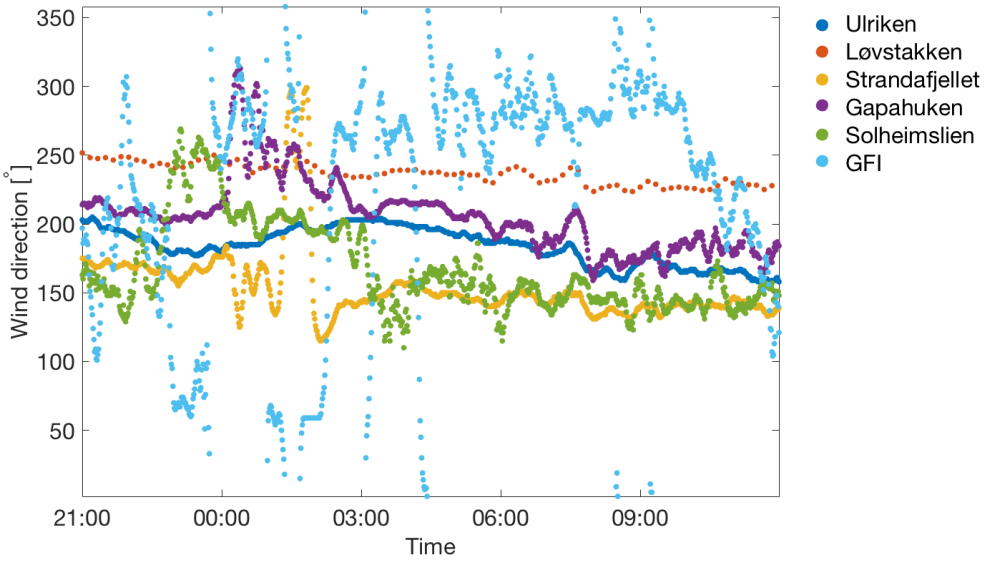

Figure 5.32: Wind direction from 08.01.18 at 21:00 to 09.01.18 at 12:00.

03:00), illustrates the situation when all stations, except GFI, have a warming trend and the ground based inversion forms. The purple line (06:50) shows the maximum inversion

between GFI and Solheimslien. The inversion strength between the two stations was 8.3 °C over a vertical distance of 88 m. If this temperature increase would have extended to Ulriken, the temperature at Ulriken would have been 56 °C.

Around midday on the 9th, the air in the valley was again well-mixed and the strong temperature inversion episode was over. The temperature difference between GFI and Ulriken was approximately 4 °C. All stations, except GFI, were back to the same temperature spread, as before the warm air advection, at 09:00.

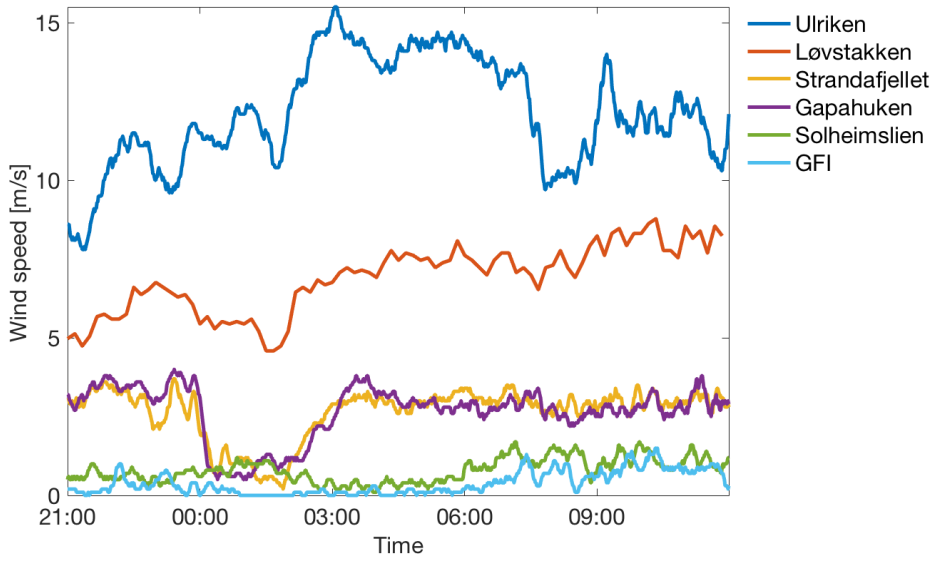

Figure 5.33: Wind speed series from 08.01.18 at 21:00 to 09.01.18 at 12:00.

Wind direction measurements from the AWSs are found in figure 5.32. For most of the stations the winds were in the range between southeast and northwest. The exception was GFI where the wind came from all direction during the measurement period. During the periods of temperature increase, the wind came from south-southwest. This supports our assumption that the warm air came from south or close to south. Løvstakken measured a rather constant wind direction from southwest, for the whole period. The stations at Solheimslien, Gapahuken and Strandafjellet got a larger spread after midnight, but from 03:00 and onward they were measuring a more constant wind direction, from southeast to south. The wind speed measured at GFI can be found in figure 5.33. The largest spread occurred where the stations were measuring the lowest wind speeds. This was

likely the reason for the large spread for the station at GFI. At midnight the wind speeds at Gapahuken and Strandafjellet rapidly decreased, indicating that those two stations might have been affected by a katabatic flow for a while. As seen in figure 5.31, these stations were located at the top or close to the top of the elevated inversions.

5.5.2 Comparison With MTP

The availability of AWS data in high spatial and temporal resolution during this event allowed also for a comparison and performance check of the MTP. Figure 5.34(a) shows the time-height cross section of temperature from the in-situ measurements from the AWSI and AWSA, and (b) from the MTP. The MTP is located at the roof at GFI, at 45 m asl and provides temperature profiles from 45 to 1045 m. Since the in-situ measurements only reached 605 m asl, the MTP profile was also cut at 605 m asl.

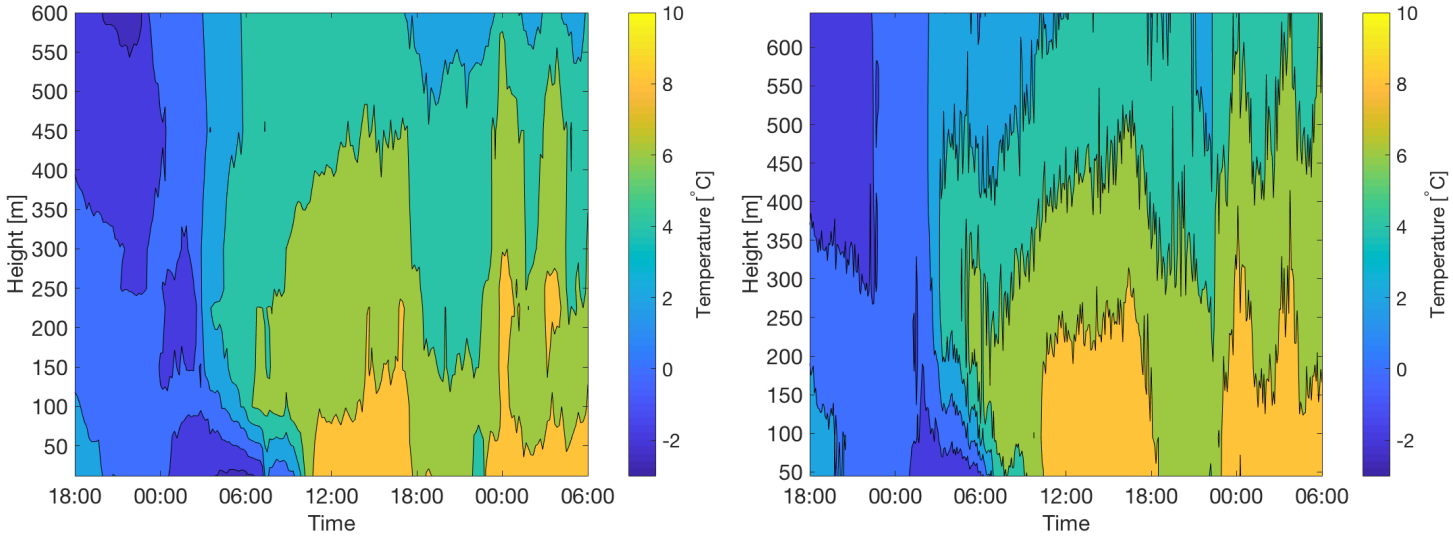

Figure 5.34: Temperature profiles from a) in-situ measurements and b) MTP-5HE at the rooftop at GFI.

Overall, the two figures show a very good agreement between the two independent measurement methods. Both present a very similar structure and development in time. The MTP measurements (5.34(b)) are based on 5 minute averages and show therefore a higher fine-scale variability than the in-situ measurements averaged over 10 minutes. The in-situ measurements were based on 50-75 m intervals for the stations in the range 100

to 300 m asl, and two 150 m intervals between 300 and 605 m asl. Also, there were no measurements between 12 and 100 m asl. The densest network of stations was in the range from 100 to 300 m asl. Even with limited measurements in some areas, the in-situ measurements were detecting small-scale features rather well. Because the MTP started at 45 m asl, it did not detect the coldest temperatures at the ground, measured by the station at GFI. For the further detailed discussion of the comparison it has also be taken into account that the MTP is averaging over a certain air volume over the center of the Bergen valley, while the AWS data represent point measurements close to a sloping surface.

Some differences between the two figures can be identified with respect to vertical structure and timing. After midnight, a region of colder air was located in between 125 and 325 m asl. The two profiles differed on the time scale. For both profiles, at around 07:00 there was an outlier between 100 and 225 m asl. Colder air from above, penetrated down to around 150 m asl. This outlier can be seen in the temperature profile for MTP, but it ranged from 200 to 350 m asl. Because of the limited measurements in the upper region, between the station at Løvstakken and Ulriken, there were some differences here. The MTP showed lower temperatures in the upper layer between 03:00 and 11:00. The MTP also showed higher temperature (yellow region) at a higher altitude, over a longer time period than the in-situ measurements. The in-situ measurements showed two outliers between 14:00 and 17:00, while the MTP showed a more constant situation over a longer time period. Between 18:00 and midnight the two profiles differed on the vertical extent, the in-situ measurements showed lower temperatures down to 150 m asl. For the MTP these low temperature only reached 200 m asl for a short time period. From midnight and during the night on the 10th, the two profiles showed the same pattern, but with different extent. The two concurred on the overall situation and pattern, but they could not be directly compared. They both detected outliers, but they differed on the how long they lasted and where they occurred.

5.5.3 Spatial Variability in the Larger Bergen Area

We included measurements from stations at schools in the Bergen area, to look at how the situation developed in the larger Bergen area. An overview of the location of the stations can be found in figure 5.35 and information about the stations is given in table 5.2. The stations were chosen to represent typical topographic conditions for the region. Garnes

and Lone from east, both located in a valley known as the Arna Valley. Hellen from north, Holen and Ortun from west. Haukeland was the chosen as the station from south, because of limited available station in the southern direction. We only had one station available further south, at Landås, but the result was the same as for Haukeland.

Figure 5.35: Overview of the stations from the "Bergen Weather" project, used for the analysis of the spatial and temporal development during the case study. The AWSI at GFI was used as a location reference. Satellite image from Google Earth.

As stated by Schönbein (2017), the Davis stations at the schools in the Bergen area have varying data quality, mainly regarding the setup. At e.g. Fløyen, wind measurements should be treated with caution because it was surrounded by woods. The stations are located at different heights and some close to rooftops, that might have affected the measurements.

Temperatures measured by the Davis stations during the event are presented in figure 5.36. The temperature from GFI was added as a reference. As presented in 5.5.1, the temperature evolution at GFI was different from the other AWSs in the Bergen Valley.

Table 5.2: Overview of the Davis station. Numbers from Schönbein (2017)

Station	**Altitude [m asl]**	**Latitude °N**	**Longitude °E**	**Logging interval**
Ortun	37	60.345	5.288	10 min
Holen	31	60.389	5.285	10 min
Hellen	37	60.438	5.461	10 min
Fløyen	305	60.398	5.338	10 min
Garnes	55	60.440	5.461	10 min
Lone	80	60.376	5.455	10 min
Haukeland	56	60.380	5.361	10 min
GFI	12	60.383	5.333	1 min

Compared to the Davis stations of the school network, mostly located at lower altitudes, the temperature at GFI showed very similar patterns. The exception was the station at Fløyen, which had the temperature increase sooner than all the other stations. This was likely because the station at Fløyen is located at 305 m asl and therefore the warm air reached this station earlier than the others.

Based on the results from the AWSs, we expected the warm air flow to reach the southern and highest located stations first. As illustrated in figure 5.36, the warm air reached Fløyen first. The station at Garnes had a decrease in the temperature at the same time as the temperature at Fløyen started to increase, before it started to increase, some minutes after the station at Fløyen. We did not see this increase for the other stations. The temperature at Garnes decreased again for a short time, before it started to increase. Short time after the last increase of the temperature at Garnes some of the other stations followed. First, the station at Haukeland increased with a maximum growth rate of 5.4 °C/40 min. At this point, also the temperature at GFI started to increase. An hour later followed Ortun, starting from a minimum temperature of -3.8 °C. Here we observed the highest warming rate with 8.4 °C/40 minutes. It reached, similar to GFI, a local maximum of 6.3 °C at 08:40, before dropping by 4 °C for about one hour and finally steeply increasing again. It was surprising that the temperature at Ortun increased hours after some of the other stations located further north, indicating additional features and processes protecting

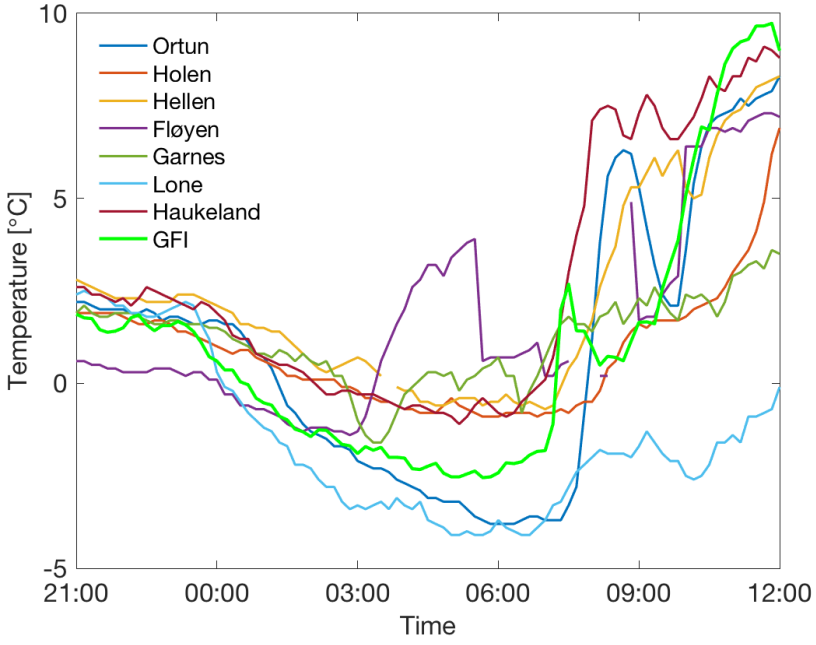

Figure 5.36: 24 hours temperature series from 08.01.18 12.00 to 09.01.18 10.00

the station from the warm flow. The temperature at Holen increased at a later time than the temperature at Ortun. This supports that the late temperature increase for Ortun was due to its location at low altitude and therefore the warm air reached the station this late.

As seen in figure 5.36, Lone measured the lowest temperature of -4.1 °C around 05:00. Compared to the other stations the temperature at Lone only had a small increase, before it decreased, and near linearly increased to a maximum of 9.3 °C at 17:00. Lone is located in the Arna Valley with mountains surrounding and is known as a cold place. Utaaker (1995) found that the area around Lone was affected by strong cold air accumulation and frequent occurrence of temperature inversions. The coldest temperatures were found when the nearby water, Haukelandsvannet, was frozen. Because the warm air came from south-southwest, the flow of warm air was likely to be affected by both the narrow valley opening southwest of the station. In addition, high mountains surrounding the station and might have delayed the warm air to reach Lone.

Our results show that elevation is clearly affecting the result. The warm air advected at higher levels has to remove the cold air in the valley. The temperatures at the stations at high altitudes were warmer than the stations further down in the valley. In figure 5.36,

this can be seen for both the AWSs and the Davis stations. Other local effects, such as surrounding mountains were also affecting the downward penetration of warm air.

Figure 5.37 illustrates as an example the temperature, relative humidity, wind speed and direction time series for two stations, GFI ((a)) and Fløyen ((b)). The station at GFI showed an increase in the temperature at a later time than the other AWS. The Davis station at Fløyen showed an increase in the temperature about four hours before GFI. As illustrated in the figure 5.37(b), the station had some missing records both for temperature, relative humidity and wind speed. In addition, the relative humidity was included in these figures. The drop in relative humidity and increase in temperature was a clear indication of warm air advection. The warm air can hold more water vapor and the relative humidity decrease. Warm air from south flowed in over the Bergen Valley, which was cold and the warm air took over for the cold air. The wind at Fløyen was from south before and during the warm air reached the station, but afterwards the wind direction changed to a east-northeast direction.

As described in this section, the strong ground-based and elevated temperature inversion occurring on the 9th of January 2018, was caused by a warm front and warm air advection. Warm air from south-southwest flowed over the cold Bergen Valley. The temperature increased at the highest located stations first. The warm air took over for the cold air in the valley and eventually the temperatures at all stations increased. When the warm air reached Solheimslien (100 m asl) it resulted in a ground-based temperature inversion, with a strength of 8.3 °C. The temperature profile from in-situ measurements showed in general a very good agreement with the temperature profile from the MTP.

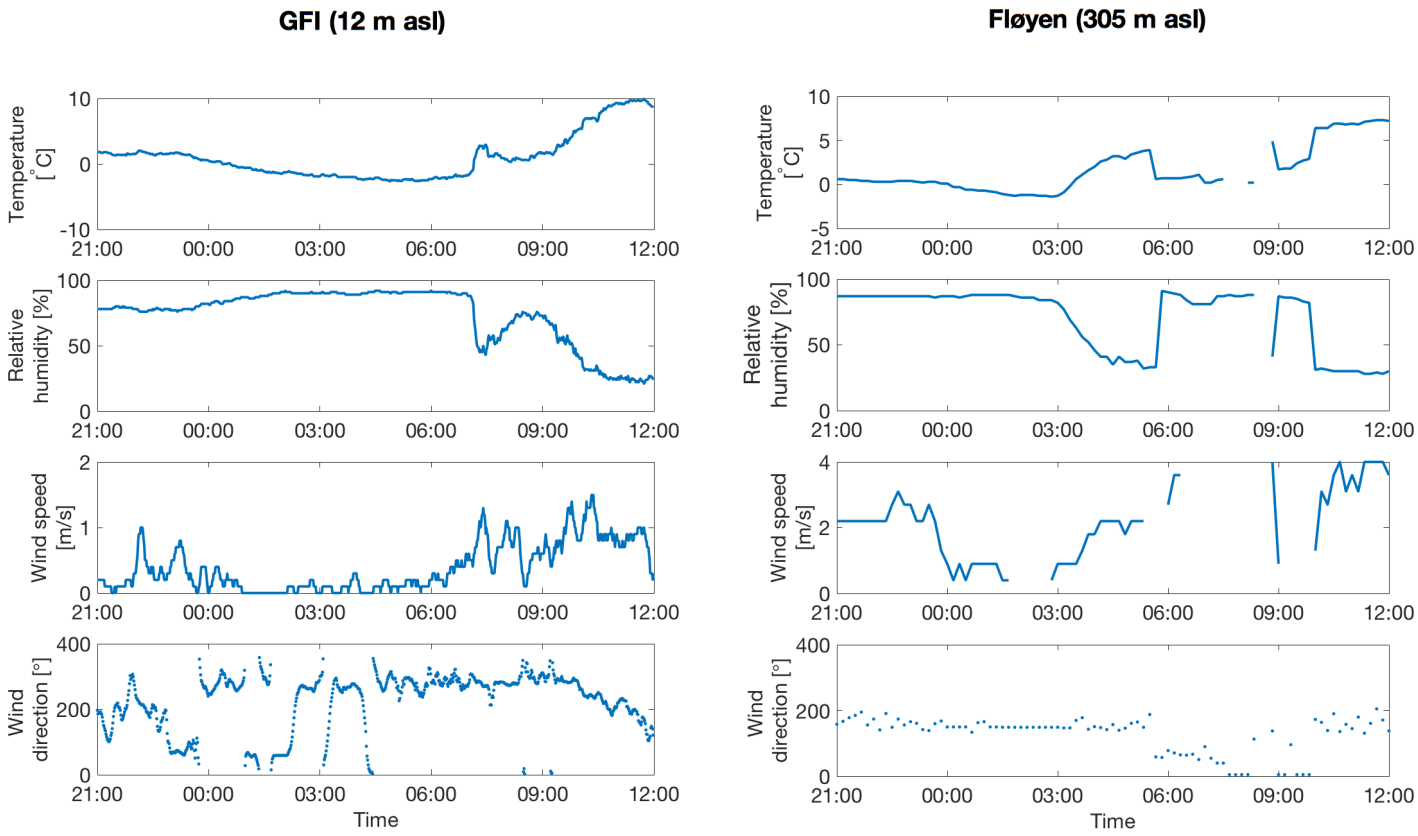

(a) (b)

Figure 5.37: Overview of the time series at GFI and Fløyen. (First panel) shows the temperature, (second panel) the relative humidity, (third panel) the wind speed and (fourth panel) the wind direction.

6 Summary and Conclusion

In this thesis we investigated the occurrence of temperature inversions in the Bergen Valley, by performing measurements in a dense network of Automatic weather stations (AWSs) along the transect of Løvstakken. In addition we tested low-cost temperature and air quality measuring instruments, in order to check their performance before installing them out in the field. We have also looked at the general weather situation during the measurement campaign. Last, we saw how a situation of warm air advection affected the Bergen Valley and how a strong ground-based temperature inversion formed.

The two tests of the EasyLog data loggers (ELs) were performed in October/November 2017, in the observational garden at Geophysical Institute (GFI). For the first test the loggers were put in a box and located close to the temperature sensor at the reference station. The result of the tests showed the same as a study by Nordhagen (2014), the ELs were prone to overheating when exposed to solar radiation. We therefore filtered the data by removing all measurements when the solar radiation, exceeded a threshold of 20 W/m^2. The filtering largely improved the result. The Root Mean Square Deviation (RMSD) decreased from values between 1.7 and 3.6 % to values between 0.44 to 0.69 %, and the correlation increased from a value between 0.58 to 0.82, to a value of 0.98. The difference in between the loggers were due to the location in the box, as one side was pointed towards the sun. The filtering only improved the overestimation due to solar radiation, but not the 2 °C underestimation during the night. The loggers went through a second test in order to check whether the loggers could be used without additional shielding. The result of the second test was similar to the first one, with overestimation when exposed to direct sunlight. The same filtering was applied and the positive spikes were removed. After the filtering the correlation was 0.98, compared to a value between 0.93 and 0.96 before the test. The systematic underestimation during the night can indicate a potential calibration error or the effect of radiative cooling of the sensor and sensor housing below

the air temperature.

The Air Quality Eggs (AQEs) went through three tests in order to check the performance of the instruments. The two first tests were performed at the official air quality measuring station, owned by the Bergen Municipality, at Danmarksplass. The result of the tests showed that the instruments were prone to overheating when exposed to solar radiation. The first two tests showed different result for the AQE measuring Nitrogen dioxide (NO_2). In the first test, the AQE underestimated the amount of NO_2 and in the second test it largely overestimation the concentration. During the first test we found a RMSD of 44.2 % and a correlation of 0.85 between the AQE and Bergen municipality reference station (BK), whereas the second test showed a RMSD of 128.9 % and a correlation of 0.24. For the second test both AQEs were tested. The AQE Particulate pollution (PP) should detect particles of size between 0.5 and 10 µm. We compared the measurements to both $PM_{2.5}$ and PM_{10} measured by the BK. The result of the comparison to PM_{10} was a RMSD of 19.3 % and a correlation of 0.33, and the comparison to $PM_{2.5}$ showed a RMSD of 6.4 % and a correlation of 0.76. The AQE was clearly underestimating the PP concentration. Both tests and both AQEs showed a better performance in temperature and relative humidity. Because temperature and relative humidity was tested against the reference station at GFI, 1 km away from Danmarksplass, a third test was preformed in the observational garden at GFI. The third test showed a clear overestimation of temperature and underestimation of relative humidity for both AQEs. The instrument measuring PP measured a systematic higher temperature. For the temperature, the AQE measuring NO_2 showed a RMSD of 7.7 % and a correlation of 0.94, and the AQE measuring PP showed a RMSD of 8.2 % and a correlation 0.96. For the relative humidity, the AQE measuring NO_2 showed a RMSD of 9.3 % and a correlation of 0.96, while the numbers from the AQE measuring PP was 20.1 % and 0.98. The large variability and non-reproducibility in the performance of the instrument disqualifies them from meaningful scientific use. Consequently those instruments have not been deployed in the field as originally intended.

The general weather situation during the measurement campaign was characterized by high temperatures and large amount of precipitation. Overall, the temperature measured at GFI was 0.7 °C higher than the normal and we found 34-49 % higher amount of precipitation than the climatological mean. The maximum amount of precipitation, 3815 mm, was found at Solheimslien (100 m above sea level (m asl)). May was the month of highest average solar radiation, due to a low amount of precipitation and clouds. We found the

weakest solar radiation in December, which we expected, due to low solar angle, short day and heavy rainfall. The result of the wind measurements were compared to the result of a study by Valved (2012). We found the same pattern for most of the stations that was comparable in location and altitude. The largest differences was at GFI, because the stations were located at two different altitudes and could therefore not be directly compared.

For the investigation of occurrence of temperature inversions, we only found few and short lasting ground-based temperature inversions. The ground-based inversions were shallow, with a maximum frequency of occurrence with tops at 100 m asl. As seen in a study by Wolf et al. (2014), it is the ground-based inversions that are problematic for the air quality in the city. They found the inversions with tops at 220 m asl to be usually connected to cases of high pollution. Our results not disagreeing with their result, because we only found a few episodes of inversions with tops at 225 m asl and these were short lasting, and we did not experience any long lasting high pollutant concentrations in the Bergen Valley during the whole 13 month campaign. Elevated inversions are typically not connected to high pollutant concentrations in the valley. We found a high number of elevated inversions between 225 m asl and 300 m asl. The stations are located close together and shading of a station might be the reason for the high occurrence of elevated inversions. More than 75 % of the elevated inversions lasted shorter than two hours. The reason for the low number of persistent inversions is likely the synoptic weather situation with a lot of frontal passages and a total amount of precipitation of more than 3000 mm.

In a case study, where we investigated the situation in the Bergen area on the 8th and 9th of January 2018, we found a strong ground-based inversion of 8.3 °C up to Solheimslien at 100 m asl, together with several elevated inversions. These inversions occurred because a warm front passed over the Bergen area, where warm advected air flowed over the cold air in the valley. Based on the measurements from the AWS along the transect of Løvstakken and the station at GFI and Ulriken we found the southern and highest located areas to have a temperature increase first. All stations showed southwesterly winds. To investigate the spatio-temporal behavior of the warm air advection in the larger Bergen area, we also compared the results of the vertical temperature structure and development from the in-situ measurements and the MTP-5HE (MTP). Overall, they showed the same pattern, but there were some differences with respect to vertical structures and timing. We also included data from the "Bergen Weather" project. These weather stations are located at more than 30 schools in the Bergen area. We used data from seven of these station, for

additional information. The result from these station confirmed the main finding from the Løvstakken AWS transect, that the warm air reached the southern and elevated stations first.

Bibliography

Aanderaa Data Instruments AS (2012), *Data Storage Unit 2990*. Last checked: 18.03.18.
URL: *https://www.aanderaa.com/media/pdfs/DSU-2990.pdf*

Aanderaa Data Instruments AS (2016*a*), *Air Temperature Sensor 3455*, d276 edn. Last checked: 27.03.18.
URL: *https://www.aanderaa.com/media/pdfs/air-temp-sensor-3455.pdf*

Aanderaa Data Instruments AS (2016*b*), *Wind Direction 3590(averaging)*. Last checked: 20.02.18.
URL: *https://www.aanderaa.com/media/pdfs/wind-direction-sensor.pdf*

Aanderaa Data Instruments AS (2016*c*), *Wind Speed Sensor 2740*. Last checked: 27.03.18.
URL: *https://www.aanderaa.com/media/pdfs/wind-speed-sensor.pdf*

Ahrens, C. D. (2012), *Meteorology Today: An Introduction to Weather, Climate, and the Environment*, 10 edn, Cengage Learning.

APIS (2017), 'Unit conversion'. Last checked: 31.03.18.
URL: *http://www.apis.ac.uk/unit-conversion*

Berge, E. & Hassel, F. (1984), En undersøkelse av temperaturinversjoner og lokale drenasjestrømmer i Bergen, Meteorological report series 2, University of Bergen.

Bergen Municipality (2017*a*), 'Hvor høye er de?'. Last checked: 31.03.18.
URL: *https://www.bergen.kommune.no/omkommunen/fakta-om-bergen/6144/article-63904*

Bergen Municipality (2017*b*), 'Tall som beskriver klima i Bergen'. Last checked: 04.05.18.
URL: *http://www.miljostatus.no/tema/luftforurensning/lokal-luftforurensning/*

Bergensværet (2018), 'Om bergensværet'. Last checked: 27.03.18.
URL: *www.bergensveret.no*

Castell, N. (2017), 'Low-cost sensor technologies, bluff or reality?', "By email".

DATAQ Instrument (2018), 'El-usb-1 temperature data logger'. Last checked: 10.02.18.
URL: *https://www.dataq.com/resources/pdfs/datasheets/el-usb-1-data-logger.pdf*

DATAQ Instruments (2018), *EL-USB-1 Temperature Data Logger*. Last checked: 20.02.18.
URL: *https://www.dataq.com/resources/pdfs/datasheets/el-usb-1-data-logger.pdf*

Ezau, I. N., Wolf, T., Miller, E. A., Repina, I. A., Troitskaya, Y. I. & Zilitinkevich, S. S. (2013), 'The analysis of results of remote sensing monitoring of the temperature profile in lower atmosphere in bergen (norway)', *Russian Meteorology and Hydrology* **38**(10), 715–722.

Fitje, A. (1972), En undersøkelse av atmosfæriske stabilitetsforhold i bergensområdet, Master's thesis, University of Bergen.

Folkehelseinstituttet (2018), 'Luftkvalitetskriterier - sammendrag'. Last checked: 30.04.18.
URL: *https://www.fhi.no/nettpub/luftkvalitet/sammendrag/sammendrag/*

Hanssen-Bauer, I. (1985), 'A simple model for diffusion of so_2 in bergen', *Atmospheric Environment* **19**(3), 415–422.

ITAS (2015), *Sammendrag ITAS/TJE*, 1 edn.

Jonassen, M. O., Ólafsson, H., Reuder, J. & Olseth, J. (2012), 'Multi-scale variability of winds in the complex topography of southwestern Norway', *Tellus A: Dynamic Meteorology and Oceanography* **64**(1), 1–17.
URL: *https://doi.org/10.3402/tellusa.v64i0.11962*

Jonassen, M. O., Ólafsson, H., Valved, A. S., Reuder, J. & Olseth, J. A. (2013), 'Simulations of the Bergen orographic wind shelter', *Tellus A: Dynamic Meteorology and Oceanography* **65**(1), 19206.

Markowski, P. & Richardson, Y. (2010), *Mesoscale Meteorology in Midlatitudes*, 1 edn, Wiley-Blackwell.

Miljødirektoratet (2018), 'Lokal luftforurensning'. Last checked: 30.05.18.
URL: *https://www.bergen.kommune.no/omkommunen/fakta-om-bergen/6123/article-63579*

NILU (2015), 'Luftkvalitetskriterier'. Last checked: 29.04.18.
URL: *http://www.luftkvalitet.info/Theme.aspx?ThemeID=6fc2e3cd-424f-4c03-ad0c-2b9c15369cd9*

NOAA National Centers for Environmental Information (2015), 'State of the climate: Global climate report - annual 2014'. Last checked: 04.05.18.
URL: *https://www.ncdc.noaa.gov/sotc/global/201413#gprcp*

Nordhagen, R. (2014), Forecast challenges associated with cold pools in norwegian valleys, Master's thesis, University of Bergen.

Norwegian Institute of Public Health (2017), 'Air pollution in Norway'. Last checked: 30.04.18.
URL: *https://www.fhi.no/en/op/hin/miljo/air-pollution-in-norway—public-he/#main-points*
degaard et al.

Ødegaard, V., Gjerstad, K., Abildsnes, H. & Olsen, T. (2011), 'Bedre byluft prognoser for meteorologi og luftkvalitet i norske byer vinteren 2010 - 2011', *MET Report* **8**.

Oke, T. R. (1987), *Boundary Layer Climates*, 2 edn, Routledge, London.

Rasmussen, R., Baker, B., Kochendorfer, J., Meyers, T., Landolt, S., Fischer, A. P., Black, J., Thériault, J. M., Kucera, P., Gochis, D., Smith, C., Nitu, R., Hall, M., Ikeda, K. & Gutmann, E. (2012), 'How well are we measuring snow: The noaa/faa/ncar winter precipitation test bed', *Bulletin of the American Meteorological Society* **93**(6), 811–829.

Resource Supply (2008), 'Ip67, what does that mean?'. Last checked: 18.03.18.
URL: *http://www.resourcesupplyllc.com/PDFs/WhatDoesIP67Mean.pdf*

Schönbein, D. (2017), A study on local weather variability in complex terrain using the bergen school mesonet, Master's thesis, University of Bergen.

Sorteberg, A. (2014), 'Nedbør i Norge siden 1900', *Naturen* **138**(06), 220–231.
URL: *http://www.idunn.no/natur/2014/06/nedboer_i_norge_siden_1900*

SSB (2017), 'Folkemengde per 1. januar 2017'. Last checked: 30.03.18.
URL: *https://www.bergen.kommune.no/omkommunen/fakta-om-bergen/6125?artSectionId=6125&articleId=63578*

SSB (2018), 'Bergen - 1201 (Hordaland)'. Last checked: 30.03.18.
URL: *https://www.ssb.no/kommunefakta/bergen*

Stull, R. B. (2009), *An Introduction to Boundary Layer Meteorology*, Springer, Vancouver, Canada.

Utaaker, K. (1991), *Mikro- og lokalmeteorologi*, ALMA MATER FORLAG AS.

Utaaker, K. (1995), Energi i arealplanleggingen lokalklima i Bergen, Meteorological report series 1, University of Bergen.

Valved, A. S. (2012), Local flow conditions in the Bergen valley based on observations and numerical simulations, Master's thesis, University of Bergen.

Wallace, J. M. & Hobbs, P. V. (2006), *Atmospheric Science: An Introductory Survey*, 2 edn, Elsevier, University of Washington.

Weiss, L. L. (1961), 'Relative catches of snow in shielded and unshielded gages at different wind speeds', *Monthly Weather Review* **89**(10), 397–400.

Wicked Device (2016*a*), *Air Quality Egg v2 - model A*. Last checked: 20.02.18.
URL: *http://shop.wickeddevice.com/wp-content/uploads/2016/02/UserManual-CO-NO2.pdf*

Wicked Device (2016*b*), *Air Quality Egg v2 - model C*. Last checked: 20.02.18.
URL: *http://shop.wickeddevice.com/wp-content/uploads/2016/02/UserManual-Particulate.pdf*

Wolf-Grosse, T. (2016), An Integrated Approach for Local Air Quality Assessment under Present and Future Climate Scenarios, PhD thesis, University of Bergen.

Wolf-Grosse, T., Pettersson, L. & Esau, I. (2016), Spredning og konsentrasjonsdannelse av NO_2 og $PM_{2.5}$ i Bergen sentrum, Technical report, The Nansen Environmental and Remote Sensing Center.

Wolf, T., Esau, I. & Reuder, J. (2014), 'Analysis of the vertical temperature structure in the Bergen valley, Norway, and its connection to pollution episodes', *Journal of Geophysical Research Atmospheres* **119**(3), 9626–9637.

Zardi, D. & Whiteman, C. D. (2012), *Mountain weather research and forecasting, Ch.2: Diurnal Mountain Wind Systems*, Springer.